Dissertation

submitted to the
Combined Faculties of the Natural Sciences and for Mathematics
of the Ruperto-Carola University of Heidelberg, Germany
for the degree of
Doctor of Natural Sciences

presented by

M. Sc. Molecular Biotechnology
born in:
Oral-examination:

Firat Terzi
Nürtingen, Germany
…….

A genetically encoded system with high spatio-temporal resolution for *in vivo* modification of neuronal network activities

Referees: Prof. Dr. Thomas Kuner

Prof. Dr. Hilmar Bading

Abstract

Despite decades of progress in the field of conditional transgene expression, acute, cell-type specific transgene induction remains difficult to achieve with currently available methods. By combining the inducible Tet system with the conditional, cell-type specific Cre recombinase system, I developed a method that allows genetic manipulation of tissues *in vivo* at cellular resolution based on adeno-associated viruses (AAV). In addition, the Cre-mediated constitutive expression of a fluorescent reporter highlights cells prior to induction of the transgene via the Tet system. Therefore, cells can be carefully characterized before, during, and after genetic manipulation. The phenotypic consequences of transgene expression can thus be temporally correlated in individual cells *in vivo*.

The TetOn system is a two-component system of a Tetracycline-dependent transcriptional activator (rtTA) and the Tet-dependent transgene, which I now flanked by Cre recombinase sites. The TetOn system was optimized to increase tightness by additionally introducing the doxycycline-dependent tTR repressor. *In vivo*, this substantially reduced the notorious leakiness of the TetOn system. The goal of my thesis research was to use this optimized Cre-dependent TetOn system for acute genetic silencing of neurons in mouse cortex by expression of Kir2.1, a potassium channel that cell-autonomously hyperpolarizes membranes. Co-injection of an AAV with the GFP-based calcium indicator GCamP6 allowed *in vivo* two-photon imaging the spontaneous activity of the same neurons over time in longitudinal experiments. Injection of doxycycline into the brain induced rapid silencing of neurons within hours that lasted for at least 80 h. Using transgenic Parvalbumin-Cre mice, silencing of inhibitory Parvalbumin interneurons significantly increased the spontaneous activity of surrounding neurons in a distance dependent manner as nearby neurons were more affected. No such effect was seen after silencing a random subpopulation of neurons. Finally, I tested if prolonged silencing influences dendritic morphology. Cre-dependent expression of red fluorescent tdTomato was used to monitor spine numbers before and 75 h after Kir2.1 expression. Corroborating previously published *in vitro* results, I could show for the first time *in vivo* that silencing individual neurons after synapse formation does not change spine numbers.

This thesis describes the entire journey from the cloning of an optimized TetOn system to its *in vivo* applications. Together with the establishment of longitudinal *in vivo* calcium imaging, an analysis pipeline has been created for registration, extracting, and processing of calcium signals for spike estimation. Despite the complexity of the combined tools and the intrinsic variability associated with manipulating and analyzing the same cells over time *in vivo*, this method yielded exciting data and will provide researchers with the possibility to use this approach in a wide spectrum of experimental settings.

Zusammenfassung

Trotz jahrzehntelangen Fortschrittes auf dem Gebiet der konditionalen Genexpression ist die schnelle und zelltypspezifische Transgeninduktion mit den verfügbaren Methoden weiterhin eine große Herausforderung. Durch die Kombination des induzierbaren Tet-Systems mit dem zelltypspezifischen Cre Rekombinase-System habe ich eine Methode entwickelt, die auf Adeno-assoziierten Viren (AAV) basiert und die genetische Manipulation von Geweben *in vivo* mit zellulärer Auflösung ermöglicht. Zusätzlich werden Zellen durch Cre vermittelte und konstitutive Expression bereits vor der Transgeninduktion fluoreszenzmarkiert. Dadurch ist es möglich die Zellen *vor*, *während* und *nach* der genetischen Manipulation zu charakterisieren. Die phenotypischen Folgen der Transgenexpression können daher *in vivo* in einzelnen Zellen über einen langen Zeitraum verfolgt werden.

Das TetOn System besteht aus zwei Komponenten: Dem doxycyclinabhängigen *transcriptional activator* (rtTA) und dem Tet-abhängigen Transgen, welches durch Cre Rekombinase abhängige Sequenzen flankiert wurde. Die unerwünschte basale Expression des TetOn Systems konnte durch die zusätzliche Verwendung des doxycyclinabhängigen tTR Transrepressors weiter verringert werden. Besonders bei *in vivo* Anwendungen führte dies zu einer substanziellen Verringerung der Hintergrundexpression. Das Ziel dieser Untersuchung war die Benutzung dieses verbesserten TetOn Systems für die schnelle genetische Inaktivierung von Neuronen in der Cortex von Mäusen. Dies wurde erreicht durch die Expression von Kir2.1, einem Kaliumkanal-Protein, das die betroffenen Neuronen hyperpolarisiert und somit deren Aktivität herabreguliert. Die gleichzeitige Injektion von AAV mit GCamP6f, einem GFP-basierten Kalziumsensor, ermöglichte die Aufnahme neuronaler Spontanaktivität mit dem 2-Photonenmikroskop *in vivo* über einen langen Zeitraum hinweg. Die Injektion von Doxycyclin führte zu einer schnellen Herabregulierung der Aktivität von Neuronen innerhalb von Stunden und hielt für mindestens 80 h an. Durch die Verwendung der Parvalbumin-Cre Mäuselinie konnte gezeigt werden, dass die Herabregulierung der Aktivität von Parvalbumin Interneuronen zu einer erhöhten Spontanaktivität umliegender Neuronen, abhängig von deren Entfernung zu Parvalbumin Interneuronen führt. Solch ein Zusammenhang konnte bei der Herabregulierung einer zufälligen Neuronenpopulation nicht festgestellt werden. Abschließend wurde untersucht, ob die langfristige Herabregulierung neuronaler Aktivität zu morphologischen Veränderungen an Dendriten führt. Die Cre-abhängige Expression von roter tdTomato-Fluoreszenz wurde genutzt, um die Anzahl von Dornfortsätzen vor und 75 h nach der Kir2.1 Expression zu untersuchen. Vormalige *in vitro* Publikationen bestätigend, konnte ich erstmalig demonstrieren, dass die Anzahl an Dornfortsätzen sich trotz veränderter neuronaler Aktivität in einzelnen, adulten Neuronen nicht ändert.

Diese Arbeit beschreibt den gesamten Entstehungsprozess der entwickelten Methode, von der Klonierung des optimierten TetOn Systems bis hin zu seiner Anwendung *in vivo*. Neben der Etablierung des *in vivo calcium imaging* wurde zusätzlich eine Analysepipeline für die Registrierung, Extraktion und Verarbeitung der Kalziumsignals zur Abschätzung neuronaler Aktivität entwickelt. Trotz der Komplexität der kombinierten Methoden und der intrinsischen Variabilität, die mit der Manipulation und Analyse von langfristigen *in vivo* Experimenten einhergeht, konnte ich mit der entwickelten Methode sehr interessante Daten gewinnen. Diese Methode ermöglicht Wissenschaftlern ein breites Spektrum an experimentellen Herangehensweisen, die vorher schwer zugänglich waren.

Acknowledgments

First of all I would like to thank Prof. Dr. Thomas Kuner for giving me the opportunity to conduct my PhD thesis in his institute and being able to use all the equipment and infrastructure that was necessary for this research project.

Especially, I would like to thank Dr. Sidney Cambridge for supervising my research and the many hours he spent discussing results, and helping me to improve my scientific writing and presenting skills, and many more. He helped and encouraged me to apply for several fellowships, which I also got in the end. My gratitude goes to the Friedrich-Ebert-Stiftung for granting me a PhD fellowship. This research would not have been possible without their financial support. I also want to acknowledge funding support from the SFB 1134.

My special thanks go to my friend Dr. Johannes Knabbe, with whom I spent uncounted hours. He introduced me to *in vivo* techniques and Matlab and helped me to establish the whole analysis pipeline. Without him, this project would have been impossible and much more boring.

Of course, many thanks go to Gabie Krämer, for helping me with a lot of daily lab work and giving me the possibility to concentrate on other research aspects. I am also very grateful for her entertaining stories and gossip of all kind that turned some frustrating lab days into enjoyment. Without her, this research would have been very boring. Noteworthy, the occasional “Kippsche & Käffsche”, we enjoyed at the balcony. I would like to thank the other technical assistants in the lab for their help with different aspects of the project. Namely, Michaela Kaiser, Claudia Kocksch, and Marion Schmitt. And also Dr. Frank Herrmannsdörfer and Dr. Hongwei Zheng who helped me brainSTORMing mathematical problems, and implementing the solutions into the code.

I also want to take the opportunity to thank Prof. Dr. Hilmar Bading for the time he took discussing the project at the annual TAC meetings.

Many thanks also go to all the colleagues in the Kuner lab for creating such a great working atmosphere. Here, I could not only find very helpful colleagues, but I also found very good friends during these years. Especially, I would like to thank Denise ‘Dr. D’ Harrach & Sabrina ‘Dr. Z’ Schröder, Dr. Christoph Körber and Janine Reinert for many funny hours, beers, and bad jokes.

I am most thankful to my beloved partner Mira E. Sevov, who I met in Heidelberg and who made my life so much better. She has always tried to be supportive of my scientist lifestyle, despite the many crazy weeks I had to spend in the 2P basement.

Throughout my whole life my family has always supported me unconditionally to achieve all my goals: My father who never questioned my choices, and my beloved mother, who has always been there for me. Also, my grandparents Feride and Hasan who also raised me. And of course, Oğulcan and Koray, my amazing brothers:

Sonsuz teşekkürler

Table of Contents

Abbreviations

µL	Microliter
µM	Micromolar
2P	Two-Photon
AU	Arbitrary Units
FCS	Fetal Calf Serum
GFP	Green Fluorescent Protein
h	Hour
kb	Kilobasepairs
kDa	Kilo Dalton
min	Minute
MIP	Maximum Intensity Projection
mM	Millimolar
ms	Millisecond
NA	Numerical Aperture
ng	Nanogram
nm	Nanometer
nM	Nanomolar
PBS	Phosphate Buffered Saline
PFA	Paraformaldehyde
PMT	Photomultiplier Tube
ROI	Region of Interest
s	Second
UV	Ultra Violet
WT	Wildtype
µm	Micrometer

1 Introduction

The mammalian brain is the most complex organ found in nature. It consists of about 100 billion cells that are under constant communication with each other by using perhaps 100 trillion synapses in total. Each and every neuron therefore has on average of 1000 synapses to connect into this complex network called brain. However, this number greatly depends on the subtype of neuron which determines its specific role within this system and gives rise to fundamental questions in neuroscience. Not only is the number of synapses formed between two neurons highly variable, but also the strength and reliability of their connection is very plastic. In 1949 Donald Hebb postulated in his "cell assembly theory" that "Cells that fire together, wire together" (Hebb, 1949). But of course, this famous postulate does not address just how the wiring and firing together maintain a stable level of activities across time and space.

In general it is considered an essential feature of brain function that the neuronal network activities are regulated. As the brain needs to adjust its activities it also needs to maintain a proper balance. To achieve this flexibility and adaptiveness to ever changing ambient inputs the brain must have developed delicate homeostatic mechanisms during the course of evolution. Balancing neuronal activity must occur at different levels ranging from acute changes at synaptic level, single cells, or small groups of cells, to large neuronal ensembles, and finally also between interconnected brain regions.

A lot of work has been done describing patterns in neuronal network activities at various developmental stages, regions, during specific tasks, or different behavioral paradigms etc. One of the main findings from these studies was for example, that a key feature of cortical function is the transmission and transformation of neuronal activity by the cortical circuitry itself (Egorov and Draguhn, 2013).

Researchers have found activity patterns in neocortical neurons *in vivo* as well as *in vitro* that are reproducibly repeated very precisely. Amazingly, there can be minutes in between such activity patterns and they nevertheless reproduce accurately. This phenomenon in interconnected cortical regions was described as a "synfire chain" (Ikegaya et al., 2004). Similar findings could also be observed in living birds. The birds showed specific patterned neuronal activities during awake singing. Then, researchers played them their own song while they were asleep. Astonishingly, the same neuronal patterns could be evoked as if the birds were singing (Dave and Margoliash, 2000). Other forms of cortical activity can be found during sleep. Scientists can measure numerous forms of

activity waves that spread through brain regions at different frequencies during sleep. By measuring these waveforms it is possible to assess the state of sleep of single individuals (Dumermuth et al., 1972). Different stages of sleep in general can be characterized as a state of immense network synchronicity of the whole brain with specific bands of waveforms. Another type of synchronization occurs early in the developmental stages in the brain and in many other neuronal tissues such as the retina or the spinal cord. This synchronized activity is supposed to have an important role in calibrating the whole circuitry to a balanced level (Mohns and Blumberg, 2008). Once established, this balanced homeostatic level is likely to be maintained throughout the whole lifespan of the organism. Therefore, these developmental network activities are crucial and essential for fine-tuning of local circuits, sensory map formation, path finding for motor neurons, and synaptic maturation, to name a few.

1.1 Homeostatic Mechanisms

In the central nervous systems (CNS) the developing network activities are a reflection of the developing network and the maturation of the synaptic connections between the neurons. This wide variety of connections that are formed at this stage will determine the strength of the network and its efficacy to propagate information. The most important physical connections between cells are of course synaptic connections, but there are also other connections such as gap junctions, and the extracellular glutamate concentration plays a role as well.

Already at very early stages during development, networks exhibit remarkable robustness against perturbations, including moderate pharmacological and genetic impairment or severe brain injuries. Therefore, homeostatic mechanisms must exist that efficiently adjust for changes in network activities. Research showed that neuronal ensembles have “target activity levels” (Turrigiano and Nelson, 2004), which were manifested through genetic and morphological means (Figure 1).

One of the key homeostatic mechanisms besides metabolic and morphological changes is based on synaptic plasticity. Of course, synaptic plasticity also depends on activity levels between neurons including the interplay between excitatory and inhibitory neurons and the surrounding network. The interaction of all these mechanisms that lead to homeostasis is far from being understood and a lot more research needs to be done in this important field of brain research.

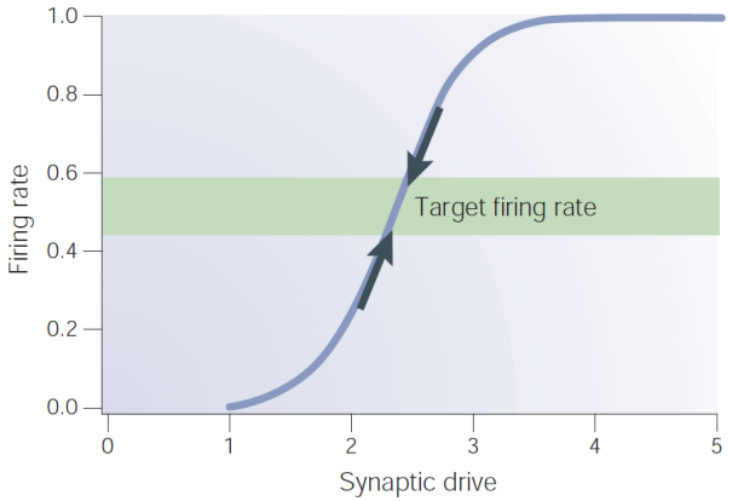

Figure 1. The graph shows the relation of synaptic drive (transmission efficiency) and firing rate of a single neuron. The scheme illustrates the idea that there is a target firing rate that the respective cell is calibrated by homeostatic changes. For example if the synaptic drive is increased by higher input of excitatory synapses and the firing rate rises above the calibrated target level, homeostatic mechanisms (arrows) will be initiated to push back down the curve towards the target area, and vice versa. [From (Turrigiano and Nelson, 2004)]

A lot of studies have been conducted in the past that concentrated on global mechanisms of homeostasis in the brain. One of the early and more vigorous experiments was aimed at identifying the origins of spontaneous activity. Entire circuits were surgically isolated in search for a "core region" of network synchronizators for the whole brain and found that GABAergic (GABA, γ-aminobutyric acid) and glutamatergic synaptic connections must be involved in the synchronization mechanism (Khazipov et al., 1997). To investigate brain wide oscillations, scientists blocked excitatory receptors in the whole brain pharmacologically. Thus, they could show that extracellular glutamate levels are essential for these oscillations (Blankenship et al., 2009). Knockout mice were generated that lack gap junction proteins in another study to examine signal transduction in their absence. The researches could conclude that the lack of gap junctions leads to a reduced electrical coupling among motor neurons (Personius et al., 2007). Several other research publications exist showing the preponderance of such approaches.

The first experiments with cultured neurons to look at their spontaneous activity and oscillation-like behavior showed that neurons would also maintain their set-point firing rate *in vitro*. For example, researchers found that inhibiting neuronal activity for an extended period *in vitro*, led to hyperactivity after removal of the inhibition (Figure 2). That was the first demonstration and indication that homeostatic mechanisms must be present also in such simple cultured neuronal networks (Ramakers et al., 1990).

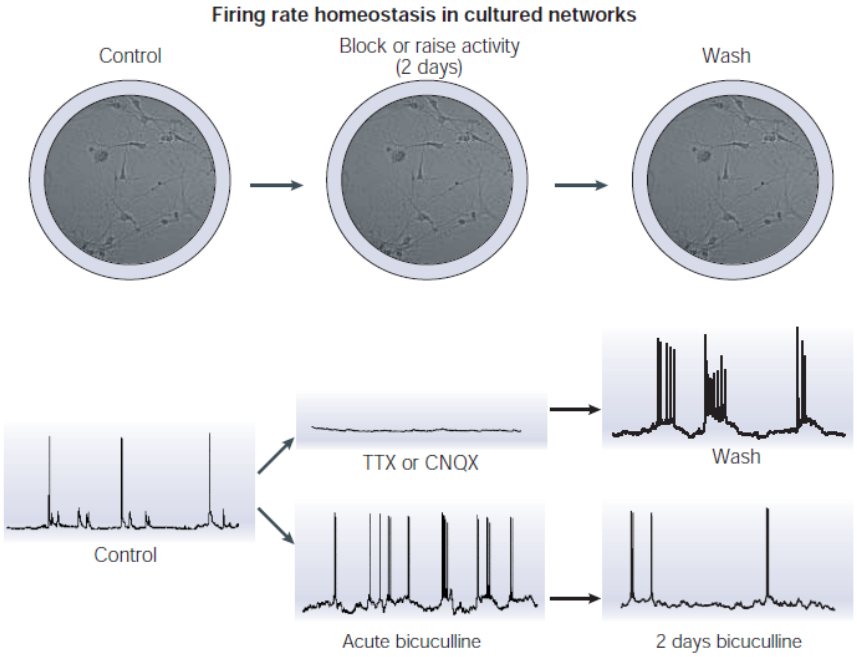

Figure 2. Evidence for firing rate homeostasis in cultured networks. Cultured cortical neurons develop spontaneous activity after a few days *in vitro*. This activity can be manipulated pharmacologically by TTX (Tetrodotoxin) a sodium channel blocker or CNQX (6-cyano-7-nitroquinoxaline-2,3-dione) a competitive AMPA receptor antagonist (both silencing) or bicuculline, a competitive antagonist of $GABA_A$ receptors (hyperactivating), treatment. Following withdrawal of these chemicals after 2 days it is apparent that homeostatic mechanisms have adjusted cellular and synaptic properties to compensate for the changes in neuronal activity levels within the networks. [From (Turrigiano and Nelson, 2004)]

However, only very few studies exist that focused on homeostatic effects after manipulating single neurons or just a subset of the neuronal population. One such study was conducted *in vitro* in dissociated neuronal cultures that were transfected with the inwardly-rectifying potassium channel Kir2.1 to genetically decrease neuronal activity (Burrone et al., 2002). The authors showed that the overexpression of the potassium channel protein Kir2.1 hyperpolarizes the respective neurons by lowering the resting membrane potential. Consequently, the excitability of this neuron was decreased. These genetically modified neurons were less electrically active than their untransfected neighboring neurons. To compensate for their decreased activity, the neurons homeostatically increased their number of synapses only if transfection occurred prior to synapse formation, which could be shown by presynaptic FM4-64 labeling.

The researchers observed changes in miniature excitatory postsynaptic currents (mEPSC) demonstrating that synaptic plasticity occurred after the genetic modification of the single cells, which they concluded to be the major parameter to direct homeostatic network activity mechanisms. These results point out that when the activity of cortical neurons is inhibited, some properties of the ensemble are altered to enhance excitability.

So the modification of single units in a wide neuronal network proved to be a very useful approach to study homeostatic effects rather than a global and unspecific modification paradigm. Nevertheless, more experiments in this direction need to be done to get a better understanding of the basic principles of neuronal networks and their homeostatic mechanisms.

A wide variety of homeostatic mechanisms is thought to play a role in neuronal activity adjustments. “Synaptic scaling”, for example is one form of plasticity. It was found that the distribution and amplitude of miniature EPSCs (mEPSC) can be scaled up or down. mEPSCs arise from spontaneous release of single vesicles at pre-synaptic sites. These mEPSCs are often used to monitor changes in neuronal activity. The higher the amount of mEPSCs and their amplitude, the higher the neurons excitability will be. Of course, the probability of vesicle release is directly correlated to the number of readily docked vesicles at the pre-synapse. For instance, mEPSC frequency will change if the number of functional release sites per bouton, or the number of synaptic boutons will increase (Prange and Murphy, 1999).

Also at the postsynaptic site the amount of synaptic receptors is homeostatically adjusted. There is evidence that changes in mEPSC amplitudes are generally due to the change in postsynaptic receptor number or conductance. This was shown directly by antibodies directed against AMPARs (α-amino-3-hydroxy-5-methyl-4-isoxazolepropionic acid receptors) after temporal increase or decrease of neuronal activity (O'Brien et al., 1998). The receptor dynamics at the synapse are believed to be a complex process, where not only the expression levels can change, but also the transport, localization, and processing of the proteins must be delicately orchestrated. There are many post-synaptic proteins that play important roles in this orchestration including proteins that manage receptor recycling (Ehlers, 2003). Interestingly, the ratio of AMPAR and NMDAR (N-methyl-D-aspartate receptor) currents appears to be remarkably constant during various homeostatic adjustments. Thus, it is hypothesized that it might be necessary to keep this ratio constant so that plasticity mechanisms can retain a balanced activity while not interfering with information processing during synaptic transmission (Malinow and Malenka, 2002).

The most crucial evidence for homeostatic plasticity in the central nervous system came from assessing the vesicle recycling processes and the morphology of the synapses in hippocampal cultures. For example, the amount of docked vesicles in each active zone and the volume of the active zones themselves are increased after a few days of activity inhibition (Murthy et al., 2001). Also, the number of the recycling vesicle pool seems to be increased. As the size of the synapses enlarges following activity inhibition, their sensitivity is increased by the extension of the post-

synaptic density and accretion of more synaptic receptor proteins. Still, the increase in synaptic volume cannot fully explain the increase in receptor accretion because of the large divergence between synapse growth and the chronologically preceding magnitude of change in mEPSC levels (Turrigiano et al., 1998). Especially during short-term plasticity, it is believed that the receptor accumulation speed in the synapse increases immediately following a stimulus. Then a slower process of expanding of the synapse volume occurs to possibly attract more receptor proteins (Turrigiano and Nelson, 2004).

Induction mechanisms for homeostatic plasticity are also not yet fully understood. It remains a mystery how the neuronal network monitors and adjusts its steady state activity levels. One possible explanation is that the average depolarization is a consequence of the average intracellular calcium levels. It might be the case that calcium plays a central role for plasticity by calcium-dependent kinases that could be involved anywhere between transcriptional as well as post-translational levels (Thiagarajan et al., 2002).

For complex cortical networks, the alteration of only excitatory synaptic strengths would probably be insufficient. So in addition to a fine-tuned system of feedback connections between and within cortical layers, there also is a balancing system of networks of inhibitory neurons.

Already minor aberrations in the balanced state between excitation and inhibition in such networks can possibly lead to hyper excitability (Chagnac-Amitai and Connors, 1989), interrupt sensory responses in the primary visual cortex (Nelson, 1991), or change experience-dependent plasticity (Hensch et al., 1998). All these findings indicate that a precise machinery must be in place that keeps the whole system in balance. For instance, this finely tuned balance is preserved by highly dynamic excitatory and inhibitory feedback onto pyramidal neurons (Kilman et al., 2002).

Summarizing research in the field of synaptic plasticity results in the acknowledgment of at least two apparently opposing mechanisms: Hebbian synaptic plasticity and homeostatic synaptic plasticity. The Hebbian plasticity can be described as establishing strong connections and favoring them. Consequently, high neuronal activity will lead to strong connections and low activity to weaker connections. On the other hand homeostatic plasticity is counteracting this process by stabilizing existing connections or counteracting changes in activity. Thus, higher activity would lead to weaker connections and lower activity to stronger connections (Fauth and Tetzlaff, 2016). Nevertheless, how Hebbian and homeostatic plasticity co-exist is not fully understood.

The study by Burrone (Burrone et al., 2002) and co-workers shows that there are cell-autonomous effects of homeostatic plasticity. Still, it is not clear if all homeostatic plasticity effects are cell-

autonomously driven. Also the study just addresses the question of adjustments that happened after the homeostatic mechanisms had taken place, rather than the whole process itself. Yet, the biggest weaknesses of most of the studies are definitely that they were conducted in cultured neuronal cells, which can only be considered a very simplified model of neuronal networks.

There are two critical aspects when studying neuronal networks. First, the time course of homeostatic mechanisms and second, the scale at which the adjustments occur ranging from local to global.

Currently there is still very little knowledge about the specific time course of homeostatic network adjustments. Thus, it is important to study the time course of the underlying molecular and cellular mechanisms. It is also not clear how these mechanisms are orchestrated, if there are short- and long-term mechanisms during adjustments or if it is a continuous process. More importantly, there is little understanding of local versus global effects, as neurons that are physically nearby might show different or greater adjustments than distant ones, for instance.

1.2 Current state

In the recent years a wide variety of tools revolutionized the neuroscience field in respect to monitoring and modifying brain activity in living animals from fruit flies to mammals. Molecular biologists were able to find and successfully optimize or even combine proteins and indicators according to their purposes.

Especially the success of genetically encoded systems to visualize and manipulate neurons proved to be an extraordinary boost for the scientific community. Quickly the field embraced the new genetically encoded proteins. But some chemical tools such as calcium indicators continue to be used in a different experimental setting (Grienberger and Konnerth, 2012). The advantages were significant: No more need for injection of chemicals into the desired brain region. Instead, the proteins could just be expressed by the desired cells using various transgene technologies. In fact, transgene expression can be limited to sub-populations of a certain cell-type compared to an injection that would reach all the cells in the respective area.

A quantum leap in neuroscience research was the possibility to detect neuronal activity by visualizing calcium transients. Tremendous efforts to not only visualize neuronal activity but also to manipulate activity with light led to the introduction of the powerful optogenetic tools. These light sensitive ion channels or pumps are now heavily used to hyper- or hypopolarize neuronal membranes.

Along with the development of these biological tools, advanced microscopy techniques became available to more scientists. Especially the introduction of two-photon microscopy would allow for the visualization of structures deep (<1 mm) within living tissue which was of great importance.

Thus, the toolbox for the neuroscience community was steadily growing to answer many questions that could previously not be addressed.

1.3 Visualizing neuronal activity in the intact rodent brain

Fluorescent imaging in the living brain requires the use of two-photon microscopy techniques (Denk et al., 1990; Svoboda and Yasuda, 2006). The two-photon microscopy technique considerably increases the detection of photons, and therefore allows imaging in highly scattering brain tissue. For two-photon excitation to take place, two photons of half the energy need to be absorbed simultaneously to allow the shift of an electron to an excited state (Figure 3A). To facilitate the simultaneous absorption of two photons a focused laser beam is used. Within this focused laser beam the highest intensity is right in the center of the beam and decreases exponentially with distance from the center in all dimensions. Therefore, fluorophores are nearly exclusively excited in a small volume in the center of the laser beam (Figure 3B). Under optimal conditions and with a high numerical aperture (NA) objective a focused laser beam can excite fluorophores almost exclusively in a volume of about 0.1 μm^3 (Zipfel et al., 2003). The precise localization of the excitation results in a resolution similar to confocal microscopy, but without the necessity of pinholes in the detection path. Consequently, an image is generated by scanning the laser over the specimen, i.e. a mouse cortex. The tissue-dependent scattering of excitation light reduces the amount of photons that reach the diffraction-limited focus (Figure 3B). Also, scattering distorts the trajectories of emitted photons after the excitation (Figure 3C). Nevertheless, as excitation only occurs in the focal volume, all emitted fluorescence photons can be collected by the microscope as relevant signal (Figure 3B). A schematic working principle of a two-photon microscopy setup is depicted in Figure 3D. Despite tissue scattering, this technique can be used with high fidelity down to depths of brain tissue of 700 µm from the surface. Combining this microscopy technique with appropriate fluorophores, scientists are able to visualize processes in the living brain tissue of rodents or whole small organisms.

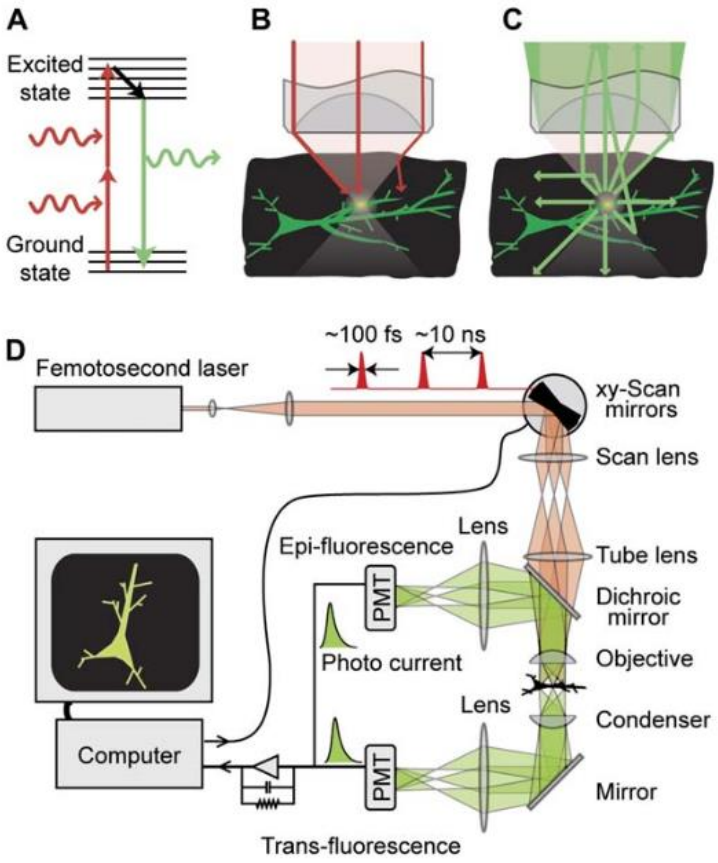

Figure 3. (A) Basic Jablonski diagram of a two-photon excitation course. (B) Excitation in a scattering tissue (black). The two-photon excitation beam (red) is focused to an exact spot of the sample through an objective and excites green fluorescence. The theoretical trajectory of two photons and one scattered photon are shown (red lines). With increasing depth more and more photons are lost due to scattering. (C) Fluorescence photons are emitted from the excited volume (green lines). All scattered fluorescence photons are collected and contribute to the signal. (D) Schematic of a two-photon microscope with epifluorescence and trans-fluorescence detection. [From (Svoboda and Yasuda, 2006)]

To visualize neuronal activity with fluorophore sensors scientists now have an extensive range of tools available to them. The most commonly used indicators detect calcium levels within neurons as a proxy for neuronal activity. Calcium plays an important role in neurons as a second messenger for neurotransmitter responses as well as driver role for neuronal membrane depolarizations. As neuronal depolarization at the membranes go together with a high calcium influx, visualizing the changes in calcium concentrations allow for estimating neuronal activity. Originally, calcium was detected with chemical indicators but more recently genetically encoded calcium indicators (GECI) have emerged.

Calcium imaging is based on calcium binding to the indicator which induces a change in its fluorescence that enables to monitor the activity of neurons and even neuronal microcompartments.

Consequently, calcium imaging became the most established method for the optical imaging of neural activity. It allows studying neural dynamics like orchestrated network activites, dendritic

processing, synaptic functionality, also with chronic *in vivo* and cultured preparations, and is appropriate for long-term imaging (Ziv et al., 2013). Depending on the cell type, cytoplasmic calcium is preserved at 50–100 nM at rest, but activity induces its influx via multiple routes (Grienberger and Konnerth, 2012). For example, excitatory neurotransmitter receptors cause an influx of calcium. Also NMDA-type glutamate receptors enable the rise of calcium in spines up to concentrations of ~1 µM (Higley and Sabatini, 2012). Most importantly, voltage-gated calcium channels permit calcium entry through neuronal membranes during action potential (AP) propagation. In cortical neurons this delicately organized calcium influx leads to an increase of ~150 nM within 10 ms and is persisting for ~100-140 ms (Koester and Sakmann, 2000). Advantages and limitations of calcium imaging are dependent on the degree and the kinetics of calcium entry and removal from the cell after the AP. For instance, a single AP can last for 3–5 ms before the calcium transients have even reached their peak. Fortunately, the much slower kinetics of the resulting calcium transients can be detected easily, as they persist 10-times longer than the APs themselves. Nevertheless, major limitations of GECI imaging are the speed of the on-off kinetics of the indicators after calcium was detected. For instance, the half-decay time for the most frequently used GECI GCamP6f is a rather slow ~140 ms (Chen et al., 2013a).

GCaMP6f is based on a circularly permuted green fluorescent protein (cpGFP), which was combined with the calcium-binding protein calmodulin (CaM), and the CaM-interacting M13 peptide. The CaM–M13 structure is in close proximity to the fluorophore inside the cpGFP β-barrel structure. When calcium is bound, dramatic conformational changes in the CaM–M13 structure cause increased brightness of the fluorophore. The changes in fluorescence levels can then be used to determine neuronal activity. Subsequent estimation of spike rates from imaging GECI data is also difficult but feasible with available algorithms (Deneux et al., 2016).

1.4 Manipulating neuronal activity

One obvious way to investigate networks is to perturb them and then to analyze the consequences of the perturbation. While the overall network activity remains constant over time, the firing patterns of individual cells or small clusters can vary substantially from one time point to the next. Thus, a tool is needed that offers high spatial and temporal resolution for interference with network activities.

1.4.1 The optogenetic approach

Optical approaches offer such resolution (Tischer and Weiner, 2014), which is why many researchers use these optogenetic tools to study acute, plasticity-related mechanisms of network homeostasis.

Dissecting and understanding the intricate neuronal connections is a delicate task. Recently, the neuroscience field has embraced optogenetic tools to regulate neuronal activity with light irradiation. The advantage, of course, is that light allows high-resolution manipulation of complex biological samples such as cells, organs, or whole organisms. By this light can be used to manipulate the spatiotemporal dynamics of signaling cascades in living cells and organisms. A breakthrough was when optogenetics were introduced to the neuroscience community — genetically encoded light-sensitive proteins that activate ion flow in response to light irradiation. The first successful applications used light-gated ion channels to manipulate the excitability of neuronal cells (Boyden et al., 2005). Quickly, more efficient versions of those channels emerged that would also allow to hyperpolarize or depolarize neuronal membrane potentials. For example, these new tools were used to identify pacemaker cells in the zebra fishes heart (Arrenberg et al., 2010), or their temporal precision and reversibility was used to reveal the importance of timing in neuronal activity for behavioral conditioning (Tsai et al., 2009).

The introduction of optogenetic tools to the neuroscience community led to totally new approaches that were impossible before. With these tools it was possible to manipulate neuronal activity with the use of light and unparalleled temporal resolution in the time scale of milliseconds. Instead of using electrodes to target a limited amount of cells, it was now possible to target any cell in the focal area of the microscope. The major limitation is that optogenetic tools are powerful for controlling the membrane potential of cells, but nothing else inside the cells can be manipulated with light. Also, applying a light source to evoke a response in the target cells can be a big problem if the target cells are for example thalamic or hippocampal neurons. In such cases the light is usually delivered by implanting optical fibers into the respective brain regions and the effects measured at cortical brain regions or in behavioral paradigms (Liu et al., 2012). The experimental procedure is mostly limited to acute effects of the manipulations due to problems with long-term illumination of the respective brain regions. Of course, having a constant source of light attached to the animals and its side effects limit the experimental procedures. Also, a general concern in the field is that delivery of light over a certain period of time might lead to cytotoxic effects because of non-physiological overstimulation, phototoxicity, or bleaching (Madisen et al., 2010).

1.4.2 The chemogenetic DREADD approach

The powerful optogenetic tools allow fast manipulation of neuronal firing by changing the membrane conductance. Chemogenetic methods on the other hand permit also long-term manipulations of neuronal activity over days to weeks and possibly months. In the recent years, one powerful chemogenetic tool emerged which was abbreviated DREADD (Designer Receptor Exclusively Activated by Designer Drugs). The DREADD system allows for chemical control of G protein-coupled signaling *in vivo* (Roth, 2016). These systems utilize G protein-coupled receptors (GPCR) that have been engineered to be exclusively responsive to synthetic small molecules, such as Clozapine N-oxide (CNO), and not to any of their endogenous ligands. CNO was chosen, because it was believed that it had the ability to penetrate the central nervous system, had favorable pharmacokinetics in mouse studies and humans (Jann et al., 1994), and most importantly it was thought to be pharmacologically inactive (Armbruster et al., 2007).

Similar to the optogenetic tools, DREADDs can also be targeted to specific cell types by means of transgene delivery vectors or cell-type specific promoters. The DREADD technology is now widely used by neuroscientists. Nowadays, the commonly used variants are hM4Di for silencing neurons by G protein-coupled inwardly-rectifying potassium channels. And on the other hand hM3Dq for hyperactivating neurons by Gαq-mediated pathways. This Gαq-mediated pathway leads to a slow depolarization and burst firing of neurons. The DREADD technology has been used to control neural activity and behavior ranging from studies with flies (Becnel et al., 2013), mice (Alexander et al., 2009), to research with nonhuman primates (Eldridge et al., 2016). However, in a study it could be shown that ~10 % of the CNO is converted to Clozapine (Jann et al., 1994) a drug used for the medication of atypical antipsychotic disorder. This very potent drug possibly has side effects that distort the results of the studies.

In fact, in a recent study it was shown that only Clozapine, and not the alleged CNO, is activating the receptors in *in vivo* experiments (Gomez et al., 2017). According to this study, CNO is not even able to cross the blood brain barrier. Therefore, only converted Clozapine is proposed to be the main source of activation of the DREADDs in *in vivo* studies. For sure, this will raise questions about many previous studies using DREADDs. The advantages of DREADDs compared to optogenetic approaches are mainly the long retention of CNO which is present in the blood stream of animals for hours and can be applied for days (Krashes et al., 2011). Additionally, it does not require specialized equipment to activate the DREADDs, compared to the light source required for the optogenetic tools. The disadvantage is the lack of precise temporal control, which is of course possible with light controlled systems (Sternson and Roth, 2014).

1.5 Targeting Parvalbumin interneurons

All neuronal networks in the mammalian brain contain glutamatergic principal neurons and GABAergic (GABA, γ-aminobutyric acid) interneurons. These interneurons represent a minority of the total neuron number (10-20 %), but are vital for balanced brain function as they regulate the overall activity of principal neurons (Freund and Buzsaki, 1996). Impaired interneuron activity can lead to the damaging of higher brain functions by unrestrained hyperactivity and seizures (Westbrook, 2013).

Until now, there are 21 subtypes of interneurons known in the hippocampus, whereas this number is thought to be higher in the neocortex (DeFelipe et al., 2013). Interneurons in general are characterized by three sets of criteria. First, morphological parameters such as the spread of the dendrites, spine numbers, and target site of the axon. Also, most inhibitory interneurons have aspiny dendrites; for example, interneurons in the Neocortex are often referred to as “local circuit neurons” because of the restricted reach of their arborizations of dendrites and axons (Hu et al., 2014); Second, by their expression profile of markers like somatostatin, cholecystokinin, vasoactive intestinal peptide, and neuropeptide-Y or calcium binding proteins such as parvalbumin, calretinin, and calbindin. Third, the characterization according to their action potential phentoype (Rudy and McBain, 2001).

As a model cell type for inhibitory neurons in general, the well characterized fast-spiking Parvalbumin-positive interneurons (PV+ interneurons) with spiking frequencies of 10-150 Hz have been chosen by many researchers so far for studies (Buetfering et al., 2014). These cells play an important role in feedback and feedforward inhibition and also in network oscillations. Still it is not known how these PV+ interneurons contribute to the complex homeostasis of maintaining proper network functions. PV cells represent only about 2.6 % of the total neuronal population but have some advantages that makes them a perfect target to investigate their effects on neuronal networks (Bezaire and Soltesz, 2013). Morphological analysis of PV cells have shown an axonal and dendritic length and reach of about 760 ± 130 µm on average (Halasy et al., 1996).

A great advantage of PV+ interneurons is their specific (>90 %) expression of the parvalbumin promoter. Using this promoter scientists created a variety of transgenic animals that would express a variety of genes in PV+ cells such as the Cre recombinase (Hippenmeyer et al., 2005). In combination with this transgenic mouse line, Cre-responsive constructs and molecular tools can now be targeted specifically to PV cells. In general, using these transgenic mouse lines expressing Cre recombinase in a sub-population of cells, scientists can cross mouse lines of interest or inject viral vectors with “floxed” transgenes that would just be recombined and expressed in Cre expressing cells. Therefore, conditional transgene expression is limited to Cre expressing cells (Figure 4).

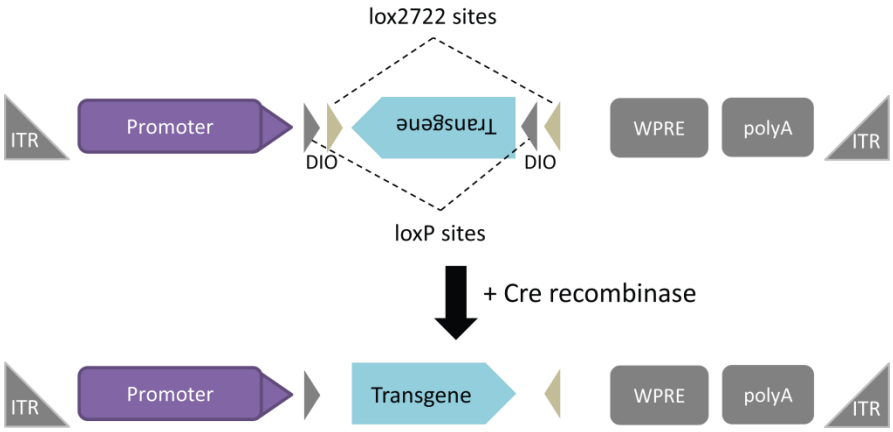

Figure 4. Principle of expressing transgenes only in Cre positive cells. The top panel shows the original, inactive construct. The transgene is not expressed in this state as it is flipped, i.e. in the wrong orientation 3'->5' and flanked by double-floxed inverse ORF (DIO) lox sites. After addition of the Cre recombinase, these lox sites will be flipped so that the transgene is in the 5'->3' orientation for proper expression.

1.6 The inducible Tetracycline system TetOn

The conditional gene expression method used in this study is based on the inducible Tetracycline system. Under control of a general or cell-type specific promoter, the TetOn system is often used for conditional transgene expression. It allows for relatively stringent, reversible (on ↔ off), quantitative, temporal and spatial regulation of expression *in vitro* as well as *in vivo*. In general, Tet-based systems require two components: First, the tetracycline dependent transactivator "reverse Tet-controlled transcriptional activator" rtTA as the effector. Second, a Tet responsive element (TRE) combined with a CMV minimal promoter cassette for transgene induction after binding of rtTA to Tetracycline or its more potent analogue Doxycycline (Gossen et al., 1995). Figure 5 depicts the genetic principle of the TetOn system.

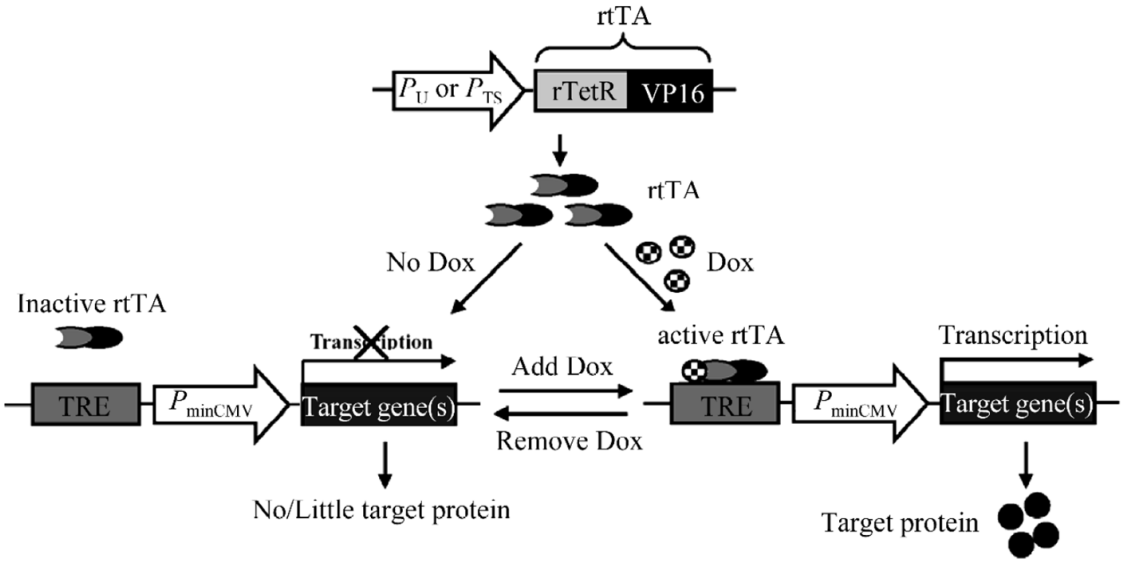

Figure 5. Schematic representation of the TetOn systems principle. The TetOn system can be utilized to conditionally activate transgene expression *in vitro* and *in vivo*. The system requires two independent constructs. One from which the regulatory protein rtTA is (constitutively) produced under the control of an ubiquitous promoter (P_U) or tissue- or cell type-specific promoter (P_{TS}). Two, a responsive construct, through which the expression of cDNA(s) of interest is under the regulation of the Tet responsive element (TRE) alongside a CMV minimal promoter. Addition of Doxycycline to the TetOn system results in transcriptional induction of the desired transgene of interest. In the absence of Doxycycline, rtTA cannot bind its target or dissociates from TRE, and therefore terminates the transcription of downstream transgenes. Administration of Doxycycline subsequently allows modulating the expression of any given transgene in a quantitative, time-controlled and ubiquitous or tissue/cell-type specific manner. [From (Sun et al., 2007)]

For experiments in which a transgene is supposed to be inactive most of the time and only expressed transiently, the TetOn system is very useful (Dogbevia et al., 2015). Unfortunately, leaky expression is also an issue with all Tet-based systems. Leakiness usually derives from the intrinsic properties of Tet systems with undesired binding of rtTA in the absence of Doxycycline and the promoter leakiness. These two origins of leakiness impair the desired tight control of transgene expression (Lewandoski, 2001). “Leaky” expression occurs because rtTA retains some affinity for TRE sequences even in the absence of Doxycycline. Also, there is residual activity of the CMV minimal promoter without active rtTA (Figure 5). This was shown by detectable expression levels of transgene activation and phenotypes of animals or cells which were not receiving Doxycycline (Lewandoski, 2001).

Only for few applications of this system the leakiness levels are acceptable. For instance, the induced expression of genetically encoded sensors or proteins which only have an impact at high concentrations, and low amounts of basal expression can be accepted. In many cases, however, the detectable and undetectable level of undesired transgenic expression unfortunately limits the use of Tet-based systems for precisely evaluating the effects of the gene product.

As these problems were known and have been a major disadvantage of the technology for dose-sensitive transgenes and experiments, different approaches have been tried to solve this problem or at least reduce the leakiness. Leakiness is possibly dependent on the binding of the effector protein rtTA to the Ptet promoter in the absence of Doxycycline and/or the intrinsic activity of the promoter itself. The synthetic Ptet promoter consists of the TetO7 region, where the effector proteins can bind, and a CMV minimal promoter. The TetO7 was constructed by monomer ligation of the bacterial Tet operator heptamers. The entirety of the TetO sequences and a minimal promoter is called the Tetracycline response element (TRE). In theory, all of these elements can be optimized to improve the TetOn system. However, most research has focused on the effector proteins rtTA and the complement transrepressor tTR that acts in opposite manner as a repressor in the absence of Doxycycline. Luckily, all of the following optimized mutants were available upon request from the respective researchers.

The rtTA is a protein, which is a fusion between the viral VP16 trans-acting protein to enhance transcription and a mutated bacterial tet repressor that is called “reverse tetR” (Gossen et al., 1995). The tetracycline-controlled transrepressor (tTR) on the other hand, is the fusion of the KRAB repressor domain (K) of the Kox1 protein (Deuschle et al., 1995) and the natural bacterial tet repressor tetR. To avoid dimerization of tTR and rtTA in the same cell that will reduce the number of active molecules for either activation or repression, class B and E Tet repressors had been chosen as proteins (Freundlieb et al., 1999). Previous studies had shown that dimerization between the Tet repressors of class B and E does not occur (Baron et al., 1999). Thus, the engineered transactivator and transrepressor have opposing responses to Doxycycline and can be expressed in the same cell without the undesirable tendency to dimerize. Therefore, the transrepressor binds the TRE only in the absence of Doxycycline to inhibit transcription and is released when Doxycycline is present. The transactivator on the other hand only binds the TRE to induce gene expression when Doxycycline is present. Previously, the positive effect of the co-expression of transactivator and transrepressor on reduced promoter leakiness was demonstrated in two studies, while maintaining the same rates of transgene induction (Freundlieb et al., 1999; Rossi et al., 1998).

Like mentioned above, an important issue that warrants discussion is the minimal CMV promoter. The minimal CMV promoter is necessary for Tet-dependent transgene expression to occur as it helps to recruit the transcriptional machinery. Nevertheless, this minimal promoter also induces undesired transcription (“leakiness”) to a certain amount. Of course, the activity of the minimal promoter is dependent on the respective cell type it is present in. Cell types with a high amount of expression activity or protein turn-over like HEK293T or HeLa cells will show higher amounts of undesired leakiness than cells with a very low transcriptional over-all activity such as primary cells. HEK293 cells

transfected with the plasmids used for rAAV production for example always showed high amounts of leakiness. In this case, the leakiness was not a limiting factor for the viral production but rather an indicator of the successful co-transfection of one of the three necessary plasmids for virus production.

1.7 Aims of this study

The aim of this study is to develop an optimized inducible transgene expression system for *in vivo* use in neuronal tissue. With this method, the neuronal activity levels of neuronal subpopulations should be manipulated transgenically and the effect on the surrounding neuronal network analyzed. The gene expression method used in this study is based on the inducible Tetracycline (TetOn) system and was combined with *in vivo* calcium and morphology imaging (Figure 6). For the challenging *in vivo* work, I further optimized the TetOn system to minimize basal expression in the absence of Doxycycline.

Of course, being able to change neuronal activity levels by genetic manipulation offers many more possibilities from a cellular perspective, such as induction of channel and receptor proteins, calcium binding proteins, proteins relevant for plasticity, etc. Such refined genetic manipulation is not possible with the popular optogenetic approach or with the available DREADD tools. Therefore, it was important to establish a tool that allows targeted genetic manipulation of neurons with high spatial and temporal resolution.

The approach I developed offers the exceptional possibility to analyze the manipulated neurons *before, during,* and *after* transgene expression. With this combination of tools, one can now begin to characterize basic principles of cellular and network homeostasis. The main goal of my dissertation is therefore to establish an *in vivo* paradigm in rodents. Using two-photon microscopy, neuronal activity will be characterized before, during, and after expression of Kir2.1, an inwardly rectifying potassium channel that cell-autonomously hyperpolarizes cells and therefore silences their firing properties. For manipulating only a subset of cells and analyzing its effects on the surrounding network we chose to target two separate populations of neurons: a random group of neurons defined by expression of Cre recombinase via the viral synapsin promoter and a group of inhibitory interneurons characterized by the expression of parvalbumin. A schematic of the working principle of this approach is visualized in Figure 5.

Consequently, an analysis pipeline has to be established that allows following the activity of single neurons over the course of the experiments. The extraction of calcium signals, their processing for estimating the actual neuronal activity also has to be implemented into the analysis pipeline.

At the end, a versatile tool should be established, which can also be used for many other applications that would require tightly controlled, high spatio-temporal transgene expression. In particular the combination with the Cre recombinase system will provide cell-type specific transgene expression and will also allow prior fluorescent marking those cells that will be manipulated by the Tet system.

My work ranges from molecular biology to a sophisticated analysis pipeline for the development and establishment of this powerful system, and I expect that this system or modules of it can be implemented into a wide range of experimental approaches.

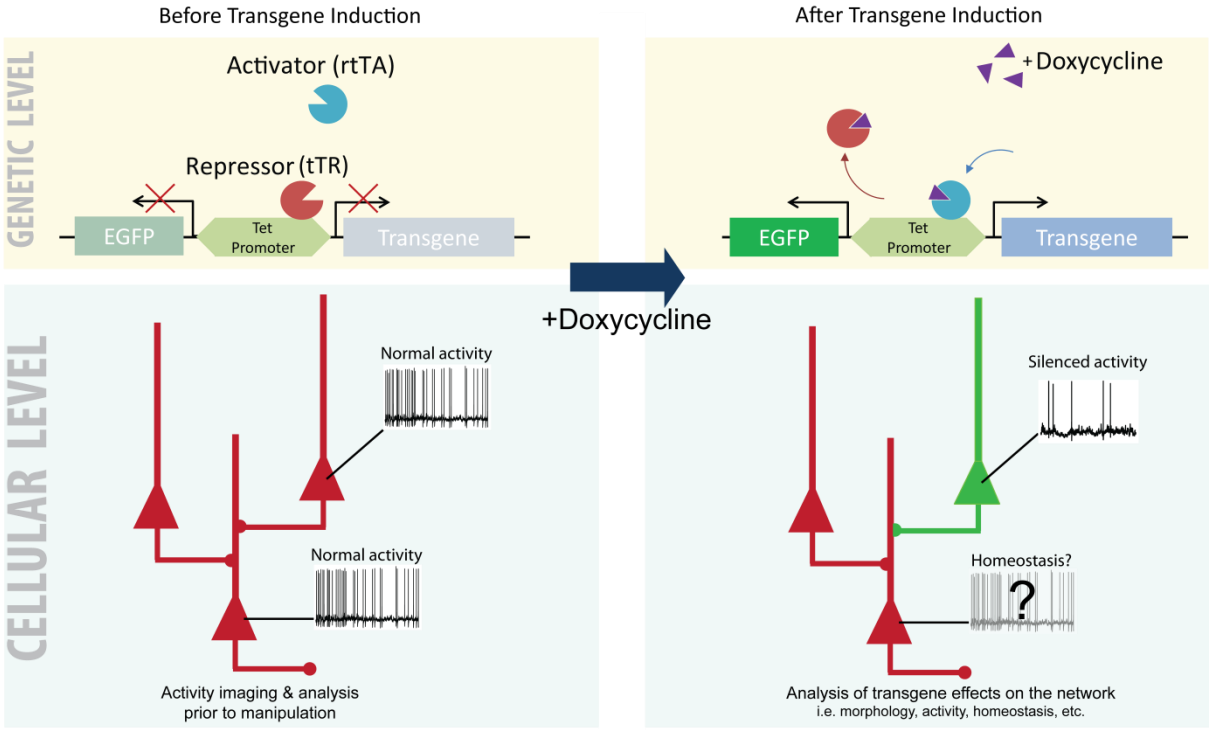

Figure 6. Schematic of the utilized gene expression method in my study based on the TetOn system. The left panel shows the inactive state of the system before transgene induction with Doxycycline. On a cellular level, one is able to observe neuronal activities and compare them to activities after induction. The right panel shows the genetic state after administration of Doxycycline, which induces the expression of the transgenes. On a cellular level one can now correlate phonotypic changes with the expression of the transgene. Here, this transgene was the Kir2.1 protein, which silences neuronal activity.

2 Material and Methods

2.1 Molecular Biology

2.1.1 Plasmid Cloning

All Plasmids described in the following section except for the DriverTET Plasmid (Table 1) were cloned with the pAM plasmid backbone and used for the generation of recombinant adeno-associated viruses (rAAV, Chapter 2.1.7). The DriverTET (DTET) plasmid was derived from a plasmid received from Rolf Sprengel (Chen et al., 2013b) and modified to fit our experimental needs. The Tetracycline responsive elements such as the bidirectional Ptet promoter region for the ResponderTET (RTET) plasmids were also optimized. Every cloning step was verified by DNA sequencing (Seqlab, Göttingen). All plasmids were cloned by me except for the purchased ones.

Plasmid name	Fluorescent protein	Wavelength (λ_{ex}/ λ_{em}/ $2P_{ex}$)	Description
DriverTET	mKO (Kusabira Orange)	548/559/960	Encodes tetracycline dependent rtTA and tTR for controlling gene expression.
RTETbi-mVenus-Kir2.1	mVenus	515/528/960	Expression of Kir2.1 transgene and mVenus after tetracycline administration
RTETbi-mVenus-NaChBac	mVenus	515/528/960	Expression of NaChBac transgene and mVenus after tetracycline administration
pAM-RTETbi-NLSmtagBFP-DIO-Kir2.1	mtagBFP (Blue fluorescent Protein)	402/457/800	Expression of Kir2.1 transgene in Cre^+ cells and nuclear localized NLS-mtagBFP after tetracycline administration
pAM-RTETbi-NLSmtagBFP-DIO-NaChBac	mtagBFP (Blue fluorescent Protein)	402/457/800	Expression of NaChBac transgene in Cre^+ cells and nuclear localized NLS-mtagBFP after tetracycline administration
pDP1rs (rep2/cap1) *	RFP	555/584	Helper & Packaging plasmids encoding proteins for rAAV2/1 production in HEK293T cells (Plasmidfactory, Bielefeld)
pDP2rs (rep2/cap2) *	RFP	555/584	

Table 1. All plasmid vectors that were used for the generation of rAAVs. (* = purchased from company)

Inserts of the plasmids for rAAV production were flanked by 5'- and 3'-ITR regions (derived from AAV2) for efficient packaging of DNA into viral capsids up to ~5.2 kb in total size (Wu et al., 2010). The human synapsin promoter (hSyn1) sequence was used to drive constitutive, neuron specific expression. The transgene sequence was followed by a Bovine Growth Hormone Poly-Adenylation Signal (bgh polyA). For DNA constructs that were sufficiently below the total packaging limit of 5.2 kb, the mRNA stabilizing Woodchuck Hepatitis Virus Post-Transcriptional Regulatory Element (WPRE) was inserted upstream of the bgh polyA signal at 3'-end (Wang et al., 2016). For bidirectional Tet responsive plasmids, the tetO7 sequences were flanked by two minimal Cytomegalovirus Immediate-Early (minCMV-IE) promoters (Gossen and Bujard, 1992). For Cre-dependent expression, the transgene was flanked by DIO-sites (double-floxed inverse open reading frame) harboring LoxP & Lox2272 sites (Sohal et al., 2009). A schematic of the generated plasmids is shown below (Figure 7).

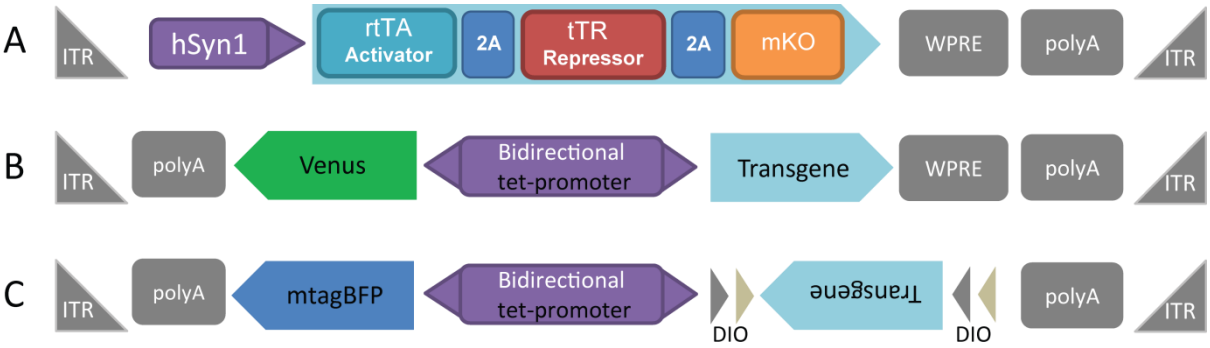

Figure 7. Scheme of plasmids for rAAV production. A) DriverTET plasmid with one open reading frame (ORF) encoding for rtTA, tTR, and mKO fluorescent protein. The 2A-peptide mediated cleavage leads to the release of 3 single proteins during translation. B) ResponderTET plasmid with a tetracycline dependent bidirectional tetO7 promoter. Induction with tetracycline leads to the expression of Venus fluorescent protein and a transgene of interest. In this study, Kir2.1 and NaChBac were used as transgenes. C) ResponderTET construct with an inducible blue fluorescent protein mtagBFP that is directed to the nucleus by a nuclear localization signal (NLS). Additionally the second transgene (with c-terminal HA-tag) is placed in a DIO cassette which will only be flipped in Cre^+ cells. Therefore the transgene will only be inducible in cells that are also Cre^+.

The generation of all the plasmid vectors described in this section was done according to the general protocols described below. If not stated differently, enzymes were purchased from New England Biolabs (Frankfurt am Main, Germany).

The design of the experimental procedures for subsequent cloning steps, sequence analysis, and annotations were performed using Clone Manager 9.3 Professional Edition (Scientific & Educational Software, Denver CO, USA).

2.1.2 DNA Preparation

E. coli carrying the plasmid vector of interest were grown over night at 37 °C in desired volumes of lysogeny broth (LB medium, for 1 L: 5 g yeast extract, 10 g trypton, 10 g NaCl) with suitable antibiotic (Ampicillin 150 µg/mL or Kanamycin 30 µg/mL) and harvested the following morning. Plasmid DNA was extracted either using the PEQGold DNA Miniprep Kit I (PEQlab, Erlangen) or Nucleobond Xtra Maxi EF Kit (Macherey-Nagel, Düren) according to manufacturer's instructions. PCR products or fragments were isolated with the Nucleospin Gel and PCR Clean-up Kit (Macherey-Nagel, Düren) either after PCR or upon cutting out the desired bands from 1 % Agarose gels (Biozym LE Agarose, Biozym, Hessisch Oldendorf). Gel electrophoresis was performed at ~120 V (Biorad PowerPac Basic, Biorad, Munich) in TAE buffer (for 20X Stock solution: 96.8 g Tris, 22.85 mL Acetic Acid, 40 mL 0.5 mol/L EDTA (pH 8.0), ad 1 L dd$H_2$0).

The concentration of purified DNA was measured spectrophotometrically with a NanoDrop 2000c machine (Thermo Scientific, Darmstadt) and the samples stored at -20 °C until further use.

2.1.3 DNA Digestion

Restriction digestion of DNA was done according to the manufacturer's instructions using the respective enzymes and their optimal reaction conditions. For plasmid vector digestions the initial DNA amount used was ~8 µg. To further increase the cloning efficiency the digested 5' and 3' ends of the DNA were dephosphorylated by adding 1 unit of CIP enzyme to the reaction and to avoid later recircularization during the ligation step. For the digestion of isolated PCR products or fragments the total eluate was used, which was ~0.5 – 1 µg. The standard reaction volume for both types was 50 µL. After 2 h of reaction time the sample was further purified as described in chapter 2.1.2, the DNA concentration measured, and used for a subsequent ligation.

2.1.4 DNA Ligation

For ligation of DNA fragments the T4 DNA Ligase was used according to the manufacturer's instructions in a 20 µL reaction volume. The molar ratio between insert and vector was 3 to 1. The molarity of DNA samples was calculated according to the following formula:

$$\mu\text{g DNA} \times \frac{\text{pmol}}{660\ \text{pg}} \times \frac{10^6\ \text{pg}}{1\ \mu\text{g}} \times \frac{1}{\text{N}} = \text{pmol DNA}$$

N denotes the number of nucleotides and 660 pg/pmol is the average molecular weight of a nucleotide pair. The ligation reaction was carried out for at least 2 h at room temperature for sticky-

end reactions or overnight at 16 °C for blunt-end ligations. The samples were stored at -20 °C or directly used for transformation of chemically competent *E. coli* XL10 gold as described in section 2.1.6.

2.1.5 DNA Assembly Cloning

In cases where suitable restriction sites were not available DNA Assembly Cloning was used. This was the case whenever additional restriction sites were also present within the sequence of interest. Alternatively, commercially synthesized DNA fragments were used directly for the assembly reaction. Synthesized DNA fragments were ordered from GeneArt Strings DNA (Thermo Scientific, Darmstadt) and ddH_2O was added to a final concentration of 30 ng/µL. The design of PCR Primers for creating overlapping regions at the flanking ends of the inserts was performed using the manufacturer's online tool (http://nebuilder.neb.com/). Vector plasmids were linearized by restriction digestion, dephosphorylated, and further purified. NEBuilder HiFi DNA Assembly Master Mix was used according to manufacturer's protocol and the product employed for subsequent transformation of *E. coli*.

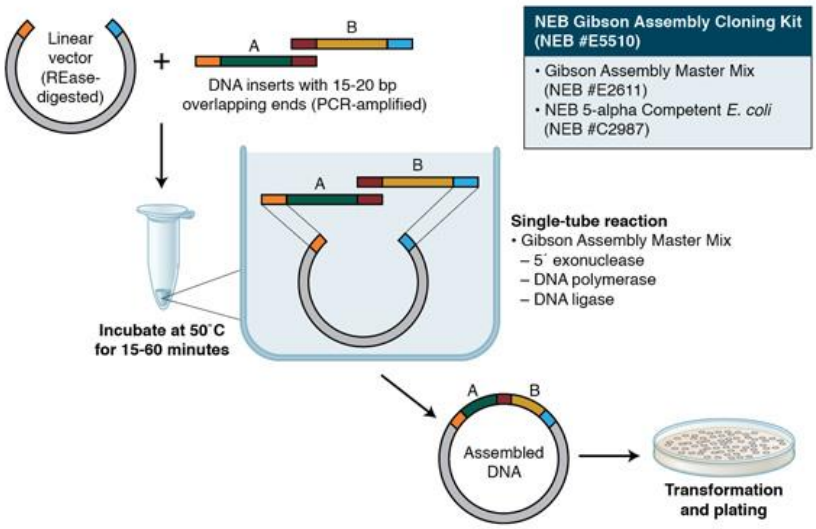

Figure 8. Schematic representation of the DNA Assembly Cloning procedure. Instead of the shown two-fragment reaction, in my research only one-fragment reactions were used. [From http://nebuilder.neb.com/]

2.1.6 *E. coli* transformation

E. coli bacteria were transformed for the amplification of plasmids. 100 µL of chemically competent *E. coli* bacteria were thawed in 1.5 mL Eppendorf tubes on ice for 10 min before the addition of 5 –

10 µL of ligation or assembly reaction to the solution. Then the cells were incubated for 30 min on ice. This was followed by a heat shock at 42 °C for 1 min. Cells were chilled for 2 min on ice again before adding of 200 µL LB medium. Subsequently the cells were incubated at 37 °C while shaking at 900 rpm on a Thermomixer comfort (Eppendorf, Hamburg) for 45 min to allow for recovery and growth. Then 150 µL of the solution were spread on LB 1.5 % Agar plates with suitable antibiotic resistance and incubated overnight at 37 °C. The next day colonies were transferred into 3 mL LB medium and incubated for 16 h at 37 °C and 160 rpm (Infors HT Multitron Pro, Bottmingen, Switzerland). The next day plasmids were isolated and a control digestion for correct insertion was performed, which was followed by DNA sequencing for confirmation.

2.1.7 Recombinant Adeno-associated virus (rAAV) Production

For rAAV production a helper-free system was used that generates capsid chimeras of AAV serotype 1 and 2 at a ratio of 1:1. On the first day $4x10^6$ HEK293T cells/cm² were cultivated in 15 cm diameter cell culture dishes (Nunclon, #168381, Thermo Scientific, Darmstadt). Routinely 10 dishes were used and cells were grown in Dulbecco's Modified Eagle Medium (PAN Biotech, #P04-03590, Aidenbach) 500 mL containing 4.5 g/L Glucose, 0.584 g/L L-Glutamine, 0.11 g/L Sodium pyruvate, 3.7 g/L $NaHCO_3$, 10 mL MEM NEAA #P08-32100 (100X), 5 mL Penicillin-Streptomycin 10.000 U/mL (Gibco, #15140122, Thermo Scientific, Darmstadt)). Transfections were performed 24 h after plating of the cells using the calcium phosphate method. DNA of the desired AAV and the two helper plasmids (pDP1rs coding for the capsid protein of AAV1 and pDP2rs coding for the capsid protein of the AAV2) were mixed at equimolar ratios to a final concentration of 37.5 µg DNA/plate. The DNA mixture was added to 6.8 mL of ddH_20 and 1 mL of 2.5 mol/L $CaCl_2$ and vortexed briefly. Thereafter 12 mL 2X HeBS buffer (280 mmol/L NaCl, 50 mmol/L HEPES, 1.5 Na_2HPO_4, pH 7.05 adjusted with NaOH) was added dropwise while vortexing the $CaCl_2$-DNA solution. A proper precipitation reaction leads to a turbid solution, while the single crystals should be big enough to be seen by eye. If the solution did not turn turbid at all or single crystals were too big, the solution was discarded and the precipitation reaction was repeated. Following 100 s incubation time, 2 mL of the transfection mixture was added dropwise to each plate. After 18 – 24 h the transfection efficiency was assessed to have at least 25 % positive cells using an inverted epifluorescence microscope. The medium was exchanged with 30 mL fresh DMEM to stop the transfection reaction. For harvesting the rAAVs two different methods were used. If high titers were necessary FPLC based purification with 1 mL HiTrap Heparin HP columns (GE Healthcare, #17-0406-01, Freiburg) were used (Chapter 2.1.9), otherwise the standard purification method with Heparin-Agarose was performed (Chapter 2.1.8).

2.1.8 rAAV purification with Heparin-Agarose

48 h after medium exchange the cells were scraped from dishes and transferred to 50 mL Falcon tubes. The pooled cells were then centrifuged at 200 x g and 4 °C for 10 min. The supernatant was discarded, 10 mL (1 mL/plate) lysis buffer (150 mmol/L NaCl, 50 mmol/L Tris-HCl pH 8.5) added, and the cells resuspended and collected in one Falcon tube. Lysis was achieved by three cycles of freeze/thaw in a dry ice-ethanol bath and 37 °C water bath, respectively. Then, 500 U Benzonase (Sigma-Aldrich, #E1014, Munich) were added to digest chromosomal DNA and the solution was incubated at 37 °C for 2 h. Cellular debris was removed by centrifugation (3600 x g at 4 °C, 15 min) and followed by filtering of the supernatant with a 0.45 µm Millex PVDF membrane filter (Merck Millipore, #SLHV013SL, Darmstadt). Crude lysates were stored at 4 °C. Purification of rAAV particles was then performed by column chromatography (Biorad, #732-1010, München). 5 mL of Heparin-Agarose (Sigma-Aldrich, #H6508, Munich) was filled into the column vessel together with the crude lysate and incubated for 2 h with gentle agitation at 4 °C. The supernatant was removed by gravitation flow and the column was washed with 20 mL washing buffer (500 mL PBS (Gibco, #14200, with 1 mmol/L $MgCl_2$, 2.5 mmol/L KCl, pH 7.2; Thermo Scientific, Darmstadt). Elution of the viral particles from Heparin-Agarose was achieved using 13 mL elution buffer (500 mmol/L NaCl, 50 mmol/L Tris-HCl, pH 7.2) and the flow-through was collected in an 15 mL Falcon tube and stored at 4°C prior to concentration. The procedure was continued as in chapter 2.1.10.

2.1.9 rAAV Purification with HiTrap Heparin Columns

48 h after medium exchange the cells were scraped from dishes and transferred in 50 mL Falcon tubes. The pooled cells were then centrifuged at 200 x g and 4 °C for 10 min. The supernatant was transferred to separate Falcon tubes and 125 U Benzonase per 50 mL supernatant were added and incubated for 2 h. The pellet was resuspended in TNT extraction buffer (20 mmol/L Tris-HCL pH 7.5, 150 mmol/L NaCl, 1 % Triton X-100, 10 mmol/L $MgCl_2$) at RT for 10 min to lyse the cell membranes. 1000 U of Benzonase were added and the solution incubated at 37 °C in a water bath for 1 h. Cellular debris was removed by centrifugation (3600 x g at 4 °C, 15 min) followed by filtering of the supernatant with a 0.45 µm Millex PVDF membrane filter (Merck Millipore, #SLHV013SL, Darmstadt). Crude lysates were stored at -20 °C prior to HPLC purification. For FPLC (ÄKTAprime plus, GE Healthcare, Freiburg) purification all solutions were degassed by vacuum-driven filtration (Stericup 500 mL Durapore 0.45 µm PVDF, #SCHVU05RE, Merck Millipore, Darmstadt). Before loading, HiTrap Heparin HP columns were first washed with 5 mL ddH_20 at 0.5 mL/min and then equilibrated with 5 mL PBS at 0.5 mL/min. Care was taken to not impair the column by introducing any air bubbles or

letting it run dry. The supernatant (<300 mL) was pushed through a 0.2 µm syringe Filter (Puradisc FP 30 Cellulose Acetate Syringe Filter, #10462200, GE Healthcare, Freiburg) and directly loaded onto the column at 1 mL/min. Afterwards the crude lysate was also filtered and loaded onto the column at the same rate, 1 mL/min. The column was then washed at a rate of 0.5 mL/min with 10 mL PBS and the virus eluted with elution buffer (500 mmol/L NaCl in PBS) at 0.5 mL/min. The fractions were collected as 1 mL aliquots. After the peak, a total of 12 mL were collected and the rest of the fractions were discarded. 1 mL aliquots were then transferred to a 15 mL Falcon tube and stored at 4 °C prior to concentration procedure. The procedure was continued as in chapter 2.1.10. Columns could be re-used up to three times if the same virus was to be purified again. Therefore the columns were washed with 10 mL PBS and then stored with 20 % Ethanol at 4 °C.

2.1.10 Concentration of viral solution

The eluates were transferred to an Amicon Ultra-15 filter tube (Merck Millipore, #UFC910024, Darmstadt). The filter tube was centrifuged at 3000 x g at 4 °C until less than 1 mL solution was left and then was washed twice with 13 mL PBS. The final run was continued until 250 µL were left. This concentrated virus solution was filtered (0.22 µm Millex, #SLGV004SL, Merck Millipore, Darmstadt) and stored at 4 °C until further use. A qualitative assessment of the virus titer was done by transducing primary rat hippocampal cultures with 0.5 µL and 1 µL and observing fluorescence increases up to 7 days. Viruses that did not produce satisfying fluorescence in cell culture were discarded and the preparation was repeated.

2.2 Cell culture techniques

2.2.1 Neuronal DNA transfection & viral transduction *in vitro*

Cultures of primary rat hippocampal neurons from P18.5 embryos were generally produced by our technician Gabriele Krämer or myself according to a standard protocol (Banker and Goslin, 1998). The cells were plated in 24 well plates (Falcon 24 Well Clear Flat Bottom TC-Treated Multiwell Cell Culture Plate, Corning, Wiesbaden) at about 30.000 cells per well using 12 mm² poly-L-Lysine (#P4832, Sigma-Aldrich, Munich) coated coverslips (thickness 1, #1001/12, Hecht-Assistent, Sondheim). The cultures were always kept in incubators at 37 °C with 5% CO_2.

Dissociated neuronal cultures between DIV5 and DIV15 (DIV, Days *in vitro*) were transfected using Lipofectamin 2000 (Thermo Fisher Scientific, Darmstadt) to achieve neuronal transfection efficiencies

up to ~5 % on average. Transfections were carried out in the 24 well plates where the cells were also plated. The original conditioned medium of the cells was saved and replaced by a freshly made and pre-warmed mixture of 400 µL Neurobasal (Gibco, #21103049, Thermo Scientific, Darmstadt), 1 x B27 (50X, Gibco, #17504044, Thermo Scientific, Darmstadt), and L-Glutamine to a final concentration of 0,5 mmol/L (100X, Gibco, #25030024, Thermo Scientific, Darmstadt). The plate with the coverslips and the kept original conditioned medium (in a petri dish) were put back into the incubator to ensure optimal conditions. 1 µg of DNA was added to 50 µL Neuobasal medium in an Eppendorf tube and 1 µL of Lipofectamin 2000 was added to 50 µL Neurobasal medium in a separate Eppendorf tube. Both reactions where incubated at RT for 5 min before mixing them together and incubating for another 20 min at RT. The total 100 µL transfection mixture was then added to the respective well. The cultures were returned to the incubator for up to 4 h. For younger cultures between DIV5 and DIV10, 1 h of incubation time was generally sufficient. The older the cultures were, the longer the incubation time was chosen. Afterwards the transfection medium was removed and the cells were washed 3 times each with 1 mL pre-warmed Neurobasal medium. Finally, the original conditioned medium was added to the cells again. This reduced neuronal cell death and increased transfection of neurons.

For viral transduction of neurons *in vitro* 0.5 µL or 1 µL of the viral stock was directly added at DIV5 to the cell culture medium. Fluorescence could usually be observed within 5 days of transduction.

2.2.2 *In vitro* induction of gene expression

For the induction of gene expression in TetOn positive cells, 10 µM Doxycycline Hyclate (#9891, Sigma-Aldrich, Munich) was added to the medium. From a stock solution of 500 ng/mL Doxycycline in DPBS (#14190094, Thermo Fisher Scientific, Darmstadt) 4 µl were added to 500 µL of Medium to reach a final concentration of 10 µM. This was sufficient to efficiently induce gene expression within one day, as could be observed by fluorescence microscopy.

2.2.3 Observation of neuronal activity *in vitro* after transgene induction

To study the impact of Kir2.1 and NaChBac on neuronal activities, cultures were transduced between DIV7 and DIV10 in poly-L-Lysine coated cell culture dishes (µ-Dish 35mm, #81151, Ibidi, Martinsried) with 1 µL of DriverTET and ResponderTET rAAVs (1:1). Also, 1 µL of a 1:10 dilution of GCamP6f rAAV as for the *in vivo* experiments was administered to the cultures simultaneously. After DIV15, cultures were treated with a final concentration of 10 µM Doxycycline and imaged consecutively once every hour, for 5 hours. The imaging was performed on a Leica SP8 confocal microscope with a live cell

imaging chamber kept at 37 °C. Using the dishes with a lid, 5 % CO_2 was superfused onto the medium via tubing. Cells were imaged for 5 minutes every hour with a 20 X objective (Figure 26). For the analysis, cell bodies were manually selected, calcium traces extracted, and the peaks counted with a Matlab script. A linear regression fit was used to statistically assess the significance of the results.

2.2.4 Fixation and staining of samples

Cultured neurons were fixated by removing the medium and immediately washing once with DPBS followed by incubation in 1 mL 4 % Paraformaldehyde (#16005, Sigma-Aldrich, Munich) in PBS for 5 min. Then cells were washed 3 times with DPBS to stop the fixation reaction. Staining was carried out with a primary antibody against the HA-Tag (C29F4, Rabbit mAB, Lot: 8, #3724, Cell Signaling Technology, Frankfurt am Main), diluted according to the manufacturers' recommendations in Blocking Buffer (5 g Sucrose [#S7903, Sigma-Aldrich, Munich], 2 g Bovine Serum Albumin (BSA) [#K41-001, PAA, Pasching], 300 µL Triton X-100 [#T9284, Sigma-Aldrich, Munich], 10 mL FCS [#P30-193306, PAN Biotech, Aidenbach] ad 100 mL 1 x PBS) over night at 4 °C.

Cells were washed 3 times with DPBS and then stained with the secondary antibody goat anti-rabbit Alexa Fluor 633 (#A-21070, Invitrogen, Thermo Fisher Scientific, Darmstadt) in a 1:1000 dilution in Staining Buffer (5 g Sucrose [#S7903, Sigma-Aldrich, Munich], 2 g Bovine Serum Albumin (BSA) [#K41-001, PAA, Pasching], 300 µL Triton X-100 [#T9284, Sigma-Aldrich, Munich] ad 100 mL 1 x PBS) for 1 h in the dark at RT. After staining, cells were first washed 3 times with DPBS and then stained with DAPI (5 mg/mL stock solution diluted 1:2500 for final use [#D9542, Sigma-Aldrich, Munich]) for 5 min. Subsequently, cells were washed again for 3 times before mounting of the coverslip onto microscope slides with a drop of Aqua-Poly/Mount (#18606, Poly Sciences, Hirschberg an der Bergstrasse). Fluorescence microscopy of samples was conducted on a Leica DM6000B upright epifluorescence microscope. Analysis of the acquired pictures was done using ImageJ Fiji distribution (Schindelin et al., 2012).

Fixation and staining of brain slices was done as follows. The animal was perfused and fixated with 4 % PFA, the brain removed, post fixated for 1 h and sliced at a thickness of ~70 µm. Perfusion, slicing, and mounting of slices was done how? Staining with the primary antibody was carried out overnight at 4 °C according to the manufacturers' recommendations in Blocking Buffer. The samples were rinsed 3 times with PBS and an appropriate secondary antibody in Staining Buffer applied to the samples. After at least 2 h at room temperature, the samples were rinsed again for 3 times with PBS and then mounted onto glass slides for subsequent microscopy.

2.3 Mouse lines

The animal experiments were carried out on a homozygous Ai14 (B6.Cg-*Gt(ROSA)26Sor*$^{tm14(CAG-tdTomato)Hze}$/J) mouse line on a C57BL/6J background in general (JAX stock #007914 (Madisen et al., 2010)). If the Cre recombinase is present in these mouse lines cells, the floxed tdTomato fluorescent protein will be activated and expressed.

For the Cre mediated targeting of Parvalbumin interneurons the Ai14 mouse line was crossed with a PVcre (B6.129P2-*Pvalb*$^{tm1(cre)Arbr}$/J) mouse line (JAX stock #017320 (Hippenmeyer et al., 2005)). In these resulting PVcre-Ai14 mice Parvalbumin interneurons would express the Cre recombinase and also tdTomato constitutively.

2.4 *In vivo* animal experimentation

2.4.1 Craniectomy, cortical virus injection and chronic window implantation

Surgeries on mice were performed as one procedure including craniectomy, injection of viruses, and the implantation of a chronic cranial window. The surgery usually required about 5 h. The animals were anesthetized by an intraperitoneal (i.p.) injection of a mixture of 40 µl Fentanyl (1 mg/mL, Janssen-Cilag, Neuss), 160 µL Midazolam (5 mg/mL, Hameln Pharma Plus, Hameln) and 60 µL Medetomidin (1mg/mL, Sedan Alvetra-Werfft, Neumünster) at a dosage of 3.1 µL/g body weight. Directly after injection the animals were monitored for up to one hour and hind limb reflexes assessed before the surgery was initiated when reflexes disappeared. At the end of the surgery animals received a subcutaneous (s.c.) mixture of three substances to antagonize anesthesia, consisting of 120µL Naloxon (0.4 mg/mL, Inresa, Freiburg im Breisgau), 800 µL Flumazenil (0.1 mg/mL, Fresenius Kabi, Bad Homburg vor der Höhe) and 60 µL Antipamezole (5 mg/mL, Antisedan, Pfizer, Karlsruhe) at a dosage of 6.2 µL/g body weight. The body temperature of the animals was kept at 38 °C during the whole surgical procedure by a feedback-controlled heating pad. After the surgery was finished the animals received a subcutaneous injection of Carprofen (Rimadyl, Pfizer, Karlsruhe) dosed 10 µg/g body weight as an analgesic. To spare the animals from further pain after the surgical procedure, the analgesic treatment was continued for at least two consecutive days or as long as the mice showed behavioral signs of pain. These signs included apathetic behavior in the cage, closed eyes, and unwillingness to move even if the animals were touched.

For the surgical procedure the heads of the mice were shaved and subsequently mounted in a stereotactic EM70G manipulator (Kopf Instruments, Tujunga CA, USA). Prior to severing the skin at

about 9 mm diameter around the bregma, ~100 µL Xylocain solution (1 %, Astra Zeneca, Wedel) was applied subcutaneously as local anesthetic. The skin was removed at the central area. After cleaning the skull surface, a 6 mm diameter coverslip (No. 0, #631-0168, VWR, Bruchsal) was used to mark a circular area around the coverslip with a pencil on the skull. This template was used to carefully thin the skull at ~6.5 mm diameter. The thinning was done using a hand-held dental drill (Osada EXL-40, Los Angeles CA, USA) until the circular bone piece was moving when applying gentle pressure to it. At this step the skull was removed by carefully lifting it up with blunt forceps (straight Dumont #2; Fine Science Tools, Heidelberg). Potential bleeding was stopped with moistened coagulant foam (Equispon, Equimedical, Münster) that contains fibrinogen. Thereafter, the dura was removed with a fine forceps (straight Dumont #5; Fine Science Tools, Heidelberg) to improve long term imaging results. Care was taken to avoid any damage to the brain surface or blood vessels. The viral solution of up to ~1.2 µL in total per brain hemisphere was delivered at cortical depths of 400 – 500 µm with an injection glass micropipette (Blaubrand IntraMARK 5 µl, #708707, Wertheim) pulled with a P97 horizontal puller (Sutter Instruments, Novato CA, USA) and had an inner diameter of 10 – 20 µm at the tips. Usually 2 – 3 sites per hemisphere were injected to have a larger infected brain area. The injections were performed at a speed of about ~3 µL/h with manually controlled pressure applied with a 10 mL syringe. It was important that the viral solution actually remained in the brain tissue and did not come out of the injection site again. Therefore, after positioning the injection micropipette in the desired depth, the tissue was allowed to tighten around the site by waiting for 2 min before starting the injection. Also, the brain surface was kept moist with sterile phosphate buffered saline at all times to avoid drying out.

When the injections were finished, the glass coverslip with the silicone filled access hole (~0.9 mm diameter, produced by the university glass workshop and sealed beforehand with Silicone [Elastosil E43 RTV-1, Wacker Chemie, Burghausen], Figure 9A) was sterilized in 70 % Ethanol and placed on the brain surface (Roome and Kuhn, 2014). It was taken care to place the access hole above the ventricle (Y= - 0.7 mm, X= ± 1.5 mm).

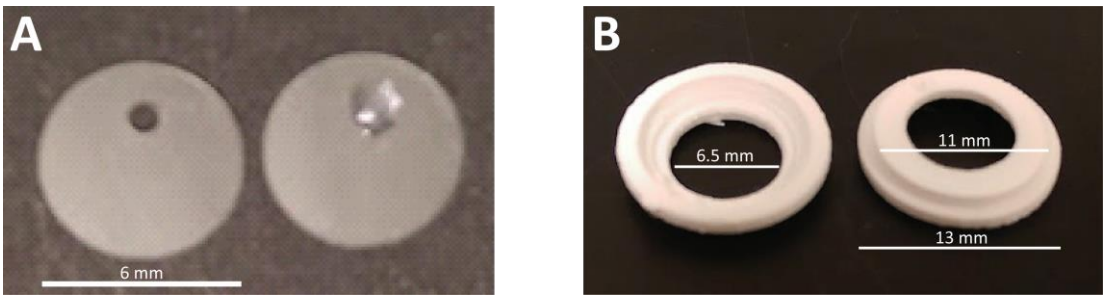

Figure 9. A) Coverslips used for cranial window implantation. Shown right is a silicone filled coverslip with the access hole, ready for use in surgery. B) Plastic crowns from top (left) and bottom view (right) for mounting of the animals at the microscope setup.

When the coverslip was in its desired place, it was glued to the skull with dental acrylic cement (mixture of glue: Cyano [Hager & Werken, Duisburg] and powder: Paladur [Heraeus, Hanau]), by avoiding contact between cement and brain tissue. To be able to mount the animal at the microscope setup, a round 3D-printed (Ultimaker 2, Geldermalsen, Netherlands) plastic crown (Figure 9B) was glued onto the skull around the craniectomy while avoiding covering the actual glass coverslip below. Additionally, the wounded skin around the surgery area was also sealed with dental cement (Figure 10). Occasionally the animals were treated with Dexamethason (100 µL intraperitoneal injection 1 mg/mL, Bela-Pharm, Vechta) for 3 consecutive days to avoid bleeding below the cranial window [surgery protocol adapted from (Holtmaat et al., 2009)].

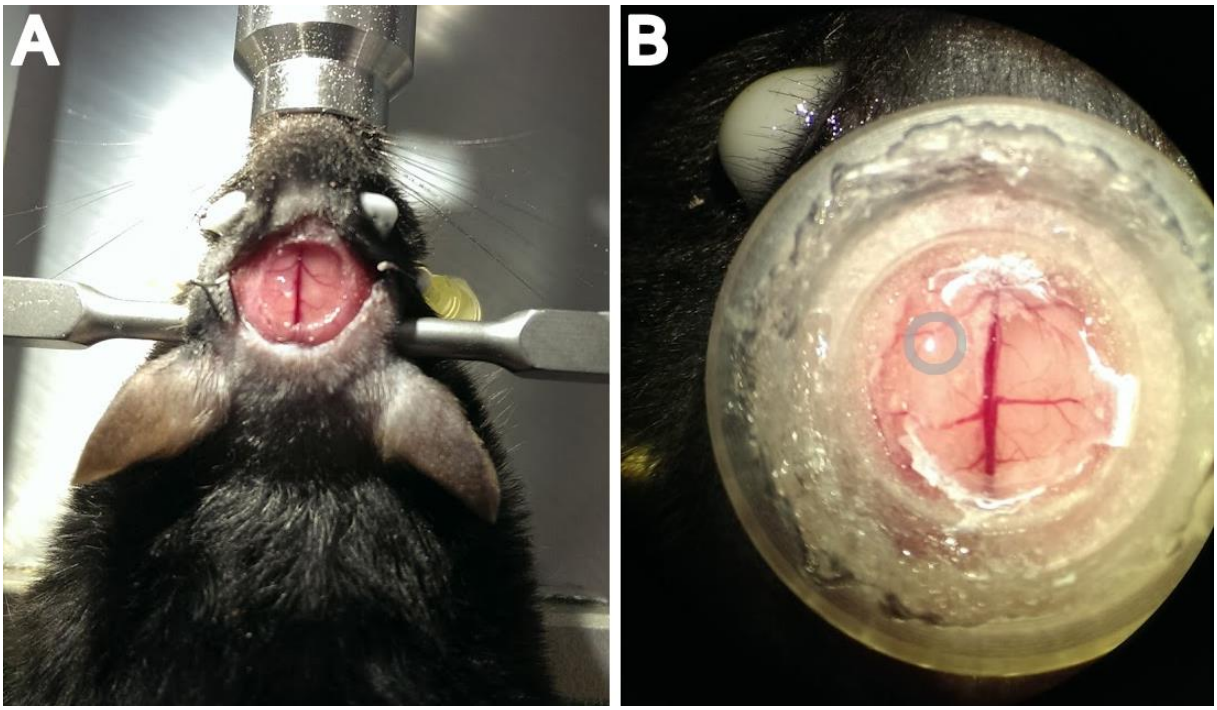

Figure 10. Chronic window surgery with a crown head holder. A) Anaesthetized mouse in stereotactic holder. The skin and a circular piece of the skull and dura were removed. B) Mouse with implanted chronic window and crown head holder glued to the skull for later mounting the animal into microscope setup. Gray circle indicates transparent silicone plug that covers the access hole within the coverslip.

2.4.2 Two-photon microscopy setup

For the *in vivo* cortical imaging of animals, an upright two-photon microscope was used (TriM Scope II Microscope, LaVision Biotec, Bielefeld). The microscope was equipped with a pulsed Ti:Sapphire laser (Chameleon Ultra II, Coherent, Dieburg) as the photon source. The wavelength was set to 960 nm which could excite Venus, GCamP6f, and tdTomato fluorescent proteins efficiently at the same time. Imaging was performed with a 25 X, 1.1 NA, apochromatic, water immersion objective with a working distance of 2 mm (Nikon, Düsseldorf). The emitted fluorescence was split by a 560 nm

dichroic mirror (Chroma, Olching) and filtered with 535/70 nm and 645/75 nm emission filters (Chroma, Olching) for green or red fluorescence, respectively. Fluorescence emission was collected with two low-noise PMTs (H7422-40-LV 5M, Hamamatsu, Japan).

2.4.3 *In vivo* two-photon imaging

I found that the best imaging conditions were 3 to 10 weeks after the window implantation surgery. Earlier imaging was not suitable as transgene expression from the viruses were not yet sufficient. And also the inflammation reaction caused by the surgery required several weeks to decay. Mice were anaesthetized with 2 % Isoflurane initially and mounted onto the imaging stage.

Before imaging, the cranial window was thoroughly cleaned with water and the volume above the cranial window was filled with distilled water. The location and expression of the fluorescent proteins was verified by epi-fluorescence microscopy (X-Cite 120Q, X-Cite; filtercube: excitation filter 535/50, dichroic mirror 565, emission filter 590 longpass) coupled to the TriM Scope II microscope. 2P (two-photon) imaging was performed at cortical depths between 80 and 130 µm and focal planes were chosen where many bright fluorescent layer 2/3 neurons were located.

2.4.4 Imaging of anaesthetized mice

Anesthesia was induced with 2 % Isoflurane (Baxter, Unterschleißheim) in O_2 briefly, and the animals were head-fixed and mounted into a custom built holder. This holder was compatible with the plastic crowns glued to the mouse skulls. After mounting the animals, Isoflurane levels were continuously adjusted to about 0.8 to 1.5 % to yield respiratory rates between 110 and 130 per minute (Figure 11). In this mildly anesthetized state the animals should exhibit substantial spontaneous cortical basal activity. At this level of anesthesia, there should not be much voluntary movement which would generate movement dependent cortical activities that are difficult to reproduce and analyze. Respiratory rates were monitored with a piezoelectric transducer (3 cm diameter, V/AC 1.3 ± 0.5 kHz, FT-31T-1.3A1-472) (Zehendner et al., 2013). To synchronize imaging and recording of breathing rates for post-hoc analysis the microscope frame trigger signal was used to mark the start of the image recording. Respiratory rates above 130 breaths per minute could lead to waking up of the animal and moving, whereas breathing rates below 90 represent a deep anesthetic state with very little cortical activity (Figure 34).

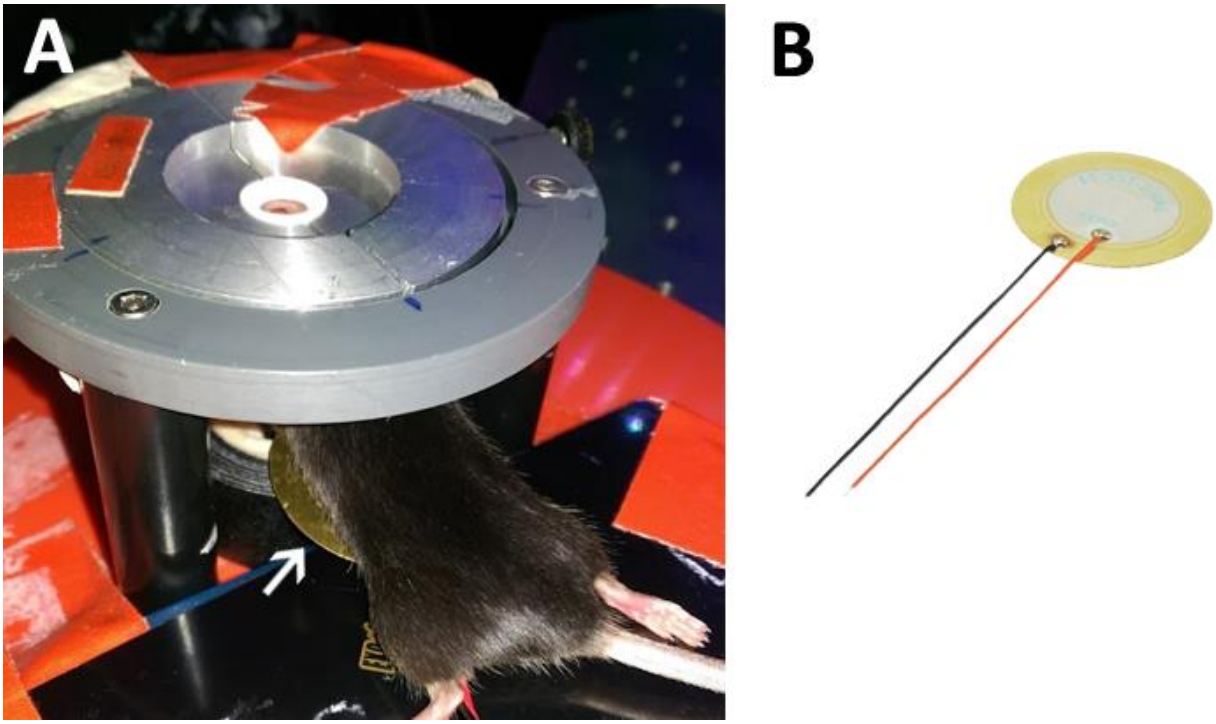

Figure 11. Simultaneous recording of breathing rates and cortical activities. A) Piezoelectric transducer is placed below the animals' thorax (indicated by arrow) to measure respiratory movements by recording electric traces. B) Piezoelectric transducer element that was used.

2.4.5 Induction of *in vivo* gene expression by intracerebroventricular injection of Doxycycline Hyclate

For *in vivo* induction of gene expression, animals were anaesthetized with 1 % Isoflurane and mounted onto the stereotactic setup. For intracerebroventricular (ICV) injection of Doxycycline the micropipette was leveled at glass surface and filled with 1.5 µL (0.22 µm sterile filtered) 8 mmol/L Doxycycline Hyclate (#9891, Sigma-Aldrich, Munich) in DPBS. Injection occurred slowly through the silicone access hole at 2.2 mm depth aiming for the ventricle (from bregma: X= ± 1.5 mm/ Y= - 0.7 mm/ Z= - 2.2 mm). As the average C57BL/6 mouse brain has a volume of 415 mm^3, i.e. 415 µL (Kovacevic et al., 2005) this amount of Doxycycline should lead to a concentration of ~30 µmol/L in the brain. 3 h after the injection, the animal was imaged for the first time after Doxycycline administration.

2.5 Analysis of calcium recordings

2.5.1 Motion correction of acquired image material

Non-rigid correction for respiratory or mechanical motion drifts between individual imaging sessions was accomplished using the ImageJ Fiji distribution (Schindelin et al., 2012) and the plugin "Moco" (Dubbs et al., 2016). Moco uses a maximum intensity projection of 500 frames from each imaging session to create a template for correction of motion artifacts. The procedure was repeated twice to ensure removal of most motion artifacts. Without the correction for motion artifacts a lot more shifts in calcium traces would be expected. Importantly, the cell-ROIs (ROI, Region of Interest) should change position across all consecutive calcium movies so that mean values can be reliably measured. Otherwise, even brief shifts due to motion will have a significant effect on the respective calcium trace. Although removal of all motion artifacts is impossible, a substantial reduction will lead to a much higher accuracy for subsequent processing and analyses.

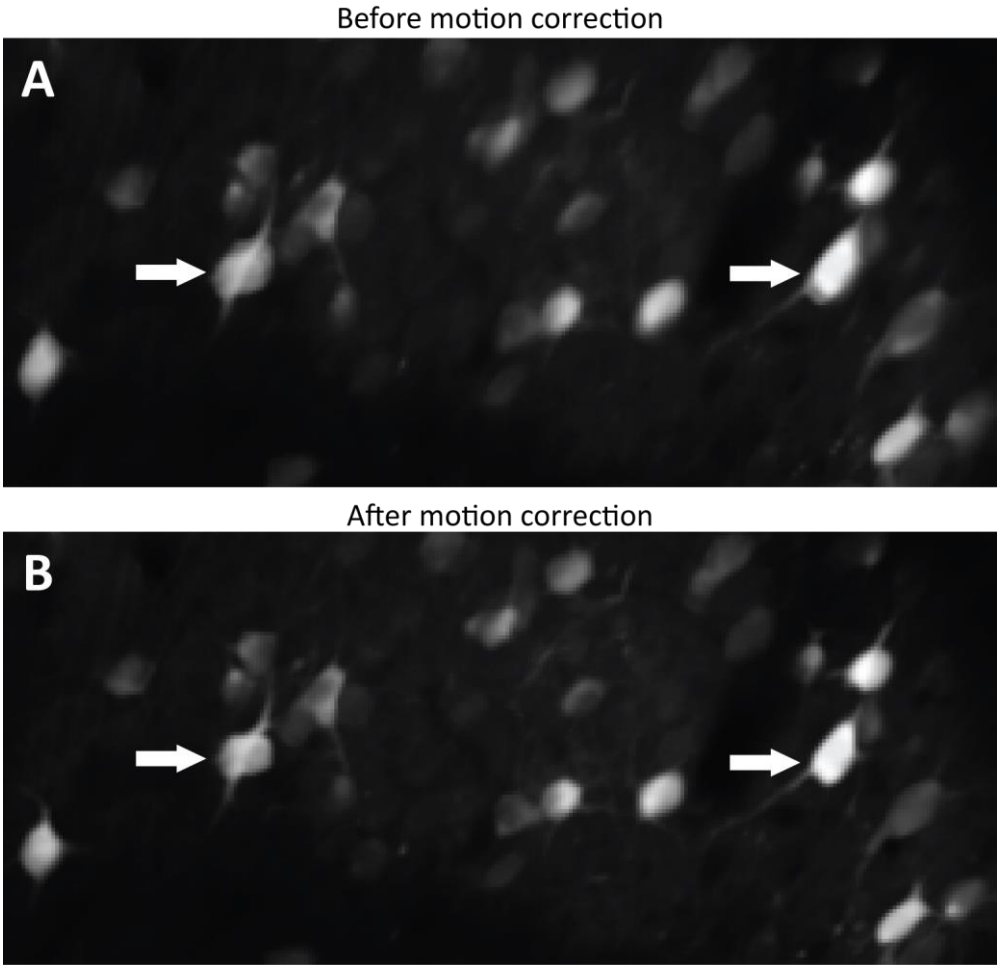

Figure 12. Example of motion correction for calcium imaging data using Moco. A) Z-Projection of standard deviations of a calcium imaging movie. Movement artifacts lead to blurry outlines and low contrast, especially at cell boundaries. B) Result of the motion correction procedure. The gain in contrast and clear outlines is a strong sign of less motion artifacts in the calcium imaging movie. Arrows indicate areas with a clear reduction of motion artifacts compared to the original projection in A.

2.5.2 Registration of consecutive calcium imaging movies

For the analysis of large datasets from consecutive time points it is necessary to correctly register the consecutive imaging sessions onto each other. To achieve a high fidelity registration of calcium imaging movies, a toolbox was created based on Matlab 2016b (Mathworks, Natick, MA, USA), as no available software solution fulfilled the requirements for this task sufficiently. The toolbox was named CaMoReg, which is an abbreviation for “Calcium Movie Registration”.

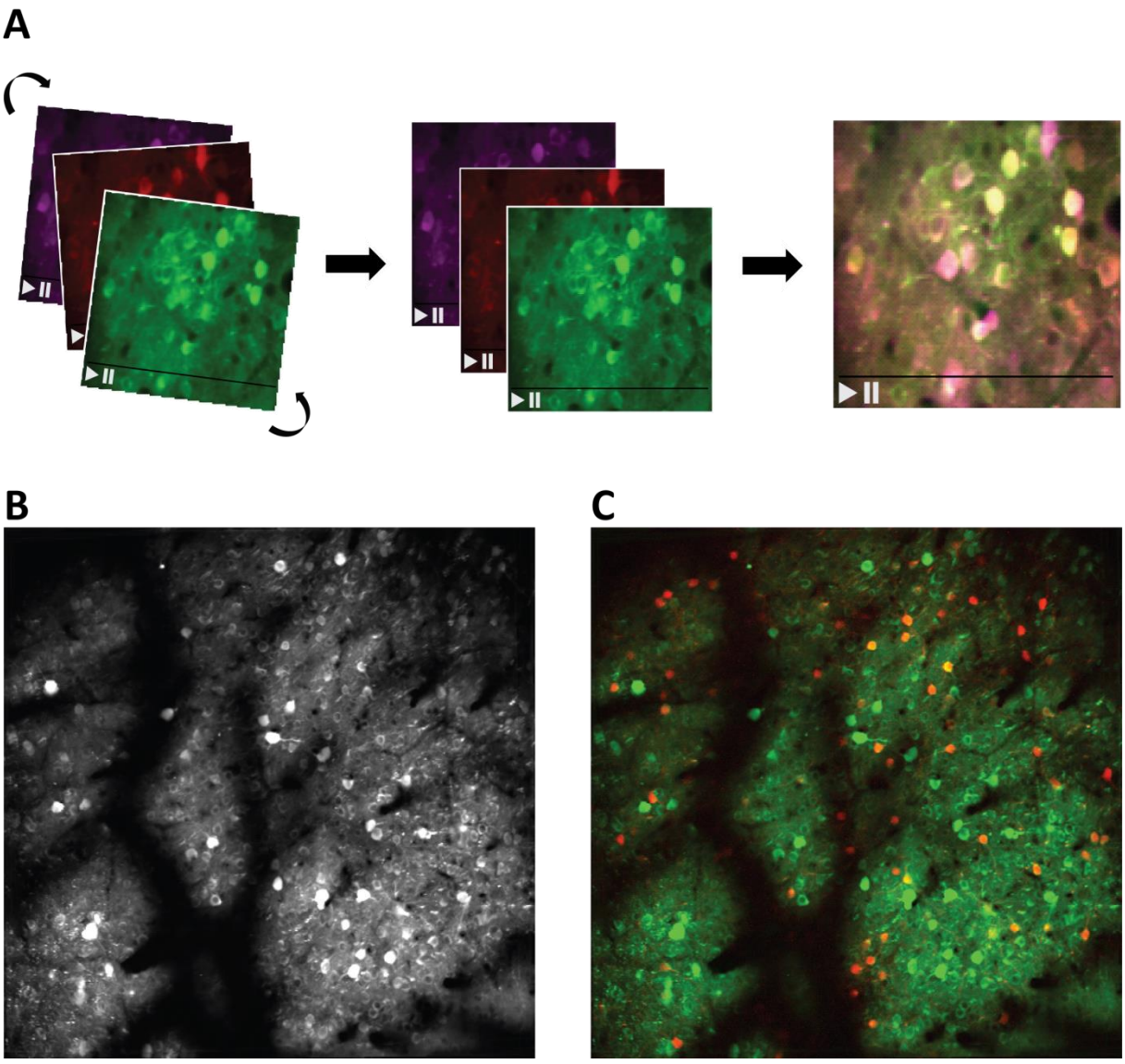

Figure 13. Registration of consecutive calcium imaging movies using CaMoReg. A) Scheme to visualize the registration process. First, the raw movies are all registered to the initial time point. The result of the registration process is verified by a maximum intensity projection across all the calcium movies. B) The result of this procedure is a near complete overlap, as evidenced by a maximum intensity projection of eleven consecutive movies, as shown here. Note the negligible deviations between all the calcium imaging movies. C) The same maximum intensity projection as in B), but with additional tdTomato positive neurons (in red) overlaid to the GCamP6f fluorescence.

The time point before gene induction was chosen as the template image to which all the other time points were registered. CaMoReg works semi-automatically as it requires the user to choose the best registration among six different affine image registration algorithm results. CaMoReg was developed by using the Matlab-App called “Feature-Based Image Registration 1.0.0.1 by Brett Shoelson”. This App utilizes all of Matlab intrinsic Computer Vision System Toolbox parameters on an interactive user interface and displays the immediate results.

I tested many parameters with different sets of my calcium imaging data to see if any were useful for the registration. If yes, the underlying Matlab function was exported and integrated in CaMoReg. In total 6 affine image registration models (i.e. “parameters”) were identified, adjusted, and integrated in CaMoReg. If none of the six predefined image registration models achieved good registrations, the user can provide a transformation matrix manually by pointing and clicking identical spots on the two images. These manual 2D affine transformation matrices are then applied to the entire stacks. The resulting registered calcium imaging movies were verified for proper registration. If the results were not satisfactory, the whole process was repeated until registration was complete across all time points.

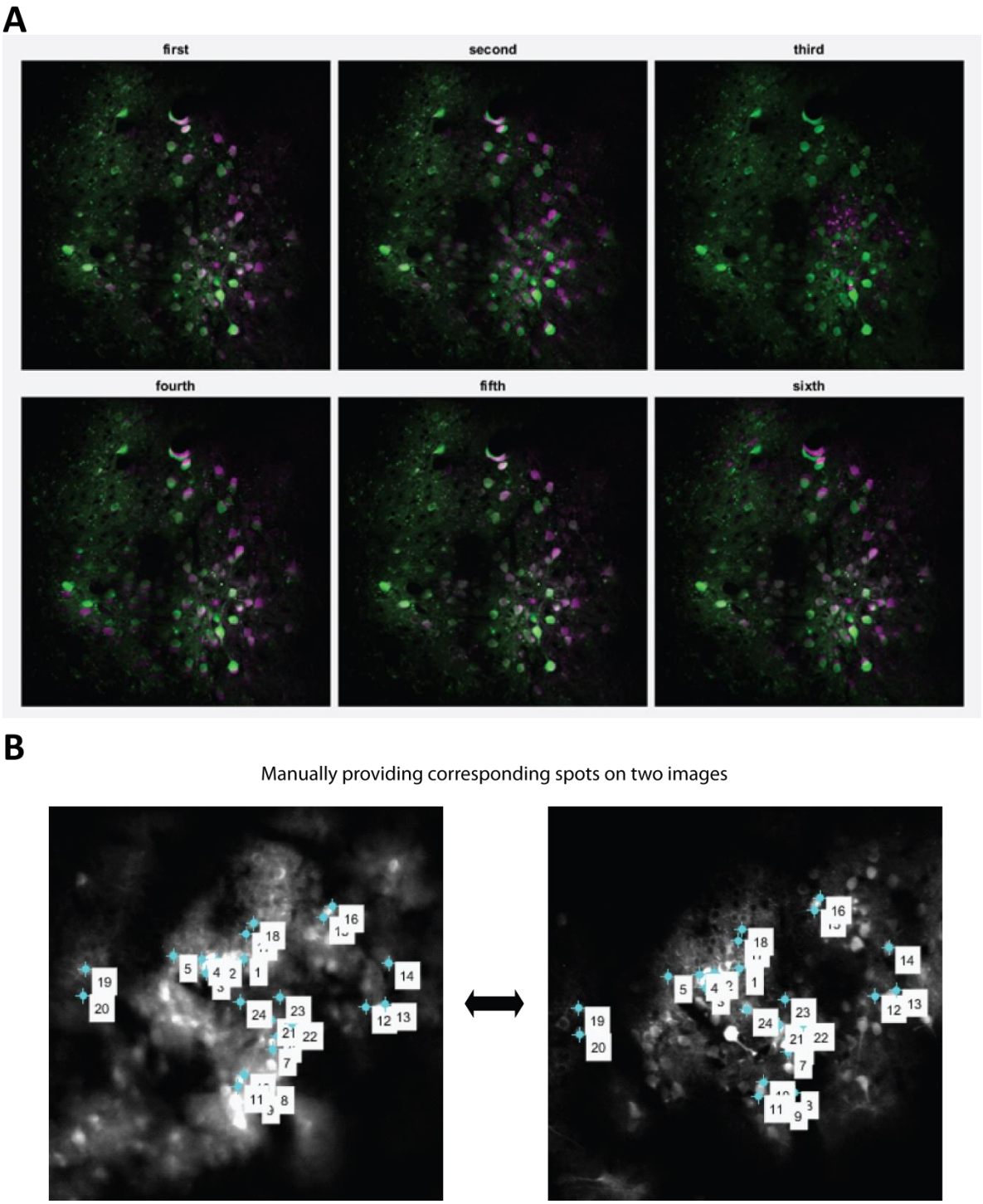

Figure 14. Affine registration of consecutive calcium imaging movies using CaMoReg. A) User interface of CaMoReg showing six different registration results of affine transformation matrices. The user has to choose the preferred registration which is then applied to the calcium movie. Here, matrix 1 and 5 show good registration between the two pseudo-colored (green and purple) MIPs from two different time points. B) Shows the possibility to create a transformation matrix manually by pointing and clicking corresponding spots on two images. This is necessary if none of the six predefined registration algorithms produces a successful result.

2.5.3 Extraction of calcium traces from acquired data

The extraction of calcium traces from densely packed regions with GCamP6f positive neurons in cortical areas is very challenging. Especially, if one wants to exclude signal from neighboring neurons or neuropil activity that is present abundantly in the focal plane. Harris and co-workers argue that neuronal activity that has not been corrected for neuropil signal from the vicinity of the corresponding cells is contaminated with a lot of false-positive co-activity (Harris et al., 2016).

Therefore, this neuropil signal is removed during the processing by our pipeline. To do this, cells were selected in ImageJ using the maximum intensity projections of all registered time points, and the respective ROIs were saved. A ROI set was created and loaded for every experiment into a Matlab based algorithm that processes each single ROI separately. Each ROI was dilated' by 4 pixels around the initial ROI without overlapping with neighboring ROIs. That created a donut-shaped, second ROI around the initial cell-ROI of which the average fluorescence value for each frame was determined. This value, which represents 'contaminant' signal from neuropils or dendrites in the vicinity of the cell-ROI, was then subtracted from the cell-ROI mean fluorescent value. The script processes every ROI for every time point of the experiment. The results of the neuropil corrected fluorescent values are saved for each ROI in a matrix for every imaging frame. (This script was kindly provided by Dr. Johannes Knabbe)

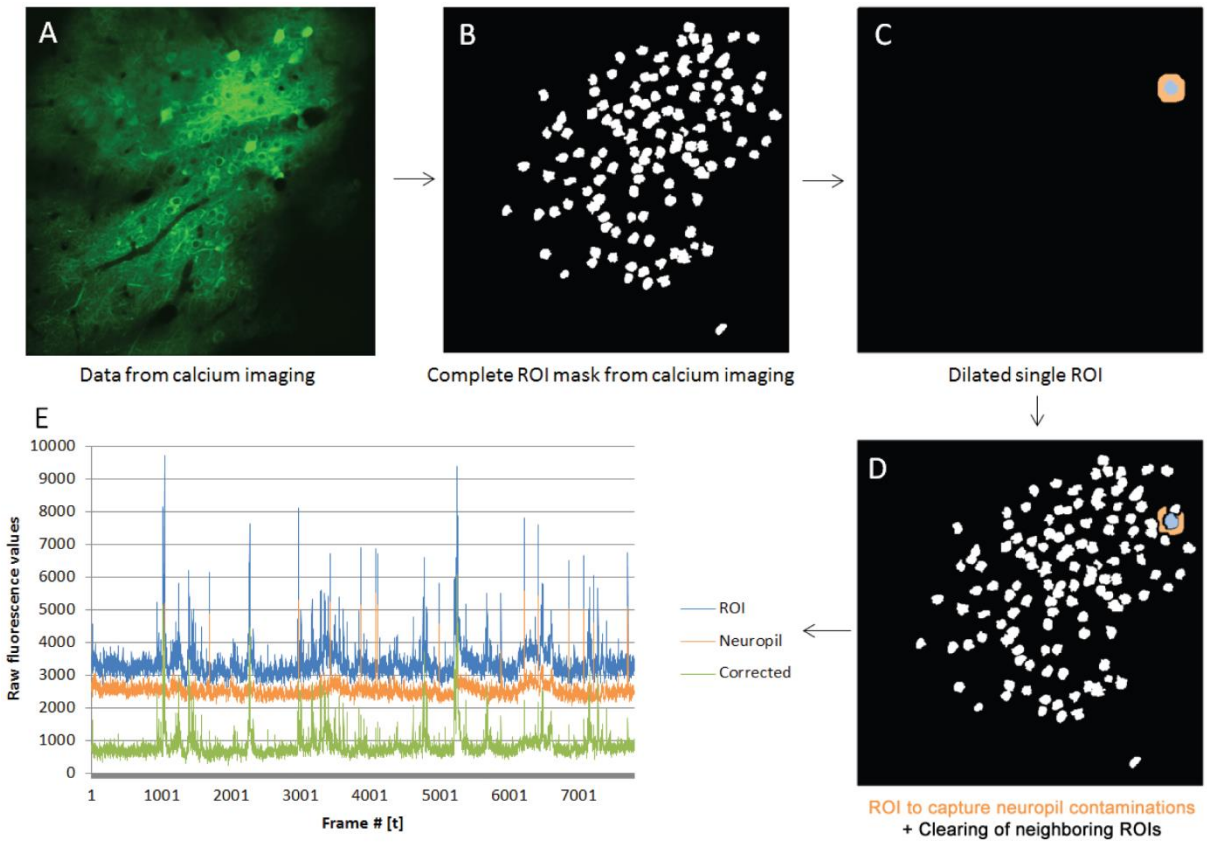

Figure 15. Workflow for improving signal quality by correcting for 'contaminant' signal from the nearby neuropil. A) Projection of all registered time points of the consecutive calcium imaging sessions. B) Manual selection of cells to create a ROI mask. C, D) Each ROI is processed separately. An area around the respective ROI is created by dilating it by 4 pixels and excluding neighboring ROIs. The resulting ROI is called 'Neuropil contaminant ROI'. E) Example traces of the resulting correction. The values of the resulting neuropil ROI are subtracted from the original ROI to correct for contaminant signal.

2.5.4 Calcium imaging baseline correction

A very challenging obstacle turned out to be the unsteady baselines of the extracted calcium traces. There are various reasons why recorded baselines are not flat, and it is impossible to describe all the underlying mechanisms that lead to this phenomenon. Mostly there are additive reasons for the phenotype of the recorded calcium trace. Sometimes it can be an artifact that was introduced by post-processing, calcium trace extraction, poor choice of the respective ROI, or a simple bleaching process. Different phenotypes of the calcium traces can be categorized into roughly six groups, which will be described in the following paragraph.

1.) The most obvious reason for a decaying baseline is bleaching of the fluorophore GCamP6f. The rate of bleaching is dependent on the amount of available GCamp6f proteins and the amount of photons that interact with the proteins' fluorophore. The number of photons is user controlled and is dependent on the laser power used to excite the fluorescent proteins. To avoid excessive

bleaching, care was taken to use the lowest possible amount of laser power while aiming to acquire images suitable for the subsequent analysis. The rate of bleaching is also dependent on the duration of the image acquisition process, but for my experiments the duration of each imaging session was fixed at about 9 min or 8000 images acquired at 15.3 Hz. Excessive bleaching was predominantly observed in Parvalbumin positive interneurons that carried a floxed GCamp6f transgene. For excitatory neurons, bleaching seemed not to occur to a high degree with the used imaging parameters as can be seen in Figure 16A.

2.) Whenever a sudden decrease in fluorescence values was observed it was often due to a high activity in neuropil-ROI around the respective cell-ROI. Subtracting the neuropil-ROI has this effect if it rapidly increases while the cell-ROI does not. The consequence is a short decrease in the baseline fluorescence of the cell-ROI, which cannot be corrected for properly (Figure 16B). As negative values are not considered for later spike prediction, these frames did not contribute to the analysis. This is the only drawback of clearing the calcium traces of contaminant signal from neighboring neuronal tissue.

3.) An obvious step-like signal change across all traces in an experiment is a clear sign of X-Y-Z displacement of the imaging plane during acquisition. Most likely this occurs whenever the animal was briefly moving. It usually is impossible to correct for such changes with post-hoc processing (Figure 16C). For these obvious cases of the animal moving substantially, the image acquisition was repeated. Slight or episodic changes that arise from breathing of the animal or blood flow could be reliably corrected for using motion correction plugins as described in chapter 2.5.1.

4.) Also, frequently observed was an increasing baseline during image acquisition. This phenomenon can only be described by a decrease in neuropil-ROI fluorescence value over time, maybe due to slight bleaching. The baseline slope cannot be properly corrected for by line-fitting, but can easily be corrected by a rigid curve-fitting algorithm (Figure 16D).

5.) Figure 16E shows a calcium trace signal shift that repeatedly occurred in excitatory neurons, usually after at least 12 h of inducing the Kir2.1 transgene in inhibitory Parvalbumin interneurons. It is only possible to correctly detect the baseline of such ‘fire-and-stay-high’ activity patterns, if there is a clear plateau at either the beginning of the trace or its end, preferably on both sides. Detecting the baselines of such neurons is particularly challenging for any algorithm as it requires excluding values above a certain value to reliably fit the correct baseline. Therefore just a constrained line-fitting or rigid curve-fitting reliably determines the correct baseline (Figure 16E).

6.) A puzzling type of calcium trace is rather often occurring. It is characterized by containing a high plateau at the center of the trace and lower arms at the beginning and the end of the recording.

This phenotype might be resulting from a combination of different effects. It is most likely a combination of heterogeneous bleaching within the cell-ROI and the neuropil-ROI at the same time (Figure 16F).

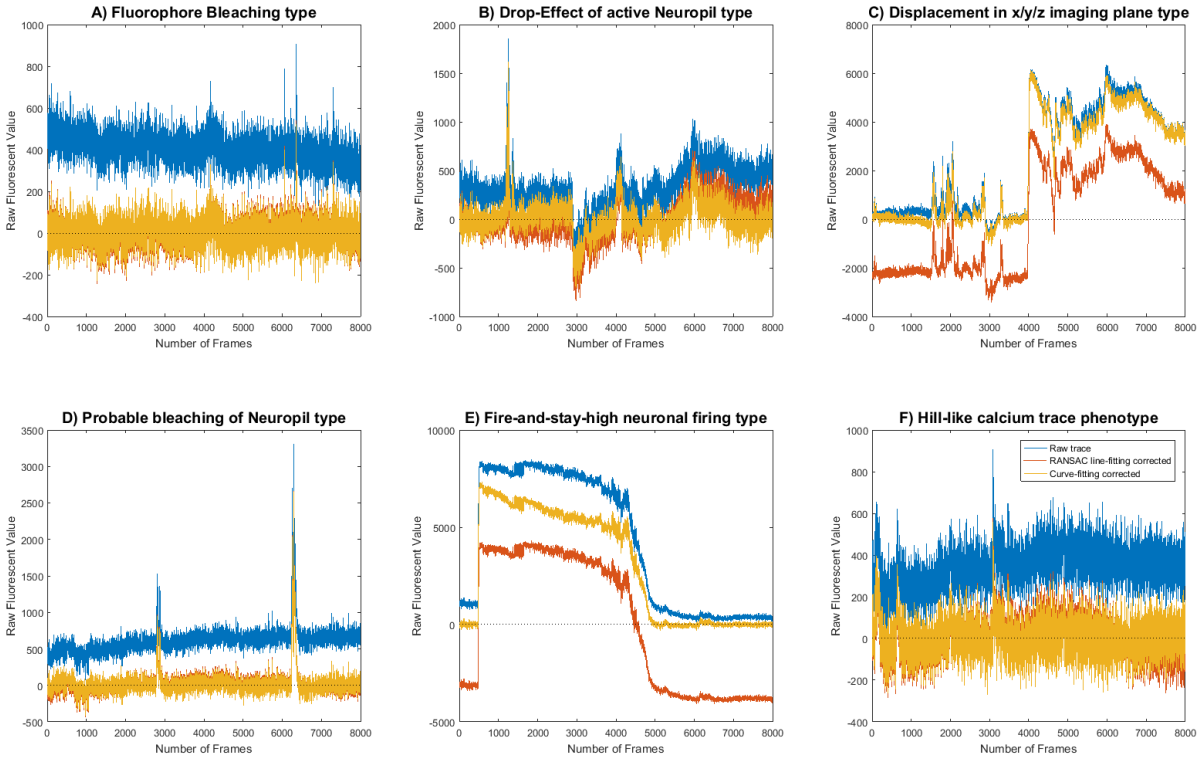

Figure 16. Examples of the six most regularly occurring calcium trace 'phenotypes' and the results of the respective correction algorithm. (Raw trace: blue; RANSAC: red; Curve-fitting: yellow) A) Moderate fluorophore bleaching is corrected successfully with curve-fitting and RANSAC line-fitting. B) Drop-Effect that occurs whenever the neuropil-ROI is active in the vicinity of the cell-ROI, obvious at Frame ~3000. C) Abrupt, strong increases or decreases in fluorescence values are usually due to displacement of the imaging plane. Curve-fitting could not correct the negative values because of animal movement. This might happen whenever the animal moves while recording the movie. If the displacement is too big, this phenotype is impossible to correct for. D) Slow increase in raw fluorescence probably due to the bleaching of the fluorophores in the neuropil-ROI. Corrected for with curve-fitting algorithms. E) Neurons that become and stay active for a while during recording lead to this 'Fire-and-stay-high' trace phenotype. These are the most challenging to correctly predict the baseline. RANSAC algorithm fails to determine the baseline correctly, while the curve-fitting algorithm performs quite well. The only drawback is the overcompensation of long lasting signals that will be slightly reduced due to the curve nature of the fitting. F) 'Hill-like' phenotype that can be corrected successfully with the curve-fitting algorithm, whereas the RANSAC line-fitting shows some weakness as for more extreme values.

2.5.5 RANSAC line fitting

For the baseline correction two different approaches were applied. The first one was a RANSAC (Random Sample Consensus) algorithm to fit a line to the calcium traces that would represent the baseline. A RANSAC implementation was modified, which is described at https://en.wikipedia.org/wiki/Random_sample_consensus (as of Sept. 27, 2017, 15:50 CET) (Figure 17).

```
function [bestParameter1,bestParameter2] = ransac_demo(data,num,iter,threshDist,inlierRatio)
% data: a 2xn dataset with #n data points
% num: the minimum number of points. For line fitting problem, num=2
% iter: the number of iterations
% threshDist: the threshold of the distances between points and the fitting line
% inlierRatio: the threshold of the number of inliers

%% Plot the data points
figure;plot(data(1,:),data(2,:),'o');hold on;
number = size(data,2); % Total number of points
bestInNum = 0; % Best fitting line with largest number of inliers
bestParameter1=0;bestParameter2=0; % parameters for best fitting line
for i=1:iter
%% Randomly select 2 points
    idx = randperm(number,num); sample = data(:,idx);
%% Compute the distances between all points with the fitting line
    kLine = sample(:,2)-sample(:,1);% two points relative distance
    kLineNorm = kLine/norm(kLine);
    normVector = [-kLineNorm(2),kLineNorm(1)];%Ax+By+C=0 A=-kLineNorm(2),B=kLineNorm(1)
    distance = normVector*(data - repmat(sample(:,1),1,number));
%% Compute the inliers with distances smaller than the threshold
    inlierIdx = find(abs(distance)<=threshDist);
    inlierNum = length(inlierIdx);
%% Update the number of inliers and fitting model if better model is found
    if inlierNum>=round(inlierRatio*number) && inlierNum>bestInNum
        bestInNum = inlierNum;
        parameter1 = (sample(2,2)-sample(2,1))/(sample(1,2)-sample(1,1));
        parameter2 = sample(2,1)-parameter1*sample(1,1);
        bestParameter1=parameter1; bestParameter2=parameter2;
    end
end

%% Plot the best fitting line
xAxis = -number/2:number/2;
yAxis = bestParameter1*xAxis + bestParameter2;
plot(xAxis,yAxis,'r-','LineWidth',2);
```

Figure 17. Matlab function for the RANSAC line fitting algorithm that was utilized.

The algorithm randomly fits lines through all available values of the graph with 10.000 iterations. The line that describes most of the values the most often is the outcome of the iterations and therefore it should represent the hypothetical baseline. This line was then subtracted from the raw fluorescence traces to correct for the deviations from baselines. Obviously, the disadvantage of this approach was its line nature. For traces with a stable baseline the results are satisfying. Problems of fitting a line occur whenever the raw calcium traces are more instable or have a phenotype as shown in Figure 18A. In general, the more exponential-like bleaching occurs, the worse RANSAC line-fitting will perform for this type of calcium trace phenotype. Calcium traces from cells that did not show any activity or change in fluorescence levels throughout recording are also a problem. The reason is that essentially too many lines describe the values as good, as there are no outliers that could be calcium peaks for example. In my case this leads to results like the example in Figure 18B. The algorithm can be applied very successfully to “proper” calcium traces, with distinct peaks originating from a perfect baseline without any decline or increase in fluorescence values over time (Figure 18C). (Thanks to Dr. Frank Herrmannsdörfer for helping with implementing the RANSAC line fitting code)

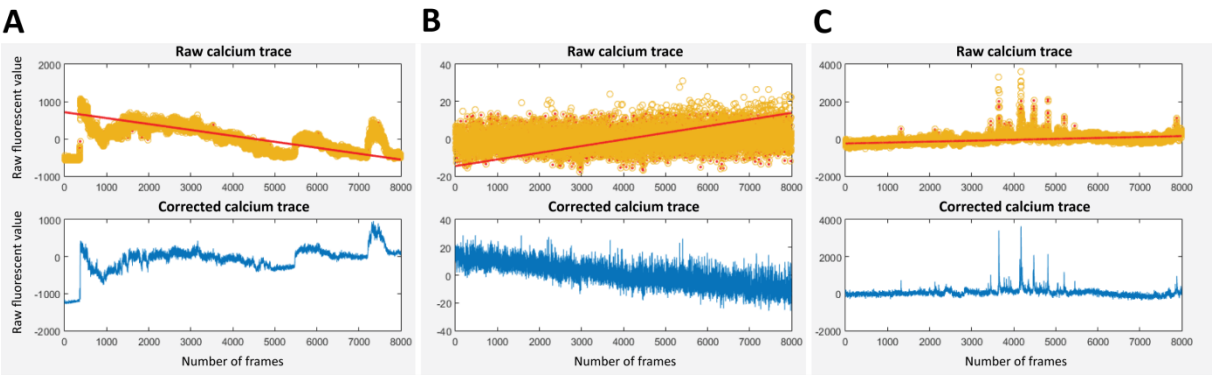

Figure 18. Examples of RANSAC line fitting algorithm results to correct for baselines of calcium imaging traces. The red line shows the 'best' found baseline of the algorithm. A) A challenging calcium trace to fit an accurate baseline. The algorithm determines the line that fits most of the values, but is clearly failing in describing the correct baseline. B) An example of a calcium trace from a cell that was inactive during recording. Here the suggested baseline is also incorrect. This is an intrinsic problem of the algorithm, which occurs when trying to fit baselines into traces that are missing any peaks. C) Example of a correct prediction of the baseline of a "text book" calcium imaging trace.

2.5.6 Calcium imaging baseline correction with curve fitting algorithms

As the problems became apparent with using the rigid RANSAC line fitting algorithm for fluctuating baselines of calcium signals, a more flexible solution was needed. The Matlab 2016b intrinsic Curve Fitting Toolbox 3.5.4 was utilized to apply one of four constrained curve fitting models, from rigid to flexible. The grade of flexibility was determined by the degree of the polynomial fit that was utilized for every model. For example, a fourth degree polynomial fit can therefore be considered as a rigid fitting and a fifth degree polynomial fit as more flexible. The most flexible model utilized for this type of data was using a seventh degree polynomial equation without constrains to fit the curves. The parameters for each fitting model were adjusted on several calcium traces from my measurements, and the functions were exported from the toolbox. A user interface was added to the script to display the result of every curve fitting model and allowed the user to choose the best fit manually. The user interface displays the raw trace with the respective fitted curve, and the result of correcting the raw trace using this curve. The correction is performed by simply subtracting the raw trace from the fitted curve that supposedly represents the predicted baseline. Also, the user can choose to keep the raw trace, when fitting the different curves would lead to incorrect baselines. The whole process is reiteratively performed on all single cell calcium traces.

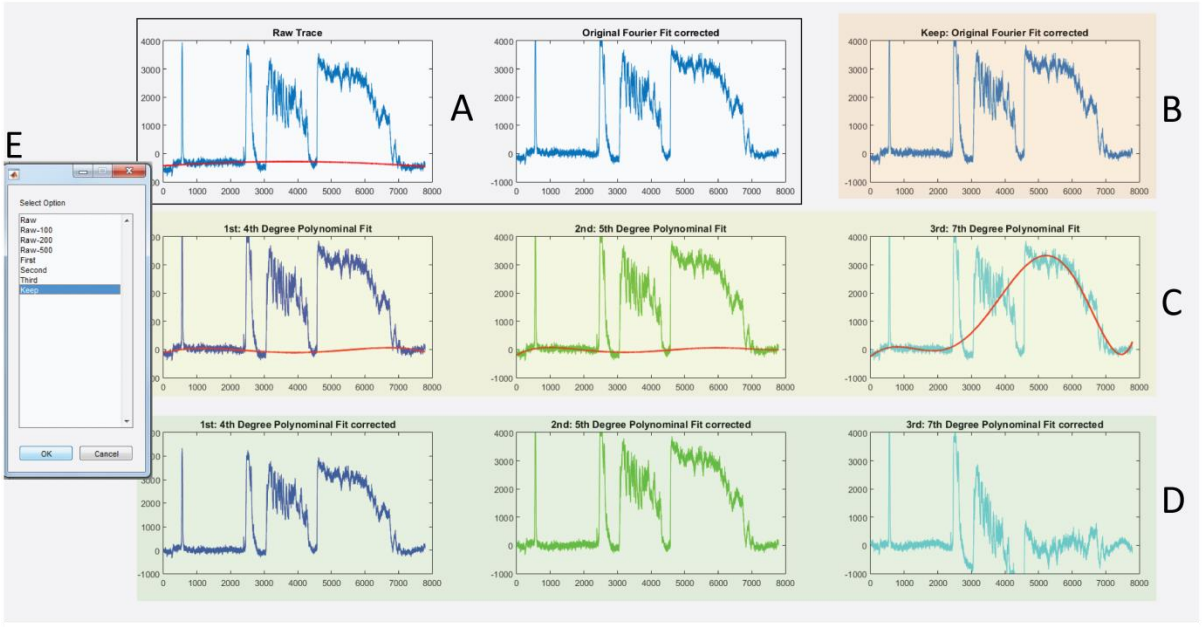

Figure 19. User interface of the calcium trace correction tool to assign a proper baseline for calcium traces. A) Raw calcium trace and the rigid type standard curve fit in red. On the right is the result of the fitted red line from the left panel. B) Rigidly corrected resulting trace after subtracting the curve from A. C) Three curves from 4th, 5th, and 7th degree polynomial fittings. D) The results of the accordingly corrected traces from C are shown. E) Pop-up window for the user input, where the corrected trace can be chosen.

To reduce the necessary user input, calcium traces from low activity cells were automatically fitted with a very constrained rigid curve fitting model. Therefore, for every experiment the standard deviations 50th percentile was determined. Calcium traces that had lower standard deviations than this 50th percentile value were considered to have a low activity. Calcium traces that showed a standard deviation above this value were displayed to the user for manual correction.

It is crucial for subsequent spike estimation from calcium traces, that they have a nearly perfect baseline. Otherwise the utilized spike estimation algorithm MLspike was not able to accurately process the calcium traces.

The problem becomes more pronounced if calcium traces of one cell are concatenated across different imaging sessions, i.e. time points.

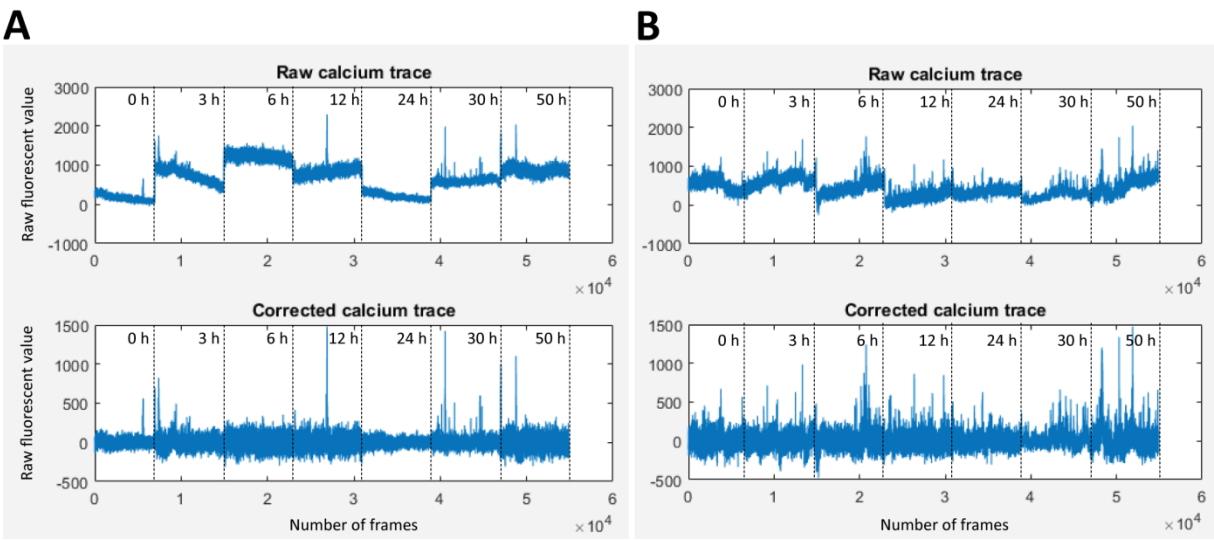

Figure 20. Two examples that demonstrate the necessity to correct the raw calcium traces. A & B) The upper graph shows the raw concatenated calcium traces from recording time points 0 h to 50 h, with shifted baselines. The lower graphs show the concatenated corrected calcium traces for the same consecutive time points with a common baseline.

2.5.7 Spike estimation from extracted calcium traces

With the established image processing pipeline calcium traces could be extracted from single cells and analyzed over multiple time points. To analyze the activity of neuronal cell populations and inferring their spiking patterns, the MLspike algorithm was used (Deneux et al., 2016). To correctly extract spiking patterns from calcium imaging data, the algorithm needed to be calibrated first. The calibration was necessary to adjust for the type of calcium signals present in the recordings. Therefore, calibration was done with a dataset from the original publication of the GCamP6f calcium indicator (Chen et al., 2013a) which was also used in my project. This original dataset consisted of 35 cells spanning from low to high frequency activity calcium recordings in combination with electrophysiological patch clamp recordings. Since the calcium signals in this published dataset are very similar to my recordings, I could calibrate the algorithm to have the lowest deviation from the true number of spikes. In total, 16 different parameter combinations were tested to approximate spiking from calcium traces. The combination of the MLspike intrinsic parameters, Hill 2.80, C(0) 0.65 and Drift 3.00 led to only a minor average underestimation of -1.85 % compared to patch clamp determined spiking numbers (Table 2).

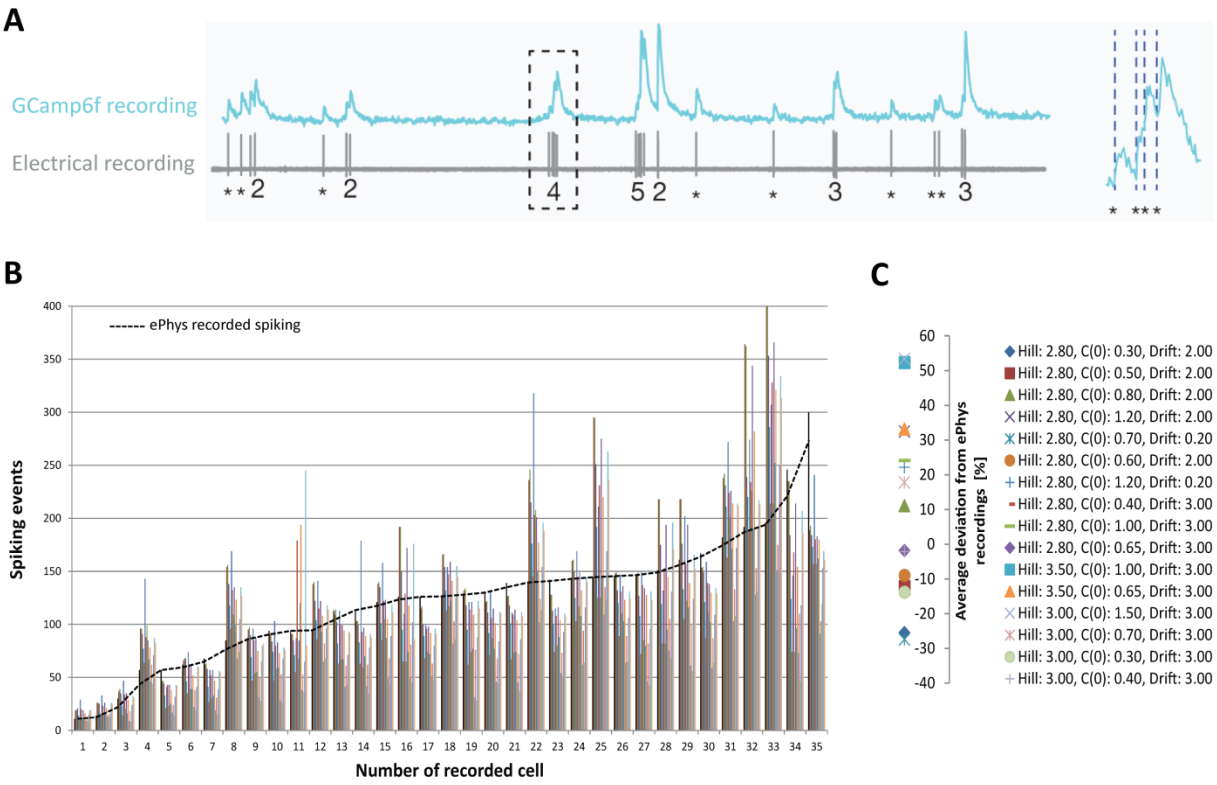

Figure 21. Calibration of the spike estimation algorithm MLspike to our type of calcium imaging data. A) Figure of the original GCamp6f publication (Chen et al., 2013a). Traces of simultaneous calcium imaging and patch clamp electrophysiological recordings are shown. Asterisks represent a single spiking event. B) Predicted spikes for each recorded cell (n=35) with different parameters. The dashed black line represents the number of spiking events which were determined by electrophysiological recordings. Colored bars represent the number of predicted spikes using the parameters shown in C. C) Average deviation of the predicted spikes from the electrophysiological recorded spike numbers with 16 different parameter combinations. The most accurate spike prediction was obtained with the MLspike parameters Hill 2.80, C(0) 0.65 and Drift 3.00.

MLSpike parameter combination	Average deviation from measurement [%]
Hill: 2.80, C(0): 0.70, Drift: 0.20	-27.42066
Hill: 2.80, C(0): 0.30, Drift: 2.00	-25.49859
Hill: 2.80, C(0): 0.30, Drift: 2.20	-24.22409
Hill: 2.80, C(0): 0.40, Drift: 3.00	-14.26479
Hill: 3.00, C(0): 0.30, Drift: 3.00	-13.89428
Hill: 2.80, C(0): 0.50, Drift: 2.00	-12.33106
Hill: 2.80, C(0): 0.60, Drift: 2.00	-8.996787
Hill: 3.00, C(0): 0.40, Drift: 3.00	-2.186652
Hill: 2.80, C(0): 0.65, Drift: 3.00	**-1.851937**
Hill: 2.80, C(0): 0.80, Drift: 2.00	11.07704
Hill: 3.00, C(0): 0.70, Drift: 3.00	17.76917
Hill: 2.80, C(0): 1.20, Drift: 0.20	22.14826
Hill: 2.80, C(0): 1.00, Drift: 3.00	24.06621
Hill: 2.80, C(0): 1.20, Drift: 2.00	32.4023
Hill: 3.50, C(0): 0.65, Drift: 3.00	33.13264
Hill: 3.50, C(0): 1.00, Drift: 3.00	52.30279
Hill: 3.00, C(0): 1.50, Drift: 3.00	53.38707

Table 2. Results of MLspike with different parameters for the spike estimation algorithm. The parameters shown in bold produced the most accurate estimation of spiking from calcium traces. The difference between electrophysiologically recorded spikes and estimated spikes from the calcium imaging is given in percent.

2.5.8 Calculation of distance and activity relations of PV/Cre+ cells to untargeted cells

The distance between untargeted cells (all GCamP6f expressing cells) and targeted ones (PV or Cre^+, tdTomato expressing) was summed up and divided by the number of targeted cells (PV or Cre^+). The term "targeted cells" is used to describe cells that were virally transduced with components of the Tet system and were potentially inducible, while "non-targeted cells" are all others. This value is low if the untargeted cell is in relative proximity to many targeted cells and high if it is further away from targeted cells. Therefore, this value shows the relative average distance to targeted cells. The calculations have been performed using Matlab with the extension called ReadImageJROI (Muir and Kampa, 2014) to extract the positions of the respective ROIs. The targeted and untargeted ROIs have been set using ImageJ Fiji distribution (Schindelin et al., 2012). The spontaneous activity before and after induction of Kir2.1 was averaged, and a ratio calculated. To avoid divisions by zero, the values were increased by 1, and all ratios above 1 were plotted ($\frac{mean\ (induced\ activity)+1}{mean(basal\ activity)+1}$>1). The relative average distance was set in relation to the ratio of activity changes before and after induction.

2.6 Statistical analyses

For the analyses Prism 6 (GraphPad, La Jolla, CA, USA) or Matlab software were used. For statistical analyses the measurement data were routinely tested if they were normally distributed or not. If they were not, and the experiment had more than 3 independent groups (for example different time points), the nonparametric ANOVA Kruskal-Wallis test was applied. In addition, follow-up tests were conducted (Matlab) to compare mutual differences between single data points from the consecutive measurements (Chapter 3.4). If single groups, i.e. time points, were compared, usually the nonparametric Wilcoxon signed rank test using median values was applied.

For experiments with high variability and insufficient n numbers below 5, a linear regression fit was applied and the deviation to zero tested (Chapter 3.7). In general, if none of the aforementioned statistical tests would indicate a significant difference, a linear regression fit was applied to test for a trend.

Since the Wilcoxon signed rank test requires median values, the One sample t-test was applied to test for significance between single measurements, if only mean values were available (Figure 38). Otherwise the nonparametric ANOVA Kruskal-Wallis test was applied (Figure 41) to test for the entire groups (Chapters 3.13 & 3.12).

3 Results

3.1 Establishment of the TetOn system

3.1.1 Testing different TetOn systems

To incorporate a system with the lowest possible leakiness I tested different available genetic constructs. During these studies I tested a version of the TetOn system with an autoregulatory induction loop. It is designated RANGE, and was designed as a polycistronic construct containing the transrepressor and the transgene of interest (Chen et al., 2013b). In this construct, the TetO7 promoter region is controlling a synapsin promoter. Minor "background" expression of the transrepressor silences its own the expression as well as the whole cassette by binding to the TetO7 region and silencing the downstream synapsin promoter. After administration of Doxycycline, this autoregulatory loop will set free the expression of transgenes by binding to the transrepressor thereby dissociating it from the TetO7 promoter site. The big disadvantage of this approach is the obvious need of an initial "leakiness" to reach effective amounts of transrepressor to inhibit expression. Therefore, this system is not suitable for experimental paradigms in which leakiness should be as low as possible. Nevertheless, it nicely incorporates all necessary elements of the TetOn system into a single rAAV vector. I tested the RANGE system to assess its usefulness my experiments. As expected, it led to expression levels higher than with the original TRE controlled plasmids in the uninduced state, in the absence of Doxycycline.

To have minimal promoters with potentially less leakiness, I obtained different plasmids from Dr. Rainer Löw, as described in the respective publication (Loew et al., 2010). In the publication different variants of the Ptet promoter were generated and tested, some of which showed great improvements in HEK293T and HeLa cells in regard to their leakiness. I tested the most promising variants in our neuronal primary cultures and could not get any visible induction at all, for none of the promoters. In HeLa cells, I found that induction was moderate with these promoters, but they still showed some leakiness. My conclusion was, that these promoters are too weak for primary hippocampal neurons even in the induced state.

At the end, bidirectional Tet-responsive constructs with CMVmin promoters obtained from Dr. Rolf Sprengel turned out to be the best. This bidirectional promoter seems to lead to low basal activity levels, i.e. leakiness in the absence of Doxycycline in neuronal cells, our target cells. After cloning in the respective transgenes, they were referred to as ResponderTET. Thus, these constructs

incorporate a bidirectional Ptet promoter with a fluorescence marker protein and a transgene of interest. All produced constructs are described in detail in chapter 2.1.1.

I combined the transactivator and transrepressor proteins in one viral vector together with a fluorescence marker protein. The original polycistronic construct from Dr. Sprengel contained rtTA, Luciferase, and a fluorescent mKusabiraOrange (mKO) reporter (Chen et al., 2013b) in a rAAV backbone. I replaced the Luciferase with a transrepressor from the Blau laboratory (Rossi et al., 1998). The resulting construct was a polycistronic transcript that was spliced during translation by the *Thosea asigna* Virus 2A-peptides to generate single proteins (Figure 7).

For experiments, the original Sprengel construct without the transrepressor tTR was used as a control to compare the effects of the transrepressor on leakiness *in vitro* and *in vivo*. Therefore, rAAV of both constructs, i.e. with and without tTR, were produced and tested.

3.1.2 Effect of transrepressor tTR on expression levels *in vitro*

The produced rAAVs were tested *in vitro* by co-transduction with the ResponderTET construct from Figure 7B. With this experimental setup the fluorescence levels of the mVenus reporter gene were used as an indicator for leakiness in the absence of Doxycycline for both constructs. Therefore, a dose-response curve experiment was conducted to observe the strength of the Doxycycline-dependent response in hippocampal neuronal cultures. The cultures were co-transduced at DIV9 (days *in vitro*) with the ResponderTET and the respective DriverTET rAAV with and without tTR. At DIV23 Doxycycline was administered to the cells at different final concentrations ranging from 0 to 50 µM. 2 days later the cells very fixated and analyzed (Figure 22).

Interestingly, in hippocampal primary cell culture I often observed cells with high amounts of leakiness that were morphologically of non-neuronal origin, while the non-dividing hippocampal neurons showed no visible leakiness.

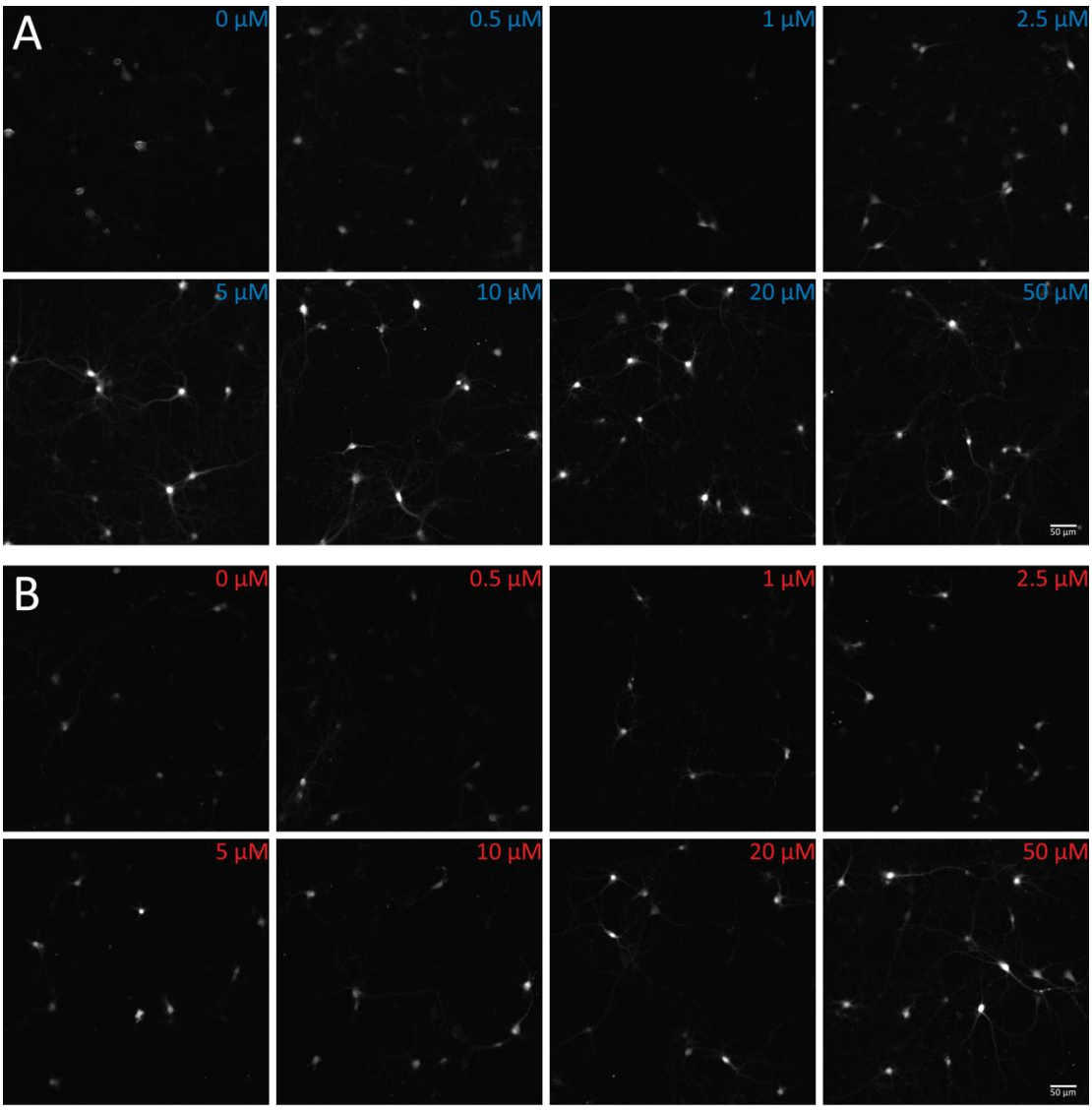

Figure 22. Assessing the effects of the transrepressor tTR on leakiness and induction levels. Dose-response experiments with increasing Doxycycline concentrations *in vitro*. Hippocampal cultures were co-transduced at DIV9 with DriverTET and ResponderTET with/without transrepressor tTR rAAVs. A) with tTR & B) without tTR show examples of cells administered with increasing concentrations of Doxycycline at DIV23. The cells were fixated 2 days later. C) Quantification of the mean fluorescence values of cell bodies with increasing Doxycycline concentrations. (Error bars: SD; n=33 cell bodies on average per condition; Scale bar: 50 µm)

The effects of incorporating the tTR into the DriverTET construct were surprising. Without the tTR the dose-response to Doxycycline was of a rather linear nature in the respective Doxycycline spectrum. The greatest impact of the tTR on expression levels appears to be changing the system from a linear dose-response do a more discrete step or switch-like response between 2.5 µM and 5 µM Doxycycline concentrations. In theory, the presence of the tTR should just have an effect on the baseline activity and not the induction levels, which has been described before (Freundlieb et al., 1999). When the tTR was present, the baseline leakiness seems to be slightly reduced at low Doxycycline concentrations between 0 µM and 2.5 µM (Figure 22C). Then at 5 µM the expression level suddenly reaches the maximum plateau level, which is the same with increasing Doxycycline concentrations. These high expression levels are not fully achieved without tTR, and it is not clear why. This step-like and almost binary on-off switch modality is ideal for experiments with a necessity for low leakiness before induction and prompt, strong onset of expression after induction.

3.1.3 Effect of transrepressor tTR on leakiness *in vivo*

rAAVS with and without tTR were also compared in *in vivo* experiments. Animals were injected with a 1:1 mixture of DriverTET with and without tTR and the ResponderTET rAAVs. Three to five weeks later the basal fluorescence levels were assessed qualitatively by comparing the fluorescence levels on the respective brain hemispheres of the animals (Figure 23).

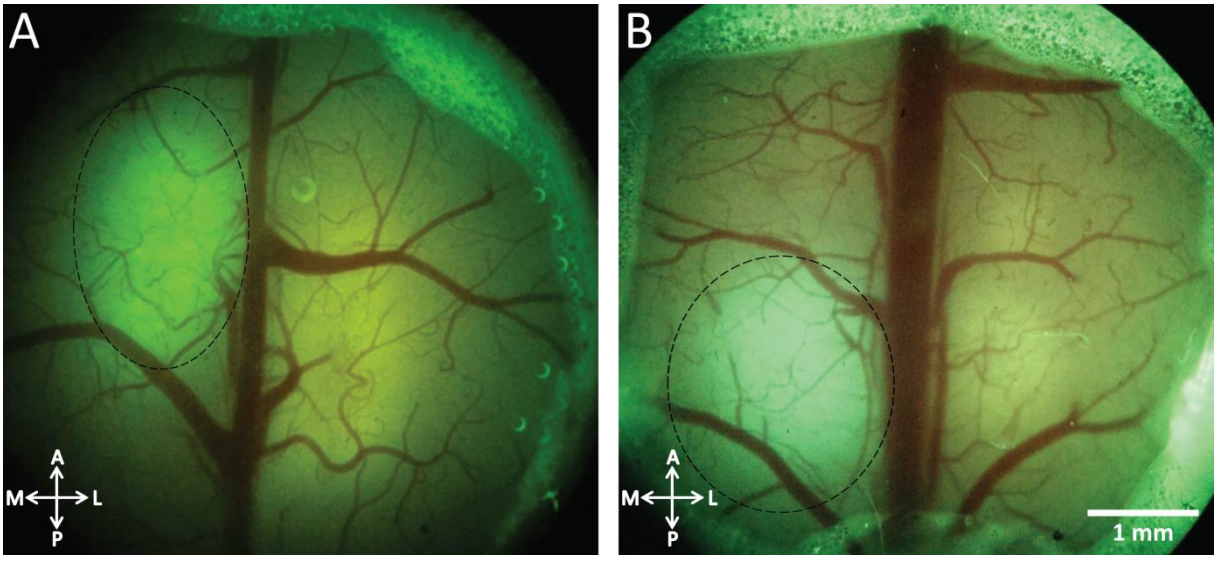

Figure 23. Assessing the effect of tTR on leakiness *in vivo*. Epifluorescence overview images of example mouse brain hemispheres injected with rAAVs 3 – 5 weeks after surgery before Doxycycline administration. A) The left brain hemisphere was injected with a 1:1 mixture of DriverTET without tTR and ResponderTET rAAVs. Right brain hemisphere with DriverTET + transrepressor tTR and ResponderTET rAAVs. B) The left hemisphere was injected with the ResponderTET rAAV only, whereas the right hemisphere was injected with a 1:1 mixture of DriverTET with tTR and ResponderTET rAAV. The dashed regions with the intense green mVenus fluorescence indicate the injection areas with

leakiness in the absence of tTR. The pale yellow color of the right hemispheres is mostly autofluorescence from the brain tissue and perhaps some mKO fluorescence from the DriverTET rAAVs. (Scale bar: 1mm)

It is apparent that the right brain hemispheres show far less leaky expression of green fluorescent mVenus and only slight yellow color most likely derived from the DriverTET rAAVs mKO fluorescent reporter. These examples show that the ResponderTET construct by itself is mostly the source of leakiness due to its TRE with a CMVmin promoter.

The results clearly highlighted that incorporating the tTR into the DriverTET construct tremendously improves the leakiness problem normally seen without tTR. It was thus decided that all further experiments would be done with constructs carrying the transrepressor tTR, together with the transactivator rtTA.

3.2 Comparison of rAAV purification methods

We decided to increase the titer of our rAAV productions because some of our rAAV batches had weak expression levels. Simply adding a larger volume of rAAVs to the cell culture wells led to toxicity, rather than increasing the expression levels. Also, this approach was not suitable for subsequent *in vivo* injections of the rAAVs, as the injection volume was limited to about 1.5 µL. Therefore, I tried a different purification method to increase the titer. The group of Dr. Rolf Sprengel was routinely applying a rAAV purification protocol utilizing a "Fast protein liquid chromatograph" (FPLC) coupled with a high-affinity chromatography column. To compare our with their purification method, a crude rAAV cell lysate was split and purified with our standard Heparin Agarose method and with HiTrap AVB Sepharose columns using a FPLC according to the protocols used by the Sprengel group.

Increasing volumes of purified rAAV solution were applied to neuronal hippocampal primary cell cultures at DIV5 and cells were fixated at DIV16. The resulting fluorescence values were used as an approximation for the transgenic expression levels of the rAAV constructs. The data showed a remarkable superiority of the FPLC based purification method compared to the Heparin Agarose method. The FPLC purified rAAV solution was obviously higher concentrated and reached 4 to 5 times higher mean fluorescence levels in cell culture (Figure 24).

It also seemed that adding larger volumes than 1 µL to the cell cultures did not lead to increased fluorescence values, but rather a decrease. One possible explanation might be a potential cytotoxicity originating from chemical residues in the purified viral solutions. Cytotoxicity originating

from a higher rAAV titer seems not to be a problem, at least not at the viral titer levels tested. An optimal volume for our cell culture wells independent of the titer seems to be between 0.5 µL and 0.75 µL.

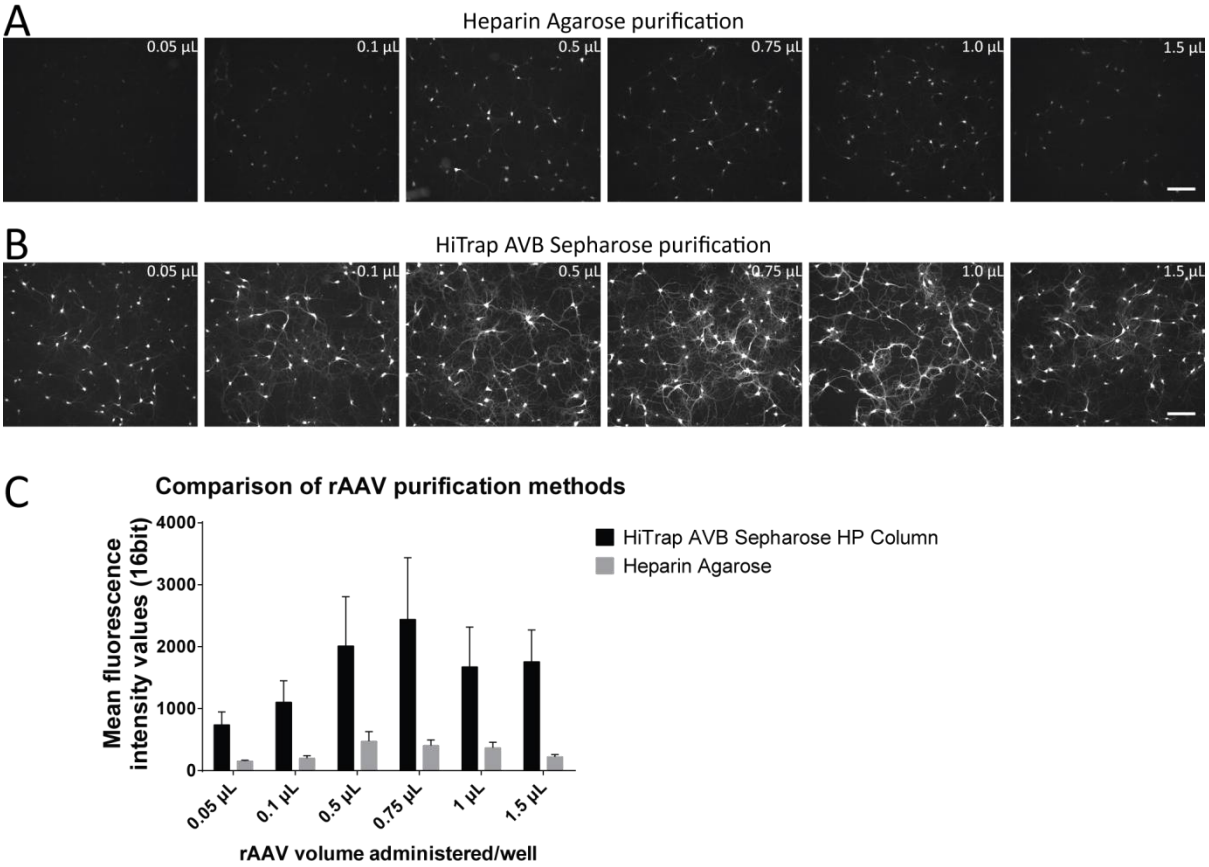

Figure 24. Comparison of rAAV purification methods using primary hippocampal cell cultures. The crude cell lysate was split and purified with two different methods. The resulting viral solutions were added to cell cultures at DIV5 and were fixated at DIV16. A) & B) The FPLC based HiTrap AVB Sepharose purification method led to much higher fluorescence levels, compared to the standard purification method with Heparin Agarose. C) Graph showing the mean fluorescence values of the cell somata with different volumes of viral solution administered to the cultures. The purification with HiTrap AVB Sepharose produced approximately 5-times higher mean fluorescence intensity values compared to the Heparin Agarose purification. (Error bars: SD; n=50 cell bodies on average per condition; Scale bar: 200 µm)

Another big advantage of utilizing the FPLC purification device was the UV spectrum readout at 260/280 nm of the elution profile. This arbitrary value is a good measure for the amount of rAAV particles in the eluate. With this value, I could compare the relative concentration of the obtained rAAV solutions and the overall success of the purification process. The use of UV absorption properties of rAAV solutions to measure the viral concentration was shown before (Sommer et al., 2003).

The HiTrap AVB Sepharose HP columns are optimized for rAAV purification, but are very costly (250 € per column). I also tested HiTrap Heparin HP columns (~50 €), which are successfully used in Prof. Dr.

Hilmar Badings department. The purification with these cheaper columns also yielded good results. Qualitative comparison of a single run with the expensive HiTrap AVB Sepharose with several runs using the cheaper HiTrap Heparin HP columns did not reveal obvious differences. Peak absorption profiles for both columns were similar; therefore the cheaper HiTrap Heparin HP columns were used for certain critical rAAV productions. The standard Heparin Agarose protocol in the lab was used for all others.

My original goal was to constitutively express GCamP6f via DriverTET by replacing mKO in the polycistronic construct. Unfortunately, this DriverTET produced only some GCamP6f signal *in vitro* and no signal *in vivo*, despite a successful column purification procedure. For GCamP6f a much higher expression level was needed *in vivo*, which could not be achieved with self-made rAAVs. A possible explanation for that might be that these constructs were polycistronic, as 3 transgenes were incorporated separated by two 2A-peptides in between. This might have reduced the expression levels of these constructs.

Instead, a synapsin promoter driven GCamP6f virus (AAV1.Syn.GCamP6f.WPRE.SV40) was purchased from UPenn Vector Core (Perelman School of Medicine, University of Pennsylvania, USA) to be utilized in my experiments.

3.3 Validation of functionality of the rAAV based TetOn system

The general efficacy and Doxycycline dependency of the TetOn system with our self-made rAAVs has been show in chapter 3.1.2. To validate the efficacy of the self-made rAAVs, they were all first tested *in vitro*. Neuronal cultures were earliest transduced at DIV5, when the cultures had overcome their initial sensitivity towards all kinds of cellular stress. Adding rAAVs to cultures prior than DIV4 was often toxic to the neurons. A week later, when the fluorescence of the constitutively expressed mKO from the DriverTET construct was visible, cells were treated with a final concentration of 5 µM Doxycycline to induce transgene expression of the ResponderTET construct. A successful induction of transgene expression was assessed by the green fluorescence from the mVenus reporter protein the day after (Figure 25).

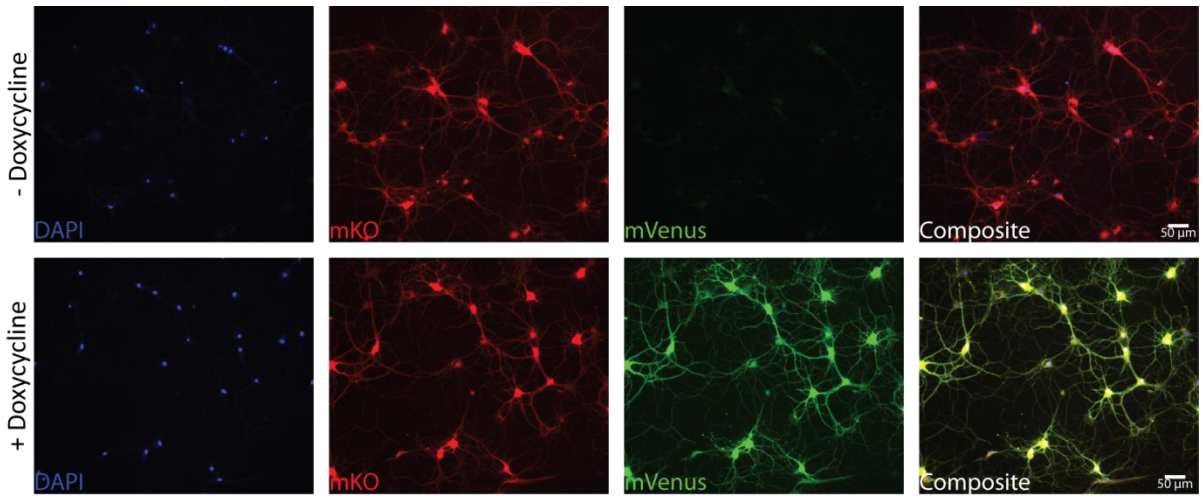

Figure 25. Transgene induction *in vitro* using the TetOn system. Hippocampal cultures were transduced at DIV7 with a 1:1 mixture of DriverTET and ResponderTET rAAVs and Doxycycline was added at DIV15 at a final concentration of 5 µM (lower row). Constitutive expression of mKO (red) originated from the DriverTET construct, whereas inducible expression of mVenus (green) derived from the ResponderTET construct. Nuclei are stained with DAPI (blue). Note the low expression of mVenus fluorescent reporter protein without induction. (n=1 culture for each condition)

3.4 Effect of induced Kir2.1 and NaChBac on neuronal activity

We wanted to acutely manipulate neuronal activity by rapid transgene expression. The potassium channel protein Kir2.1 was chosen to hyperpolarize the resting membrane potential of neurons and by this reduce their activity (Burrone et al., 2002). Hypopolarization of neuronal membranes was achieved through the expression of the sodium channel NaChBac. Neurons expressing NaChBac should therefore increase their activity.

In total six different experiments for the Kir2.1 induction and four for the NaChBac and Control experiments were conducted. For each experiment, approximately 100 cell bodies were imaged.

While there was a high variability of neuronal activities across all the different cells on average, the induction of the transgenes led to a rapid change of calcium activity levels, i.e. GCamP6 fluorescence signals, *in vitro*. In these experiments, the induced expression of Kir2.1 led to a decrease of activity on average by ~40 % within 5 h after administration of Doxycycline (Figure 26). The induction of NaChBac on the other hand, led to an increase of about ~70 % after 5 h. The steady change in activity starting one hour after induction appears to be a reflection of rapid transgene expression. Also, the basal activity levels were similar compared to control experiments without Doxycycline. This also indicates the low levels of leakiness that can be achieved with this system.

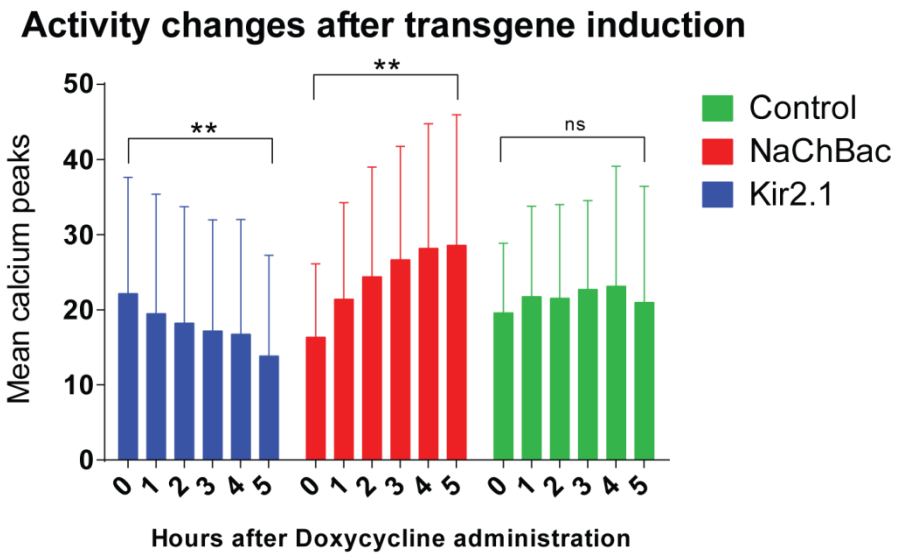

Figure 26. Effect of the induced transgenes Kir2.1 and NaChBac on neuronal activity *in vitro*. Cells were transduced with either a mixture of DriverTET and RTETbi-mVenus-Kir2.1 or DriverTET and RTETbi-mVenus-NaChBac together with a GCamP6f rAAV at DIV7-10. Approximately one week later, cultures were induced with Doxycycline at a final concentration of 10 µM. Live cell imaging was performed for up to 5 h. Cells were imaged every hour for 5 minutes and spontaneous calcium transients were quantified. Kir2.1 expression decreased the average number of the calcium transients from 22 to 13 (n=622 somata from 6 cultures; p=0.0011; R^2=0.9461). For NaChBac the transients increased on average from 16 to 28 (n=422 somata from 4 cultures; p=0.0035; R^2=0.9055). The control cells were not treated with Doxycycline and did not show any significant change in activity levels over time (n=568 somata from 4 cultures; p=0.295; R^2=0.2660). (Error bars: SD; statistical test: linear regression fit)

These findings demonstrate that from activation of the transactivator rtTA after Doxycycline administration, to the transcription of the DNA, and translation, and trafficking of the proteins to the neuronal membrane, Doxycycline dependent protein expression must be rapid. In fact, there was a significant difference observed after 2 h for Kir2.1 (p=0.0026) and after 1 h for induced NaChBac (p<0.0001) with the Wilcoxon signed rank test.

Presumably, one or two hours after induction only a small number of channels have been synthesized and incorporated. Yet, there is a clear trend of changing neuronal activities suggesting that these channels are quite potent in small amounts. Therefore, a small number of these channel proteins will have an effect on the neuronal resting membrane potential and the spontaneous neuronal activity. Concluding, it is apparent that the induction of Kir2.1 and NaChBac has a rapid and significant effect on the spontaneous activity of neuronal cultures *in vitro*. By having tested two oppositely acting channel proteins, one can exclude toxicity effects of the transgene induction with Doxycycline. Of course, it could be argued that the Kir2.1 dependent decrease in activity might simply be due to overexpression toxicity, but this could then not explain the increase in activity seen after NaChBac expression.

With these experiments the efficacy of the rAAV based TetOn system, as well as its robust and rapid inducibility, while having low levels of leakiness were confirmed. Additionally, the transgenes for the manipulation of neuronal activity levels, Kir2.1 and NaChBac showed a rapid and significant effect on neuronal activity after induction.

3.5 Validation of Cre dependent expression in ResponderTET constructs

To be able to target specific cell types the ResponderTET constructs were further optimized. As a lot of available transgenic mouse lines express Cre recombinase in a cell-type specific manner, the transgene in the ResponderTET constructs was rendered Cre recombinase dependent ("floxing"). The fluorescent reporter of the bidirectional ResponderTET was not inactivated by floxing and is therefore expressed in the presence of Doxycycline independent of the Cre recombinase. However, the original idea was to monitor induction with Cre-dependent fluorescence originating from the reporter protein in live cells. Floxing both, the transgene and the fluorescent reporter was not possible with the same DIO sequences. Instead, to validate expression of the transgene after unfloxing and induction with Doxycycline, a C-terminal HA-tag was added to Kir2.1 and NaChBac (Lobbestael et al., 2010). Therefore, cells had to be additionally Cre recombinase-positive in order to recombine and activate tet-dependent inducibility of the transgenes. Then, induction was possible with Doxycycline and cells should express the same amounts of protein as in the original constructs without the DIO sequences.

To validate the efficacy of these floxed and inducible transgenes of the ResponderTET constructs, the cells were transduced with DriverTET and RTETbi-NLSmtagBFP-DIO-Kir2.1 (Figure 27A) either with or without a Cre expressing rAAV. In both conditions the cultures were induced with Doxycycline. As a negative control the cultures were not treated with Doxycycline (Figure 27B).

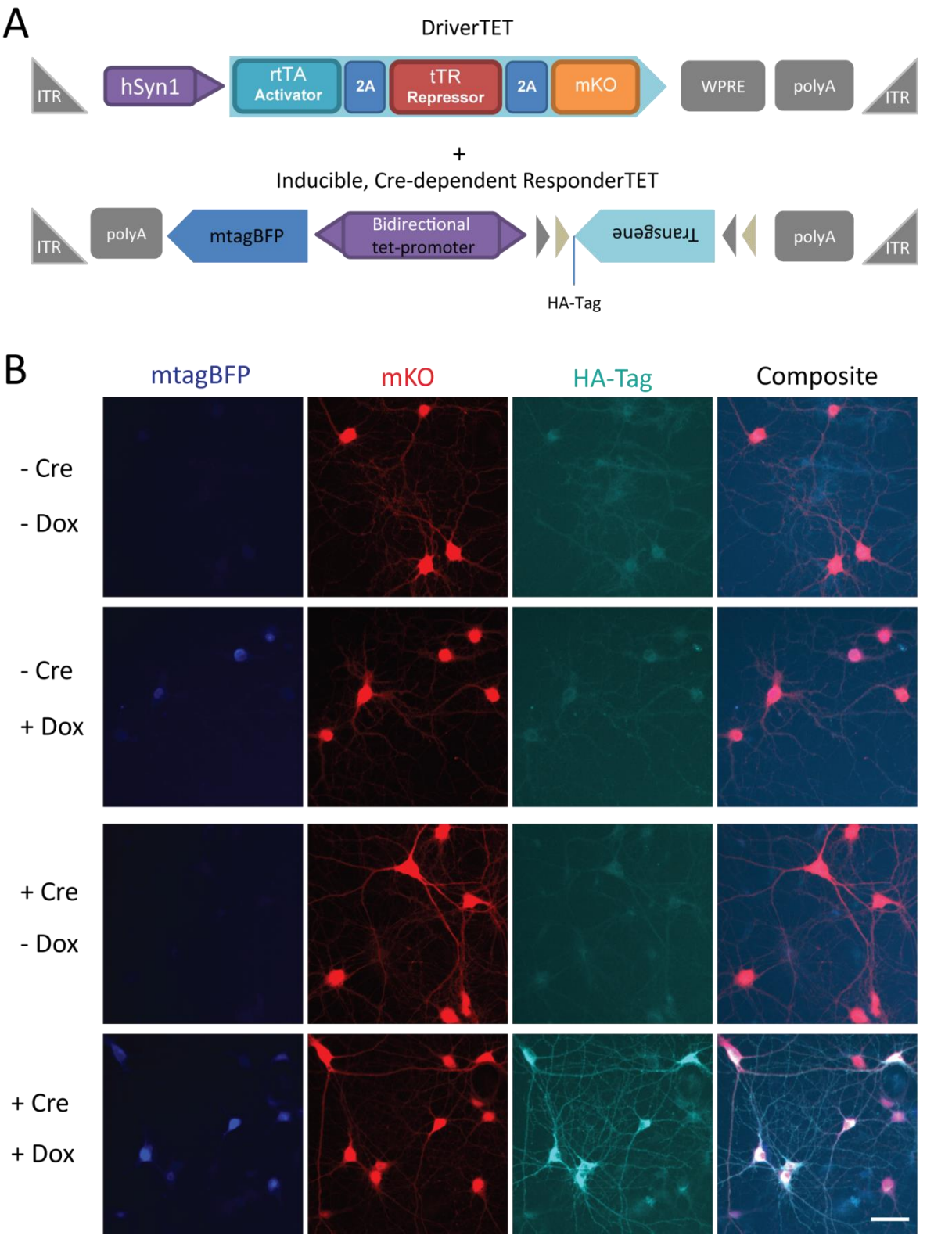

Figure 27. ***In vitro*** **validation of the Cre dependent TetOn system. A) Schematic representation of the rAAV constructs for the Cre dependent and inducible TetOn system. The ResponderTET construct will express the transgene only if the Cre recombinase is present in the respective cell and only after induction with Doxycycline. B) Neuronal primary cultures were transduced with the rAAVs from A, with or without a synapsin driven Cre recombinase rAAV. Note the nuclear localized mtagBFP fluorescence of the RTETbi-NLSmtagBFP-DIO-Kir2.1 construct. In the absence of either Doxycycline and/or Cre recombinase, little signal is observed. (Scale bar: 50 µm, n=1 culture for each condition)**

The idea was to have constructs for *in vivo* experiments would allow three color imaging. With the red spectrum occupied for constitutively expressed tdTomato (and some mKO expression from DriverTET) and the green spectrum used for the calcium indicator GCamP6f, only blue or near infra-red fluorescence was suitable. Since there are some limitations of the 2P excitation for long wavelengths with our setup, I decided to use a blue fluorescent protein. I cloned and compared the blue fluorescent proteins EBFP2 (Ai et al., 2007) and mtagBFP (Subach et al., 2008) qualitatively. The fluorescent protein mtagBFP was chosen as it was much brighter by visual inspection.

In a recent publication the brightness levels of mtagBFP (32.8 x $10^{-3}M^{-1}cm^{-1}$) were demonstrated to be not as bright as mVenus (52.5 x $10^{-3}M^{-1}cm^{-1}$) values (Cranfill et al., 2016). To overcome this, mtagBFP was localized to the nucleus by adding an N-terminal NLS (nuclear localization sequence) peptide (Kalderon et al., 1984). By this, the fluorescent protein should be more concentrated in the nucleus and its detection should be easier. Also, spatial mixing of spectral signals with GCamP6f would be avoided, as GCamP6f is efficiently excluded from the nucleus. Taken together, while the brightness of mtagBFP after induction was lower than mVenus, it was easily possible to detect mtagBFP expression *in vitro*.

Detection of the HA-Tagged protein by antibody staining was hampered by low staining efficiency and high non-specific staining, which can also be observed in Figure 27B. The limitations of the HA-Tag antibody staining approach were surprising, as it was expected to show high levels of specific staining. Yet, it was possible to show that the RTETbi-NLSmtagBFP-DIO-Kir2.1 construct is bidirectionally inducible and the transgenes are successfully unfloxed in the presence of the Cre recombinase.

3.5.1 Validation of induced transgene expression *in vivo*

Validating the successful induction of gene expression *in vivo* was not possible with the mtagBFP fluorescent reporter. Neither with 2P *in vivo* imaging nor in post-hoc fixated and sliced brains could any signal from the mtagBFP spectrum be detected. For the 2P *in vivo* image acquisition the physical limitations of the approach because of photon scattering and absorbance of the emission wavelengths in the tissue coupled with the low brightness and efficiency of mtagBFP, might have been the reason (Salomonnson et al., 2012).

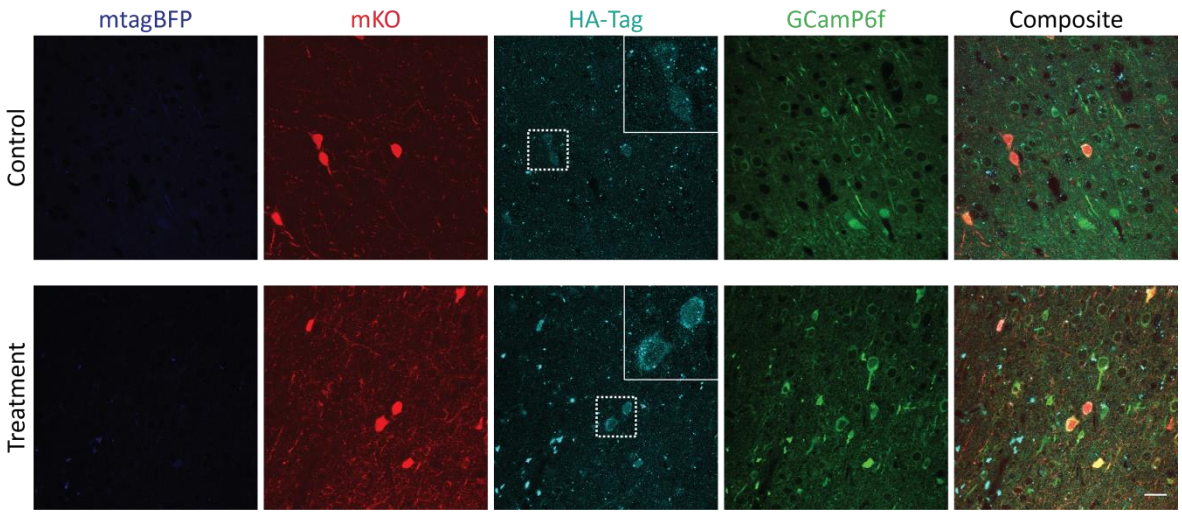

Figure 28. Example of a sliced and stained Ai14 transgenic mouse brain 80 h after induction with Doxycycline. Control hemisphere was not injected with TetOn rAAVs. Whereas the treatment hemisphere was injected with TetOn rAAVs containing an inducible HA-Tagged Kir2.1. Comparing control and the treatment experiments for the HA-Tag staining, one cannot validate the expression of the transgene with a high confidence. Yet, an apparent slight fluorescence signal could be observed for the mtagBFP in the treatment hemisphere compared to control . (Scale bar: 25 µm)

For post-hoc validations mice were perfused after the last image acquisition step and brains were sliced for subsequent HA-Tag antibody staining (Figure 28). Animals were previously injected with a mixture of DriverTET, RTETbi-NLSmtagBFP-DIO-Kir2.1, GCamP6f, and a diluted Cre virus. The control brain hemispheres were injected only with GCamP6f and diluted Cre rAAVs similar to the *in vitro* data (Chapter 3.5).

Also, for the slices I observed substantial non-specific staining and low staining of cells where expression and positive staining was expected. Although, this procedure was repeated with many animals, only on rare occasions was the staining higher than the control hemispheres. An example of this can be seen at the magnified areas of cellular somata of the HA-Tag stained pictures in the upper right edge (Figure 28).

No blue fluorescence of the mtagBFP protein could be observed either. Perhaps 80 h after Doxycycline induction mtagBFP had already been degraded. Concluding, one can say that it was not possible to detect any induced fluorescent reporter expression in the *in vivo* experiments. Therefore, one needs to extrapolate from the *in vitro* results (Chapter 3.6), that the induced expression of the transgenes should also work *in vivo*.

3.6 Assessing the protein turnover rates of transgenic proteins after brief induction *in vitro*

A key question for the *in vivo* silencing experiments is the length of the time window during which Kir2.1 protein level is sufficiently high to achieve hyperpolarization of neurons.

To be able to estimate the turnover and abundance of proteins after their induced expression over time *in vitro*, I transduced hippocampal cultures with the same rAAV constructs that I also used for *in vivo* experiments. For both sets of experiments the cells were only briefly induced for 4 h with 10 µM Doxycycline. The short exposure to Doxycycline was meant to qualitatively approximate the time course, i.e. pharmacokinetics of Doxycycline in the brain after direct injection. I analyzed protein turnover of mVenus and Kir2.1, by quantification of live mVenus fluorescence or immunofluorescence of HA-Tagged Kir2.1.

In general, the amounts of protein levels after the induction for only 4 h were quite low. With such a brief induction I was able to observe levels of induced protein expression under non-saturating conditions. We believe that this approach more closely mimics the *in vivo* situation in respect to protein dynamics and abundance compared to induction for 24 h or more.

The induced HA-Tagged Kir2.1 expression seems to be surprisingly long-lasting (Figure 29B). After 96 h there was still significantly more fluorescence observed than in the control experiment without Doxycycline induction. Of course, it is not clear whether this prolonged presence of Kir2.1 is due to mRNA or protein stability or persistent expression from the locus because of the continued existence of the Doxycycline-rtTA complex. Only between 96 h to 168 h, which corresponds to 8 days *in vitro* after brief Doxycycline induction, the fluorescence vanished to the values of the control experiment.

GFP and its derivatives such as mVenus are generally considered to be very stable and resistant against degradation (Saeed and Ashraf, 2009). Surprisingly, the average fluorescent value of induced mVenus dropped below significance after 96 h (Figure 29). In *in vivo* experiments no such drop could be observed after 72 h (Figure 30A-B). This might be due to its longer circulation of Doxycycline at high concentration in the blood stream of the animals and a subsequent accumulation of mVenus fluorescent proteins. *In vitro*, after 120 h the average fluorescent levels had reached the ones of the control experiments without Doxycycline induction. One can assume that the induced mVenus protein had been degraded within 5 days *in vitro*. Another explanation could be that the fluorescent proteins had been bleached by subsequent imaging over the course of the experiment.

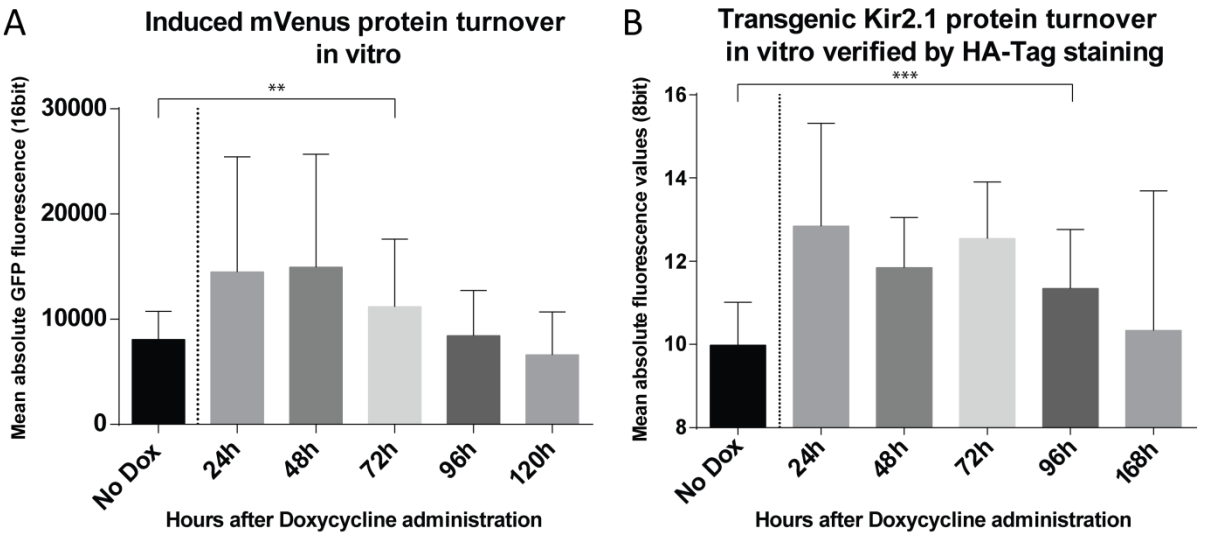

Figure 29. Validation of the protein turnover of transgenic proteins after a brief induction of 4 h *in vitro*. A) mVenus fluorescence was followed for 5 subsequent days after induction. Significant amounts fluorescence could still be observed 72 h after the induction (p=0.0035; n>25 somata, 3 separate cultures). After 96 h the fluorescence decreased to the initial values without Doxycycline induction. B) The protein turnover of the induced Kir2.1-HA-Tag protein was persisting in the cells an even longer time. Until 96 h the fluorescence values were still significantly higher (p=<0.0001; n>70 somata, 2 separate cultures each) compared to the control experiment without Doxycycline induction. Only 168 h after induction the values were insignificant compared to the initial values. (Error bars: SD; statistical test: Wilcoxon signed rank test)

Even though the *in vivo* conditions are different from these *in vitro* models, the acquired results point out that the induced transgene Kir2.1 should be present for at least 80 h also *in vivo*. This is important, as the *in vivo* experiments were conducted for up to 80 h after Doxycycline induction and subsequent validation of the presence has not been possible either by reporter mtagBFP fluorescence, nor HA-Tag antibody staining in brain slices after the experiments were finished (Chapter 3.5.1).

Concluding, one should expect that a one-time induction with Doxycycline administration *in vivo* may be enough to maintain transgenic protein levels for at least 80 h. This can also be concluded from the *in vivo* experiments with transgenic Kir2.1 expression that showed silencing at least up to 80 h after induction (Chapter 3.12).

3.7 Administration routes of Doxycycline for efficient *in vivo* induction

For the *in vivo* experiments we wanted to achieve a rapid onset of transgene expression after administration of Doxycycline. The key to an effective induction is the availability of Doxycycline at high concentrations to drive gene expression in the injected brain regions. Most researchers prefer to inject Doxycycline intraperitoneally assuming resorption into the blood stream and availability in

the brain. Also, some researchers administer Doxycycline through the drinking water and food to the animals (Hasan et al., 2001). To further boost induction efficiency researchers are recently using a Doxycycline analogue that is considered exhibiting a 10-fold greater transgene induction compared to the standard Doxycycline. 9-tert-butyl (9TB) Doxycycline is more hydrophobic than Doxycycline which may help to cross the blood brain barrier more readily and enrich in more lipophilic environments such as brain or lung tissue (Zhu et al., 2007).

I wanted to see if it would be possible to directly inject Doxycycline into the brain. By this, it would immediately be available in high concentrations in the brain and could induce gene expression more rapidly. According to a published protocol (Roome and Kuhn, 2014), the coverslips for the chronic window implant were prepared to have a small (<1 mm), decentral hole to inject Doxycycline into the brain directly. Unfortunately, it was not possible to inject 9TB Doxycycline into the brain directly. Due to its lipophilic nature and poor solubility in PBS it was clotting the injection electrodes when trying to load the solution. Therefore, the experiments to assess the benefits of direct injection of Doxycycline into the mouse brain were all performed with standard Doxycycline hyclate.

As we wanted to achieve a high concentration in the whole brain very fast, the idea was to target the injected Doxycycline to the ventricles. The injected Doxycycline should be able to readily diffuse into the whole brain from there. For this approach, the silicone filled holes of the coverslips were placed above the respective ventricles during the chronic cranial window implantation surgery.

The contralateral brain hemisphere that was not receiving the injection directly, but through diffusion was also monitored (Figure 30C). Therefore, I compared transgene inducibility after intraperitoneal (IP) injection of Doxycycline with either ipsilateral or contralateral direct injection into the brain. The animals were injected with a 1:1 mixture of DriverTET and ResponderTET rAAVs during surgery. After administration of Doxycycline the increase in mVenus fluorescence was followed up to 72 h.

Direct-ipsilateral injection produced much higher increase in fluorescence levels as compared to the standard IP injection of Doxycycline (Figure 30). A clear difference could already be observed 18 h after induction. At the end of the experiments, induced mVenus fluorescence was about 6 times higher than the initial values (Figure 30B). Interestingly, the fluorescence intensities of IP and contra lateral intracerebroventricular (ICV) injections were comparably high.

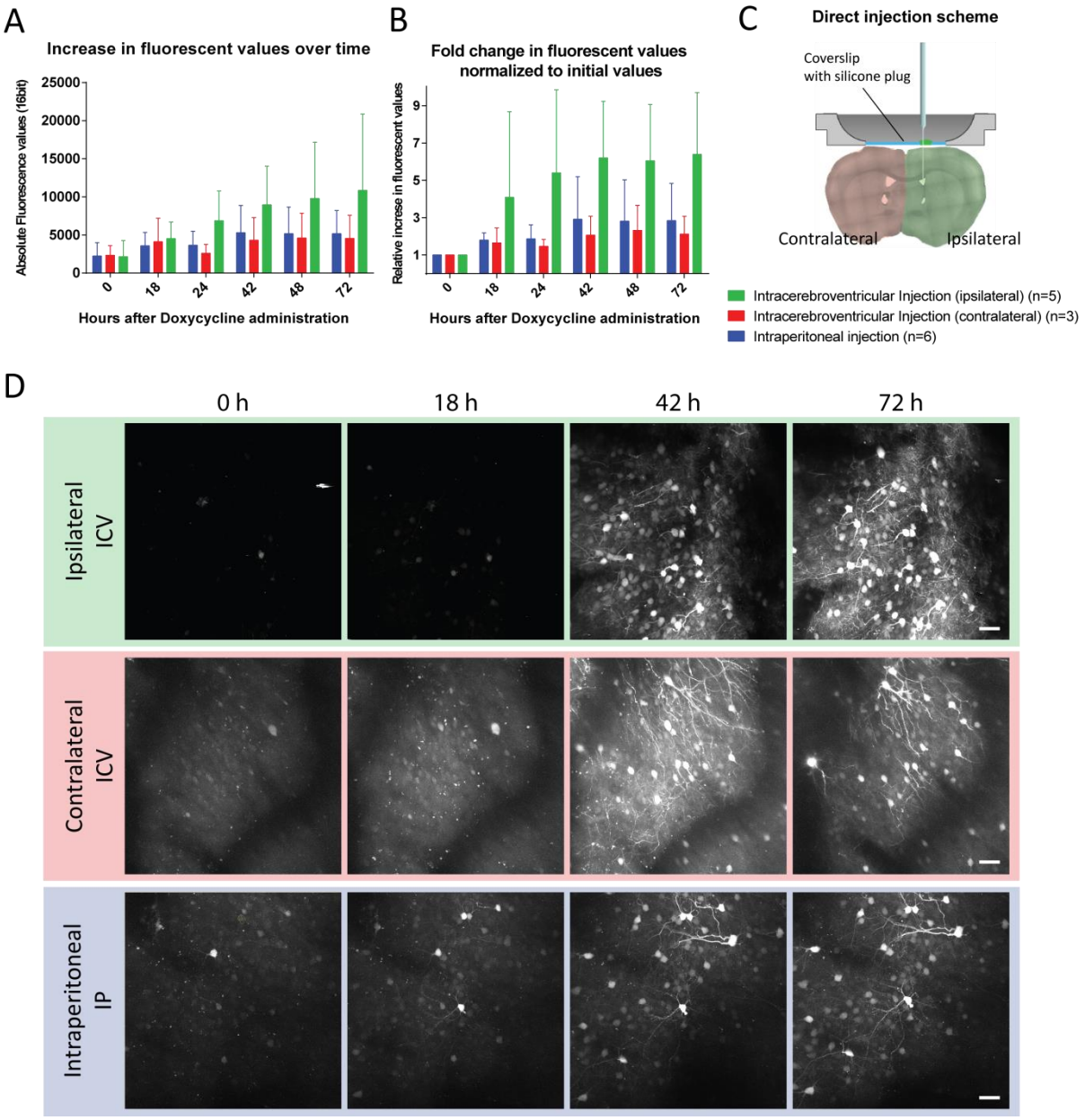

Figure 30. Comparison of different administration routes of Doxycycline *in vivo*. Animals were injected with DriverTET and ResponderTET rAAVs and Doxycycline was administered intraperitoneally (IP) or by direct intracerebroventricular injection (ICV). The ICV injection targeted one hemisphere (ipsilateral), but also the contra lateral hemisphere was monitored, see C. A) Direct ICV injection of Doxycycline shows a substantial increase in fluorescence after transgene induction (n=5). It exceeds the values of IP (n=6) or contralateral ICV (n=3) injections by a factor of about 2. B) Fold change of fluorescence values normalized to the initial value at time point 0 h. After 42 h, ICV ipsilateral injected animals showed a 6-fold increase in fluorescence values. IP and ICV contra lateral injected animals showed about a 2 to 3-fold increase. C) Scheme of experimental setting for intracerebroventricular injections. D) One example of each Doxycycline administration route analyzed with 2P *in vivo* imaging. Cortical areas of animals are shown over time, from prior to Doxycycline administration up to 72 h thereafter. (Scale bar: 50 µm; Error bars: SD)

Statistical analysis using a linear regression fit of the values in graph A (Figure 30) showed that the fluorescence increase is significant for ipsilateral ICV (n=5; p=0.0068) and IP (n=6; p=0.0239) injections, whereas no significance could be detected for contra lateral ICV (n=3; p=0.2088) injections with a linear regression fit analysis. No significance could be produced with Wilcoxon signed rank test comparing each measurement to the initial median value, due to the small n numbers, except for the IP injection experiments after 18 h (p=0.0313). It seems that a single IP injection of Doxycycline might not be sufficient to induce transgene expression to the full extent. Presumably, the injected amount of 2 mg Doxycycline did not reach high sufficient concentrations in the brain over the necessary time periods to effectively induce transgene expression. Surprisingly, the contralateral brain hemisphere of ICV injected animals exhibited only a minor increase in fluorescence intensities comparable to the IP injections. Therefore, one can conclude that a sufficiently high local concentration of Doxycycline is the limiting factor for induction of transgenes.

According to these results, all subsequent experiments were conducted with direct injections of Doxycycline hyclate ICV. To achieve maximal expression levels, 9TB Doxycycline was IP injected additionally to the ICV injections. Thus, 2.5 mg of 9TB Doxycycline dissolved in 500 µL PBS was injected at the same time as the ICV injections (1.5 µL, 5 mg/mL). Administration of Doxycycline via the drinking water or food was not attempted because the time and level of uptake could not be properly controlled.

3.8 Injections of GCamP6f rAAV for 2P *in vivo* calcium imaging

Several publications suggest diluting the GCamP6f rAAV prior to injection into the animals (Resendez et al., 2016), due to cytotoxicity occurring from overexpression or the intrinsic calcium buffering properties of GCamP6. Cells in which GCamP6f entered the nucleus are excluded from analysis, as this is generally considered as a sign for unhealthy overexpression of the transgene (Chen et al., 2013a). Due to its size of ~50 kDa it should not be able to passively translocate into the nucleus under normal physiological conditions (Wang and Brattain, 2007).

To determine a suitable injection titer for the purchased GCamP6f rAAV, two different dilutions of 1:6 and 1:18 in PBS were injected into separate brain hemispheres of the same animal. The titer of the viral solution was given with 2.82e13 GC/mL (genome copies). Imaging was conducted under constant, standard conditions at the 2P microscope four weeks after surgery, and average intensity projections of the movies were generated to compare the two different dilutions (Figure 31).

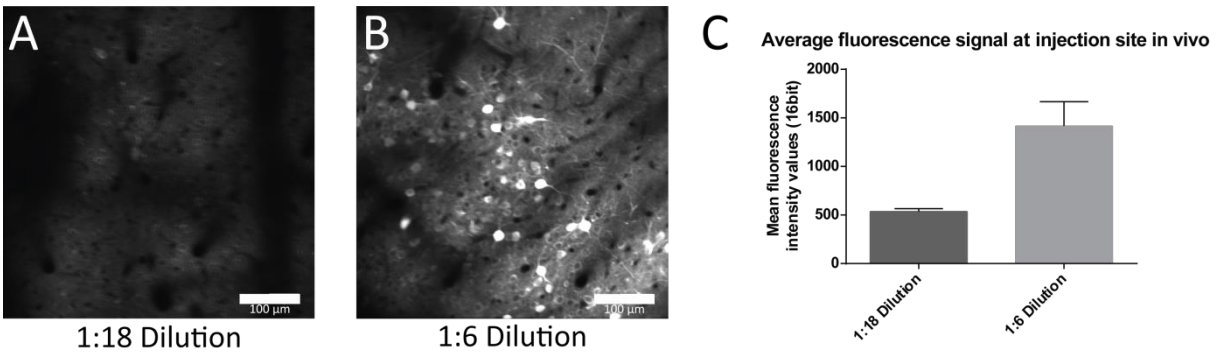

Figure 31. *In vivo* 2P Comparison of two different dilutions of GCamP6f rAAV injected into cortical brain areas. A) A dilution of 1:18 led to low fluorescence levels of GCamP6f. B) A 1:6 dilution of GCamP6f rAAV shows very high expression levels, but also neurons with filled nuclei. C) The graph shows that the dilution of the rAAV by a factor of 3 leads to a decrease in average fluorescence levels also approximately by the factor of 3 (1500 → 500 and 1:6 → 1:18). Mean fluorescence intensity values are derived from figures A & B. (Error bars: SD; Scale bar: 100 µm; each dilution n=1)

At a high dilution of 1:16, very low fluorescence levels were observed, that might be insufficient to reliably image calcium activity (Figure 31A). With low dilutions such as 1:6 some cells showed filled nuclei (Figure 31B). This can be considered as an indication for unhealthy overexpression, and thus a sign that the viral solution should be diluted more (Resendez et al., 2016).

Subsequently, all the following injections of the purchased GCamP6f rAAV were done at a 1:10 dilution of the virus with PBS prior to injection. This dilution led to sufficient expression levels for effective calcium imaging, while not showing too many pathologically "filled" neuronal nuclei.

I could observe that the same concentration of GCamP6f virus particles produced different expression levels dependent on how many other viruses were co-injected. Additional virus particles (DriverTET & ResponderTET) decreased GCamP6f fluorescence. This suggests that the capacities of neurons to be transduced are limited.

3.9 Transduction efficacy of the different rAAVs *in vivo*

To gain insight as to how far rAAV particles following injections would spread and transduce cells *in vivo*, a few brains of treated animals were sliced after experiments. The animals were injected with a mixture of 1 to 1.5 µL of DriverTET, RTETbi-NLSmtagBFP-DIO-Kir2.1, and GCamP6f. The main concern was that maybe not all the cells in the imaged area would have been transduced and be inducible by Doxycycline. Especially for the cases where the neuronal activity of surrounding cells were measured after inhibitory PV+ cells were targeted. Moreover, it was not possible to monitor a successful induction by a reporter gene or activity changes within these neurons. The only bright fluorescence

was originating from the highly concentrated GCamP6f rAAV. Therefore, one can only conclude that the cells would be transduced if they were within the central areas of GCamP6f expression, as a rAAV mixture was always applied (Figure 32). For the imaging part of the experiments it was consequently taken care to choose areas that were surrounded by bright green GCamP6f fluorescence. That way I expected that all the cells were connected to PV cells, which would be manipulated by Doxycycline administration and subsequent expression of the Kir2.1 transgene.

By extrapolating the number of PV+ cells in the area of GCamP6f neurons one can expect to be manipulating around 5000 PV interneurons by a cortical injection of ~1 µL into a mouse brain. Of course this is only the case, if we assume that the far less concentrated rAAVs of the self-made DriverTET and RTETbi-NLSmtagBFP-DIO-Kir2.1 have the same spread as the highly concentrated GCamP6f rAAVs. Taking into account that the viral AAV capsids have the same physical properties for diffusion, they should also spread comparably in the brain after injection. For that reason, the only difference should be the amount of multiplicity of infections per rAAV and neuron. And this is more essential for fluorescent reporter proteins, where high amounts of expressed protein are necessary to detect the signal. For functional proteins such as Kir2.1 already few proteins will have an effect on the neuronal resting membrane potential.

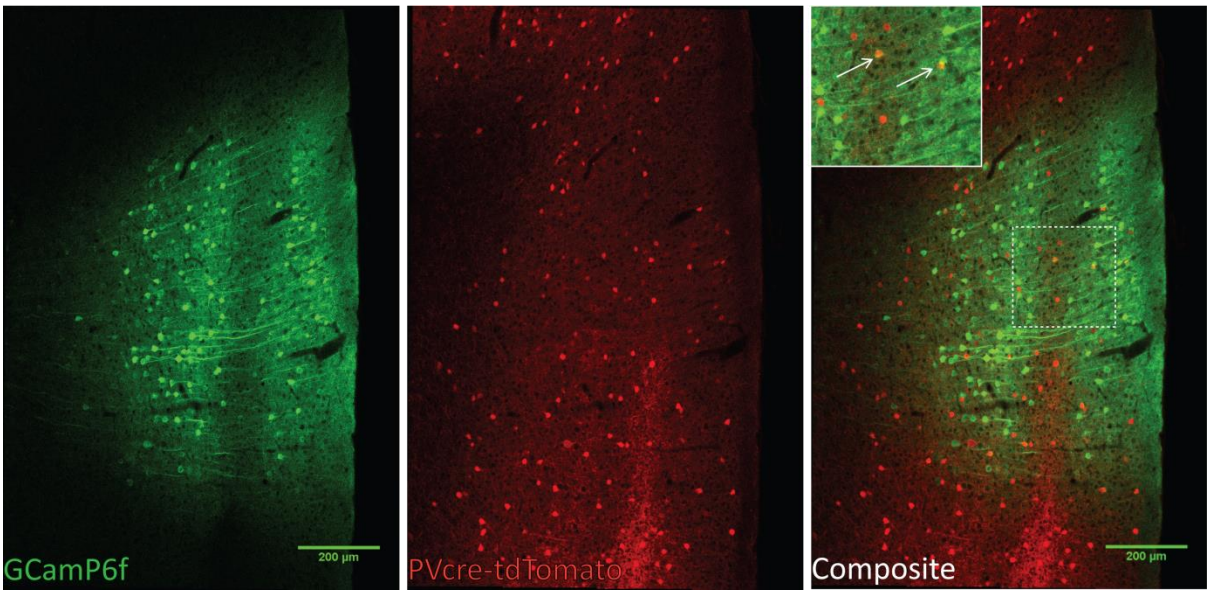

Figure 32. Spread of fluorescence after injection of 1 µL of a synapsin promoter driven GCamP6f rAAV into a PVcre-Ai14 mouse brain. In this example brain slice one can nicely see the circular spread of fluorescent GCamP6f signal from a presumed injection site in the center, below the surface. In the red channel inhibitory Parvalbumin interneurons expressing Cre dependent tdTomato fluorescent reporter can be seen. In the composite picture it is apparent that only very few PV+ cells are expressing synapsin driven GCamP6f. Two examples are pointed out in the magnified area by arrows. This is due to the fact that the synapsin promoter is not active in the vast majority of PV+ interneurons. (Scale bar: 200 µm; Slice thickness: 70 µm)

3.10 Assessing spontaneous activity of Parvalbumin interneurons with GCamP6f was impossible

Visual inspection of transduced cells revealed, that the majority of PV+ cells was not expressing synapsin promoter driven GCamP6f, but only a fraction of PV neurons did (Figure 32, magnified area). However, we wanted to measure changes in activity levels after induction of Kir2.1 in these cells. By being able to image PV cell activity one could have possibly assessed the induced changes in activity in a quantitative manner. For example, the actual Kir2.1-dependent decrease in PV cell activity could have been correlated with the extent of activity increase of the surrounding neurons. To improve GCamP6f imaging in PV cells, a floxed and ubiquitous CAG promoter driven GCamP6f rAAV was co-injected in some experiments. Unfortunately it was not possible to assess spontaneous activity in these cell types with GCamP6f (Figure 33). The main problem was that these cells have a different firing pattern than the synapsin 'positive' cells that expressed GCamP6f because of the synapsin-GCamP6f virus. Parvalbumin interneurons are high frequency firing inhibitory neurons (Hu et al., 2014). Their firing is so frequent, that it basically results in a "line of activity" when trying to monitor activity with a calcium indicator such as GCamP6f. The most plausible explanation would be that GCamP6f is too slow to resolve single action potentials of these high frequency firing patterns of Parvalbumin interneurons. This is one of the reasons why most scientists characterize PV interneurons electrophysiologically, rather than using calcium sensors such as GCamP6f (Buetfering et al., 2014).

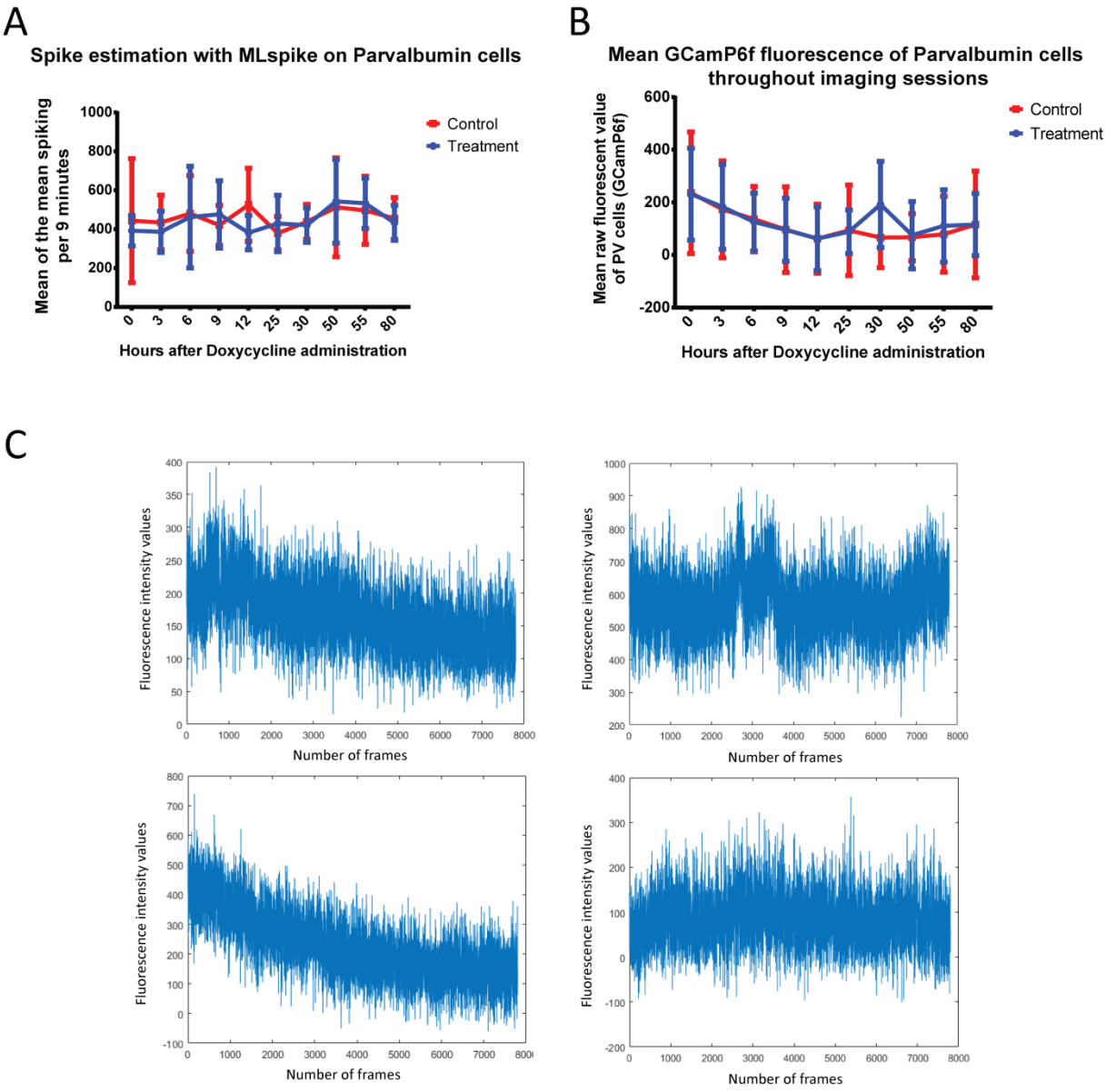

Figure 33. Attempts to measure spontaneous activity of Parvalbumin interneurons with a GCamP6f calcium sensor. A) Inferred spiking for calcium recordings with MLspike algorithm and loose, standard parameters. No difference between control and treatment brain hemispheres could be observed. B) Mean raw fluorescent values over the course of the experiments suggest minor bleaching of the GCamP6f fluorophore. Also, no difference between treatment and control brain hemisphere could be observed. C) Four examples of calcium traces of PV+ interneurons imaged for 9 minutes. It is apparent from these traces that there are no distinct events that could be quantified and compared. Most likely the high frequency activity pattern of PV cells leads to slowly fluctuating calcium signals. (Error bars: SD; n=7 for control and treatment experiments)

The recorded calcium traces resembled broad lines without distinct changes over time (Figure 33C), which made it impossible to quantify spontaneous activity in slightly anaesthetized mice.

Inferring spiking from these calcium traces was unsuccessful with the calibrated MLspike parameters for excitatory neurons (Chapter 2.5.7). The algorithm was not able to identify any spiking events in these PV calcium traces. Therefore, I decided to run the algorithm on PV calcium traces with very

loose, standard parameters. This resulted in very high numbers of inferred spiking, which was also expected for such high frequency firing patterns. Unfortunately, again no difference could be observed over time after induction of Kir2.1 transgene between treatment and control hemispheres. The levels of activity remained more or less constant over the course of the experiments (Figure 33A).

Another idea was, to quantify mean fluorescence levels of these cells. The rational was that the level of fluorescence would be related to the levels of activity of these cells, i.e. cells with more activity would display higher levels of fluorescence. Thus, if the PV cells would decrease their activity after the induction of Kir2.1, their mean fluorescence level would also decrease. Regrettably, no such effect could be observed comparing control and treatment hemispheres, as the fluorescence levels did not change over the course of an experiment besides a general loss of fluorescence due to bleaching of the fluorophore GCamP6f (Figure 33B). Of course, Kir2.1 induction must have occurred because the surrounding neurons did change their activity levels.

Taken together, it was not possible to assess the levels of basal activity of PV cells using GCamP6f with our current methods in slightly anaesthetized mice.

3.11 Keeping a constant depth of anesthesia

To compare spontaneous activity of cortical neurons over a long period of time, it turned out to be necessary to keep the animals state of anesthesia at a constant level. When high doses of Isoflurane (>1.5 %) were applied to the animals, the spontaneous cortical activity diminished and was not evident any more. On the other hand, when very low doses of Isoflurane were applied (<0.5 %) the animals would start to move occasionally. These movement artifacts had tremendous effects on neuronal activity, but also substantially distorted imaging quality. Additionally, having such states of occasional movement makes it impossible to compare activity over time. To have comparable neuronal states at every time point, I monitored the breathing rates of the animals and adjusted Isoflurane levels accordingly. Constant breathing rates are considered to reflect constant stable baseline activity (Zehendner et al., 2013). In my experience, keeping the breath rates between 110 and 130 Breaths/min was the most suitable target (Figure 34). At these values anesthesia was deep enough to prevent the animals from moving, while being able to observe cortical neuronal activity with GCamP6f.

By maintaining the breath rates constant the calcium imaging could be conducted under comparable conditions at each time point . This way it was possible to follow spontaneous neuronal activity levels over a long time course to conduct longitudinal experiments.

For most of the animals one could keep the Isoflurane levels constant over the imaging session. Some animals needed constant supervision of the breath rates and continuous adjustment of the Isoflurane levels. In general, the Isoflurane dosage could usually be reduced slightly towards the ends of the imaging sessions, which took around 20 minutes in total.

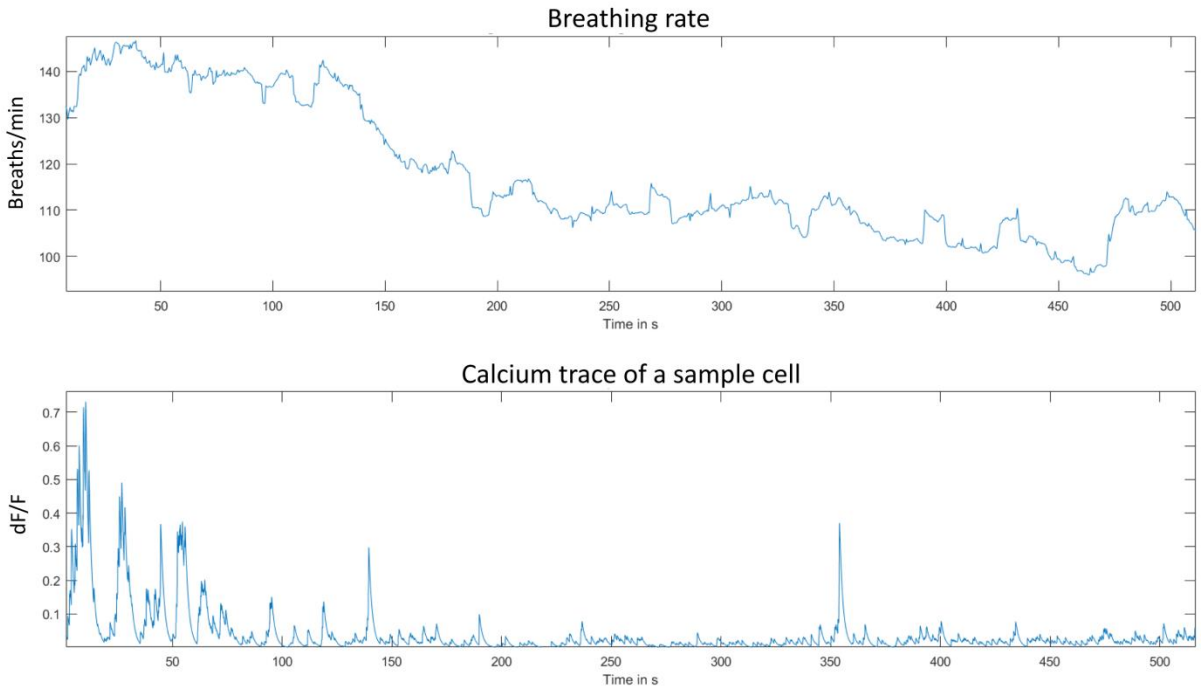

Figure 34. Example of correlation between breathing rate and neuronal activity. Upper trace shows the breathing rate of the animal using a 10 s sliding window. The lower trace is the calcium trace of a sample cell that was recorded simultaneously. It is apparent that elevated breathing rates of 140 Breaths/min represent a lower anesthetic state and therefore more neuronal activity is recorded.

For all the *in vivo* experiments, breathing rates of the animals were recorded and analyzed (Figure 35). Over all, one can conclude that keeping constant breathing rates was a key parameter to observe and to compare spontaneous neuronal activity levels in cortical regions.

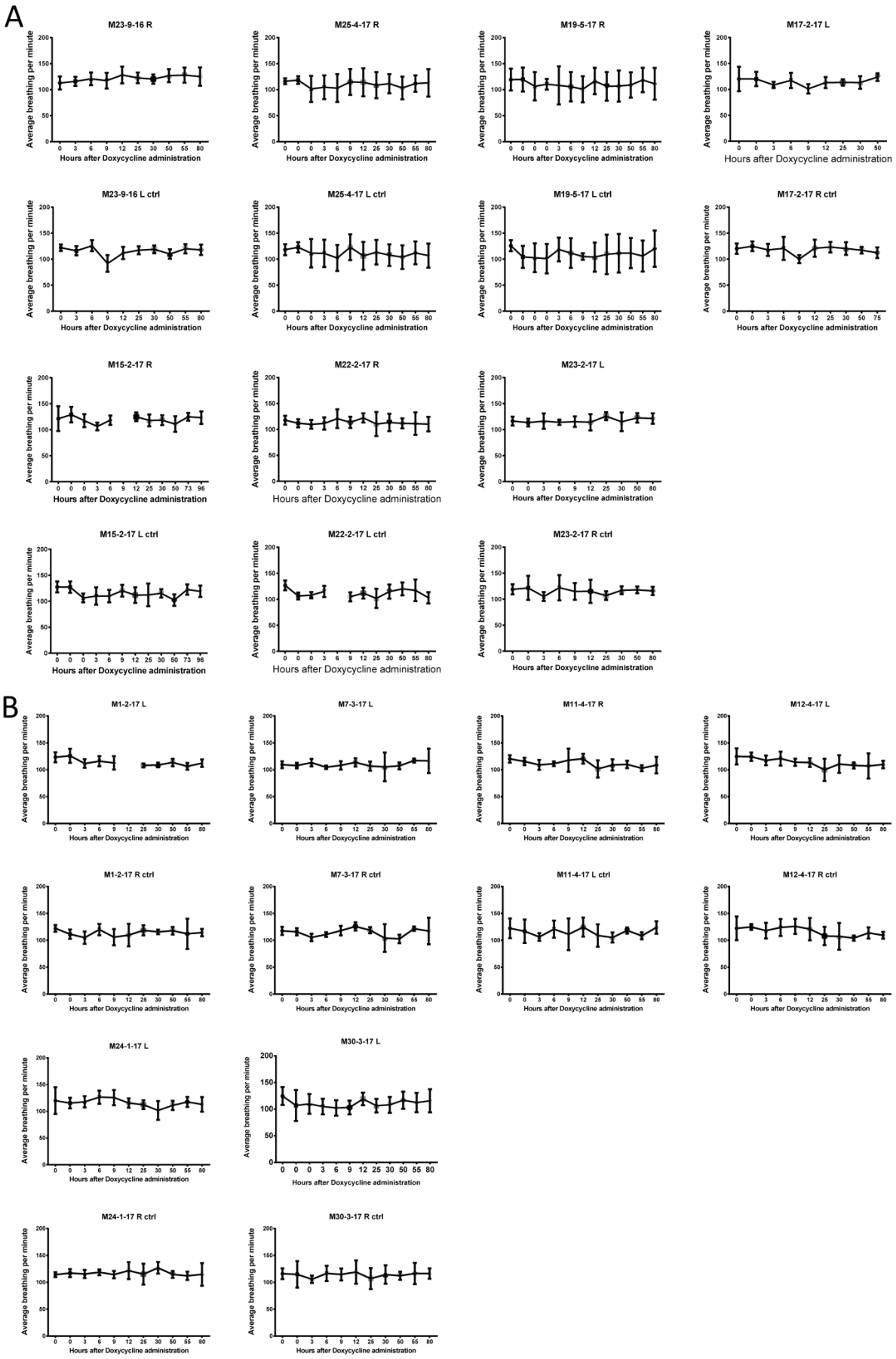

Figure 35. Breathing rates of (A) PVcre-Ai14 and (B) Ai14 animals during image acquisition over time.

Experiment name	'Dilute Cre'	Parvalbumin
Mouse line	Ai14	PVcre-Ai14
rAAVs	DriverTET	DriverTET
	RTETbi-NLSmtagBFP-DIO-Kir2.1	RTETbi-NLSmtagBFP-DIO-Kir2.1
	Synapsin GCamP6f	Synapsin GCamP6f
	Synapsin iCre (1:2000)	Synapsin floxed-GCamp6f
Manipulated cells	Random Cre^+ cells	Parvalbumin interneurons
Calcium signal from	Surrounding & manipulated neurons	Surrounding, untargeted neurons. No signal from manipulated interneurons
Chapter	3.12, 3.14.1, 3.15	3.13, 3.14.2

Table 3. Overview of *in vivo* experiments with the most important experimental parameters.

3.12 Silencing of a small and random subpopulation of neurons by induced Kir2.1 expression ('Dilute Cre')

To study which effects the silencing of a small subpopulation of neurons has on the larger network, I used an approach that we designated 'Dilute Cre'. The two TetOn viruses and the GCamP6f virus were used at standard concentrations. However, to achieve only sparse manipulation of neurons, a method developed in our institute was used and adopted to my experimental needs with a highly diluted Cre rAAV that was co-injected with the other three rAAVs. By changing the Cre virus dilution, the number of cells that can be manipulated with the TetOn system can be adjusted. Of course, the GCamp6f transduction and signal are unaffected by the Cre rAAV.

The surgeries were carried out on adult mice after the age of 6 weeks. Experiments were conducted at least four weeks after the surgeries were performed to allow the injuries to heal and the inflammation reaction in the brain tissue to cease. Then, the animals were imaged for 1-3 times before the administration of Doxycycline to assess the basal neuronal activity in the injected cortical region. Each imaging session lasted for about 9 minutes and the breathing rates of the animals were monitored and Isoflurane levels adjusted if necessary to keep them at about 120 Breaths/min. A constant breathing rate was considered to ensure a constant level of spontaneous neuronal baseline activity. This is important for the identification of activity changes in a subset of cells. After each

imaging session animals were returned to their cages to recover from anesthesia until the next imaging session took place.

With some effort, it was possible to always acquire images of the exact same region. This was important, as the goal of this project was to follow the changes of neuronal activity of the same individual cells over the course of the experiments. By being able to assess the same cells before and after the induction of Kir2.1, increases the probability of detecting phenotypic changes compared to always analyzing different cells at different time points.

I injected Ai14 mouse line animals with a 1:2000 dilution of a synapsin driven iCre rAAVs along with the TetOn cocktail consisting of DriverTET, RTETbi-NLSmtagBFP-DIO-Kir2.1, and GCamP6f rAAVs. As a result, roughly 10-25 % of the GCamP6f positive neurons were Cre positive, which was validated through the Cre-dependent expression of tdTomato in these cells. As these cells were expressing Cre recombinase, they were also amenable to the induction of the Tet-dependent Kir2.1 transgene via the RTETbi-NLSmtagBFP-DIO-Kir2.1 rAAVs (Figure 36).

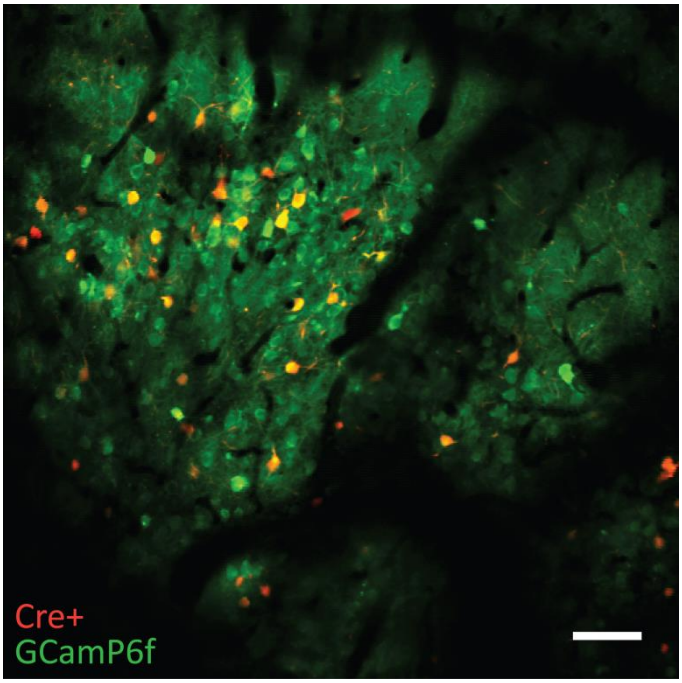

Figure 36. Example composite image of a cortical region after injection with a diluted (1:2000) synapsin driven iCre AAV at a depth of ~100 µm. In the red channel, Cre^+ cells can be seen as they were expressing the tdTomato fluorescent protein. In the green channel, the GCamP6f calcium indicator is visualized. Maximum intensity projections of both channels are merged. (Scale bar: 100 µm)

The goal of using this set of experiments was to silence a subpopulation of neurons and to measure the effects on the local network. Unlike in the experiments in which PV cells were targeted, here also the activity of the manipulated Cre positive cells could be measured as they were presumably mostly

excitatory neurons with characteristic firing patterns that could be characterized with GCamP6f. The control brain hemispheres were injected with GCamP6f rAAVs only. In total, 6 animals were used and the experiments were carried out the same way as described before (3.13).

No change in activity levels could be observed for untargeted neurons that surrounded the manipulated Cre positive neurons (Figure 37). A linear fit showed no significant difference between nearby and cells further away ($p=0.4243$). The control brain hemispheres were displaying a high variability but did not change their spiking activity level on average ($p=0.8314$). Only the Cre positive neurons substantially reduced their activity levels already 3 h after Kir2.1 induction by Doxycycline administration. A linear fit test almost reached criterion ($p<0.05$) with $p=0.0751$, and a nonparametric Wilcoxon signed rank test could confirm that the activity values from 25 h were significantly different ($p=0.0313$) except the 50 h measurements, compared to the initial activity level at 0 h. No significance was detected either for control ($p=0.8737$) or for the untargeted ($p=0.8716$) cell populations (linear fit analyses). At the final time point the activity had decreased 13-fold, compared to the average initial activity level (40.6→3.1). After 6 h the activity had dropped about 27 %. This result is in good agreement to the *in vitro* experiments in which the expression of Kir2.1 led to a reduction of activity on average by ~40 % within 5 h after administration of Doxycycline (Figure 40).

Despite this sizeable impact of Kir2.1 on the Cre positive cells, no obvious effect could be seen for the surrounding, untargeted cells. One could have expected an increase in activity levels to compensate for the short-term loss of activity from the Cre positive neurons or a decrease in activity levels as excitatory signals in the local network would be missing. Conversely, the number of 10-25 % targeted cells was too little to have a significant effect on the surrounding network.

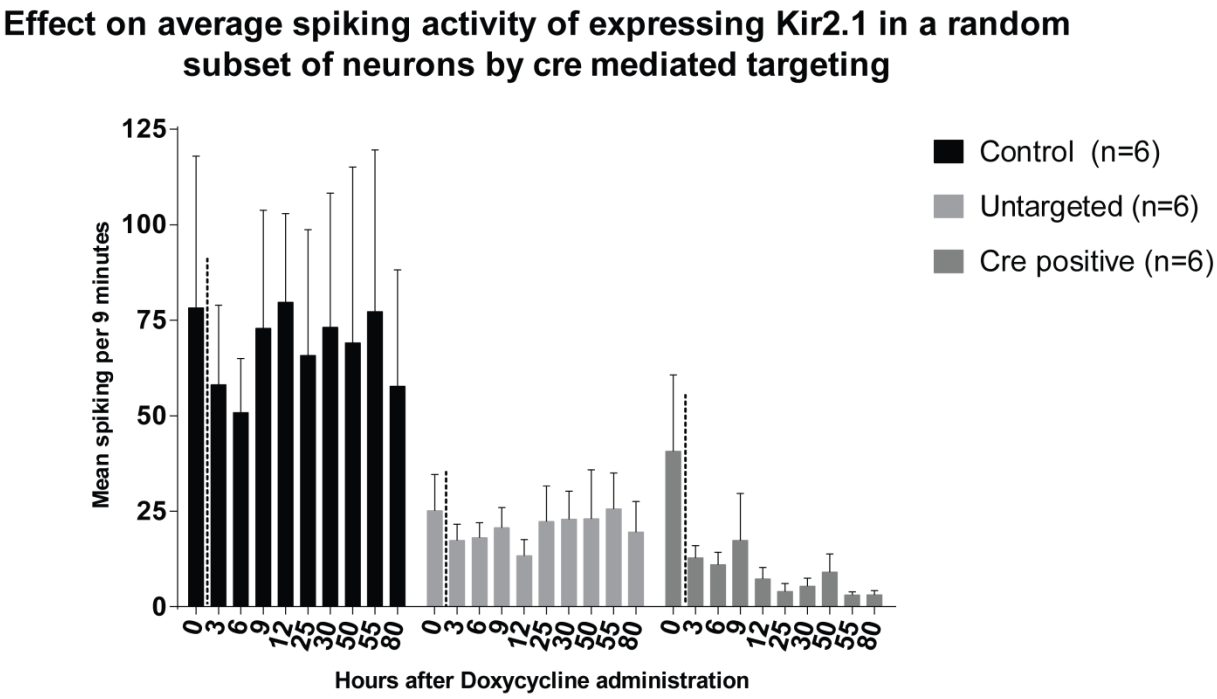

Figure 37. The effects of a Cre mediated silencing of a subpopulation of neurons in a local network. After transgene induction, a substantial decline of the mean spiking was observed for Cre positive and Doxycycline responsive neurons. No significant changes in activity levels can be seen either for the control (p=0.8737) or the untargeted, surrounding neurons (p=0.8716), but for the Cre positive, targeted neurons (p=0.0285). Spiking activity was assessed in neuronal populations for 9 minutes at every time point. Measurements at time points 0 are each an average value of 13 independent measurements, all the other time points are the average value for the respective time point of each animal. (Error bars: SEM; Statistical test: Kruskal-Wallis, nonparametric one-way ANOVA; n=6 for each condition)

As expected, analyses of single experiments showed a rapid response to the induced expression of Kir2.1 (Figure 38A & B) as the activity levels decreased. For some time points (for example 55 h and 80 h in both figures) no activity could be observed. The activity levels of the untargeted, non-tdTomato cells did fluctuate generally but without any significant change. Thus, these results nicely match the *in vitro* silencing data. However, if single experiments were analyzed, the variability from one time point to the next became more obvious. For example, despite the clear overall decrease after induction in Figure 38C, an outlier can be seen. All time points after Doxycycline induction exhibited lower values than baseline except for the measurement at 9 h. Careful inspection of the measurement did not reveal any obvious imaging artifacts. Also, the breathing rate was normal at 9 h. The reasons for such an obvious artefact are unclear. In another experiment, the activity levels of targeted neurons only decreased significantly after 9 h (Figure 38D). Importantly, for all experiments, the untargeted, surrounding cells did not react to the silenced activity of targeted cells in their vicinity. Overall, most the experiments point to a very rapid effect of induced Kir2.1 to the neuronal activity.

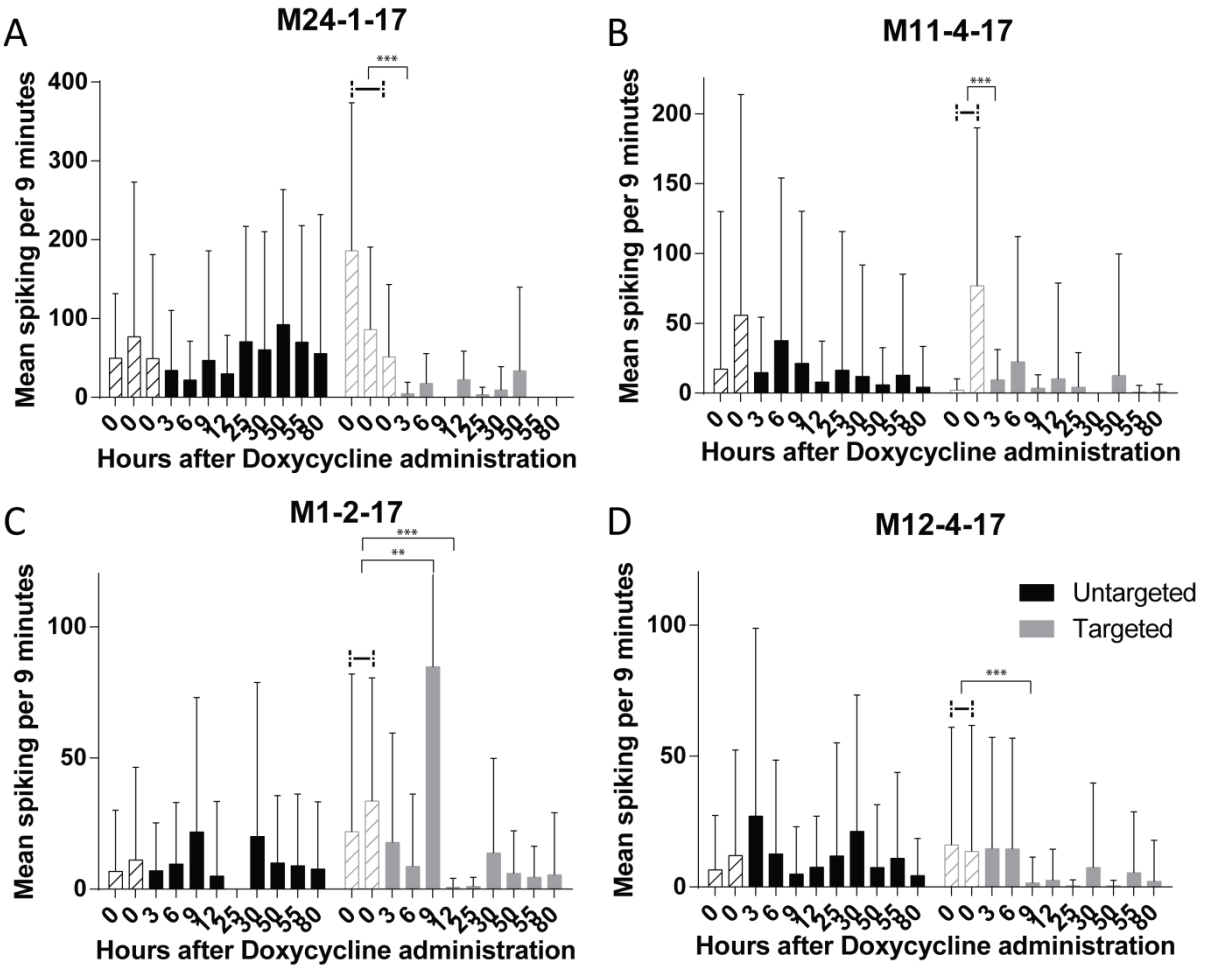

Figure 38. Examples of average inferred spiking of four different animals with a randomly silenced subpopulation of neurons (Treatment hemispheres only). A) In this animal one can see the low fluctuation of the untargeted cells activity, while the targeted cells are almost entirely silenced after 3 h (p=<0.0001). (Untargeted cells: n=35; Targeted cells: n=10). B) The targeted cell population shows a significant decrease in activity already after 3 h (p=<0.0001) but is showing only low levels of activity, except for the second 0 h recording. (Untargeted cells: n=112; Targeted cells: n=48). C) Despite high variability in the targeted cells activity, an underlying trend towards silenced activity is still apparent. Even though, the signal recorded at 9 h is significantly different from the initial average. The first significant silencing occurs at 12 h (p=<0.0001). (Untargeted cells: n=78; Targeted cells: n=30). D) A sharp decrease in activity levels can be observed only 9 h after Doxycycline administration (p=<0.0001). The untargeted cells are relatively stable in their low, but fluctuating activity (Untargeted cells: n=110; Targeted cells: n=57). Average values of basal recordings at 0 h were used to determine significance compared to activity after induction (basal values joint by hyphen). (Error bars: SD; Striped bars were averaged; Statistical test: One sample t-test)

With these experiments I could show rapid and strong activity changes after Doxycycline induced expression of Kir2.1. A simple pulse of Doxycycline provided sustained silencing of neurons for at least 3 days comparable to Kir2.1 *in vitro* expression data (Chapter 3.6). Combined with its low levels of leakiness, this tool could be valuable in diverse experimental settings in which transgene expression needs to be tightly regulated, fast, and cell-type specific. (Graphs of all conducted experiments can be seen in the appendix under Figure 48.)

3.13 Silencing of Parvalbumin interneurons by induced Kir2.1 expression

To study the effects of silencing PV interneurons by Doxycycline induced expression of Kir2.1, seven PVcre-Ai14 animals were injected with DriverTET, RTETbi-NLSmtagBFP-DIO-Kir2.1, and GCamP6f rAAVs before implanting a chronic cranial window. One brain hemisphere of each animal was injected with this virus cocktail while the other was injected with GCamp6f rAAVs only. This brain hemisphere was used as a control, as it was not responsive to the Doxycycline administration.

As it was not possible to assess the activity rates of the PV interneurons (Chapter 3.10), the analyses focused on the surrounding GCamP6f positive neurons.

Following each experiment, between 30 and 80 neurons were manually selected and their activity levels investigated over time (Figure 39). Spiking was inferred using the MLspike algorithm.

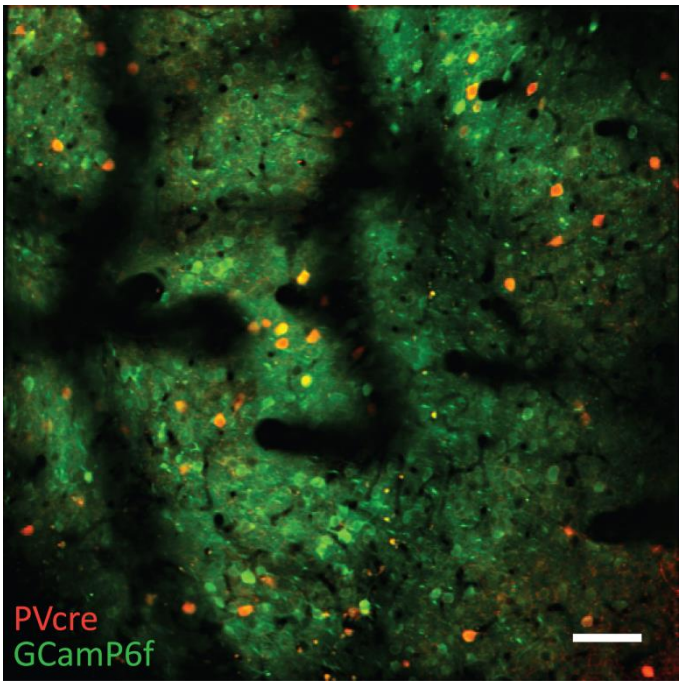

Figure 39. Example composite image of a cortical region used for image acquisition in PVcre-Ai14 mice at a depth of ~100 µm. In the red channel PV cells can be seen as they were expressing the tdTomato fluorescent protein. In the green channel the GCamP6f calcium indicator was visualized. Maximum intensity projections of both channels were merged. (Scale bar: 100 µm)

6 h after induced expression of Kir2.1 one could observe a clear trend of increasing spiking activity in surrounding neurons if inhibitory PV interneurons were silenced (Figure 40). The same effect could not be observed in the control hemispheres, where activity levels were also highly variable, but did overall not change significantly from the initial values (linear regression fit analysis, p=0.3653). After

80 h, the surrounding neurons had almost tripled their activity levels compared to the basal levels. A linear regression fit analysis of activity changes over time produced a p-value of below 0.001 for the pooled 7 experiments, showing that the observed phenotype was significant. Other statistical tests such as Wilcoxon signed ranks test did not produce significance for either control or treatment brain hemispheres.

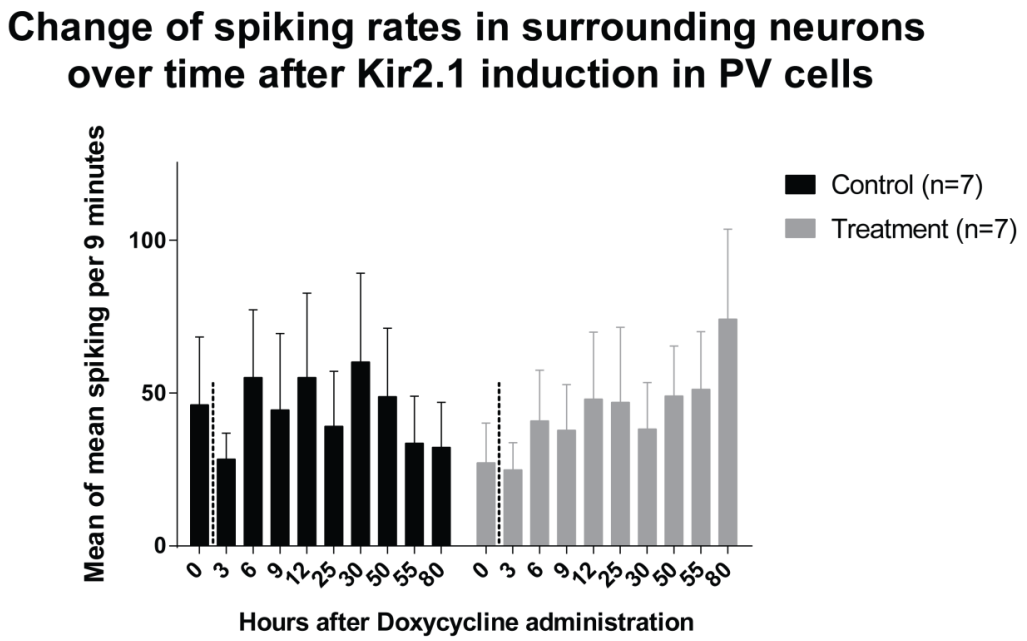

Figure 40. Effect of silencing PV cells by Doxycycline induced Kir2.1 expression on surrounding neurons over time. Each animal was injected with DriverTET, RTETbi-NLSmtagBFP-DIO-Kir2.1, and GCamP6f rAAVs, whereas the control brain hemisphere of each animal received only GCamP6f rAAVs. Spiking activity was assessed in surrounding neuronal populations for 9 minutes at every time point. One can clearly see the trend of increasing spiking activity of neurons, if nearby inhibitory PV cells were genetically silenced (p=0.001). There was no significant trend for the control experiments (p=0.3653). Measurements at time point 0 are an average value of 19 measurements, all the other time points are the average value for the respective time point from each animal. (Error bars: SEM; statistical test: linear regression fit; n=7 for each condition)

With these experiments I could show that it was possible to use Cre mouse lines to specifically target a neuronal subpopulation with the constructs I developed successfully. Thus, the combination of Cre/lox and TetOn systems allows cell-type specific genetic manipulations *in vivo* with high spatiotemporal resolution. Even though the PV cells turned out to be a complicated target for assessing their intrinsic activity, I could show that their manipulation has a significant effect on surrounding neuronal activity levels, as expected. Behavioral differences of the animals could not be observed during the entire experiments.

Overall, the variability in these kinds of experiments turned out to be the most challenging issue. For example, a long recording window of roughly 9 minutes appears not sufficient to represent the basal neuronal activity faithfully at all times. Also, the depth of anesthesia, level of fear, nervousness, the

animals' current day-night cycle at the time of the recording, their hydration level or when they had eaten before, might have an influence on basal brain activity levels. The general level of variability between the experiments is apparent from the error bars in Figure 40. If experiments from single animals are compared, one can see these levels of variability also being high between control and treatment hemispheres.

Interestingly, an effect could be observed where the overall neuronal activity of the treatment hemisphere increased with an intermediate drop in between. This phenomenon was observed at least twice, one can be seen for example in Figure 41A, or in the appendix in Figure 47 (M15-2-17). In both cases the activity first increased, and then decreased before increasing again, between 9-25 h and 55-80 h after Kir2.1 induction. This phenomenon might reflect some sort of population homeostatic adjustment of the network to initially counteract the reduced PV cell activity. From the previous *in vitro* and *in vivo* experiments it is clear that Kir2.1 activity and thus silencing is constantly high during these time phases. Thus, the activity decrease in non-PV cells appears to be the consequence of possible homeostatic counteractive mechanisms.

Some cortical areas just seem to have an intrinsic level of variability that is higher in general (Figure 41B-Control). Also, some experiments did neither lead to an obvious effect nor a trend after the silencing of PV cells (Figure 41C). The most difficult cases have been experiments where almost no cortical activity could be observed (Figure 41D). In this specific case also the control brain hemisphere did only show very little spiking activity. The rate was on average 10 spikes per 9 minutes, whereas in other experiments the general activity was around 40 spikes within 9 minutes. These much lower levels of activity might be a consequence of damage during surgery. However, at a cortical depth of 100 µm these cells did exhibit GCamP6f and tdTomato fluorescence and also did look healthy by visual inspection.

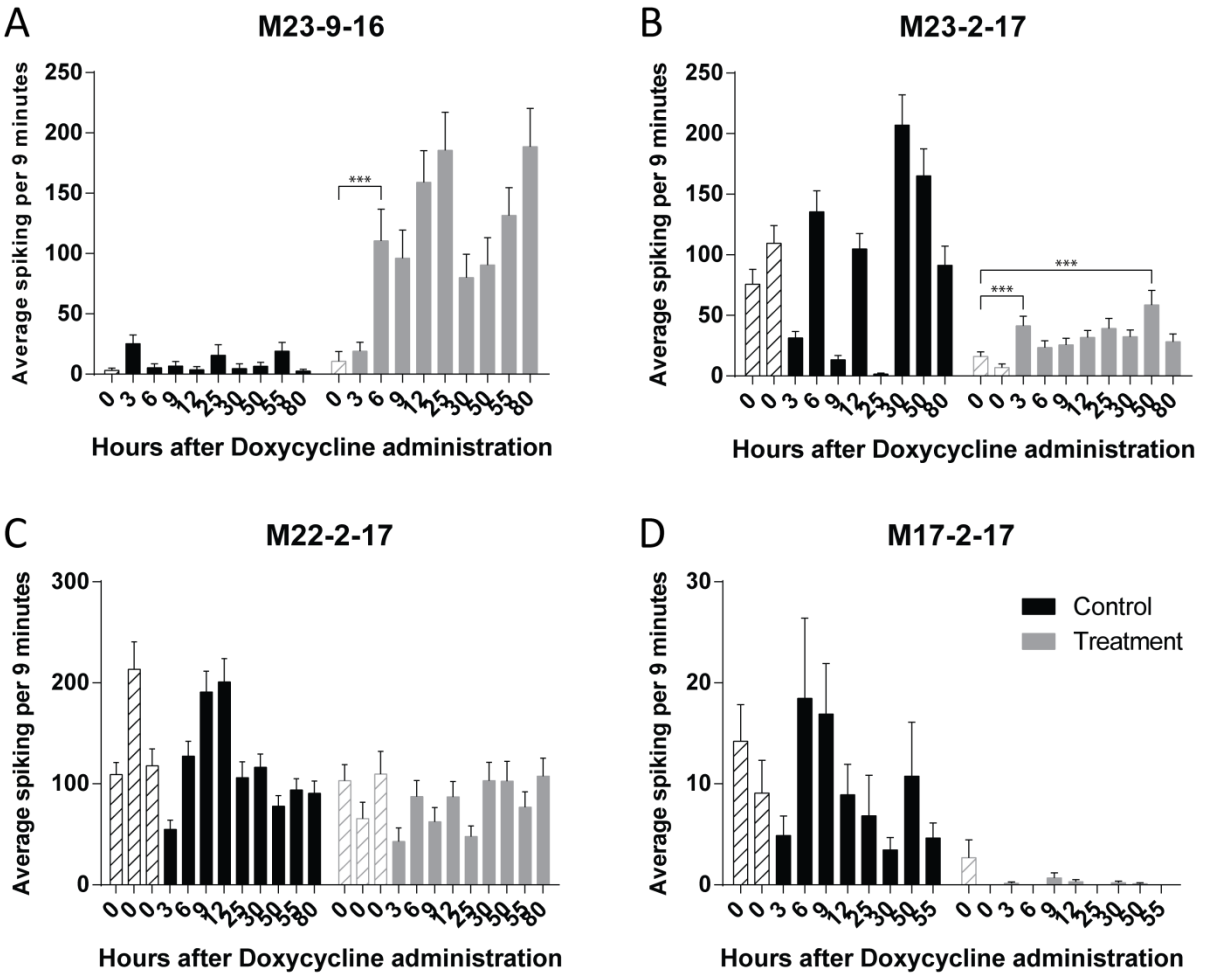

Figure 41. Examples of inferred spiking of four different animals with silenced PV cell populations. A) Low basal levels of activity, but then a high increase of activity can be observed for the treatment hemisphere. Already 6h after Doxycycline administration there is a significant difference compared to the initial value before transgene induction (p=<0.001). (Control cells: n=51; Treatment cells: n=72). B) There is a high variability of neuronal activity levels within the control brain hemisphere. The treatment hemisphere shows a significant increase already after 3 h (p=<0.001), and a trend to higher neuronal activity after induction is also apparent here. (Control cells: n=112; Treatment cells: n=123). C) Example where transgene induction did not work or did not have a measureable effect on neuronal activity levels. (Control cells: n=123; Treatment cells: n=93). D) Example where chosen cortical area did not show much neuronal activity despite expressing the calcium indicator GCamP6f. In this case the control hemisphere also showed very low neuronal activity levels. (Control cells: n=92; Treatment cells: n=79). (Error bars: SEM; Striped bars were averaged; Statistical test: One sample t-test)

These levels of variability in general are what had to be dealt with for the experiments and analysis. Therefore, it is even more remarkable that a clear statistically significant trend could be observed that validated the efficacy of the method (Figure 40-Treatment).

(Graphs of all conducted experiments can be seen in the appendix under Figure 47.)

3.14 Relation between proximity and change of activity levels

3.14.1 Proximity to manipulated random Cre+ neurons (Dilute Cre)

With the Dilute Cre experiments it could be shown that only the Cre^+ cells changed their activity levels after manipulation. The surrounding untargeted cells did not change their average firing rate as a consequence of silenced targeted cells in their vicinity (Chapter 3.12) in contrast to the experiments with manipulated PV interneurons (Chapter 3.13).

While there was no effect on overall activity levels of non-targeted cells, conceivably, nearby neurons might increase and more distant neurons decrease their activity (or vice versa), so that the overall activity levels remained constant.

However, the surrounding, untargeted neurons did not adjust their firing activity to counteract such an activity decrease in Cre^+ cells. Thus, no significant changes in activity levels related to the distance to manipulated cells were observed, if the average activity changes were correlated to the average distance of untargeted cells to targeted Cre^+ neurons. The average activity changes of each of these cells over time were compared to the initial activity levels before Doxycycline administration (Figure 42). In Figure 42A and B one can see that there is no correlation between distance and changes in activity levels as the distribution of the neuronal activity is roughly resulting in a horizontal line for treatment ($p=0.0967$, $R^2= 0.009892$) and control ($p=0.6966$; $R^2= 0.0005746$) hemispheres. Figure 42C depicts an example cortical region with Cre^+ cells in red and GCamP6f expressing neurons in green. Figure 42D shows the same cortical region but color coded with changes in average spiking levels over all recordings compared to the initial recording.

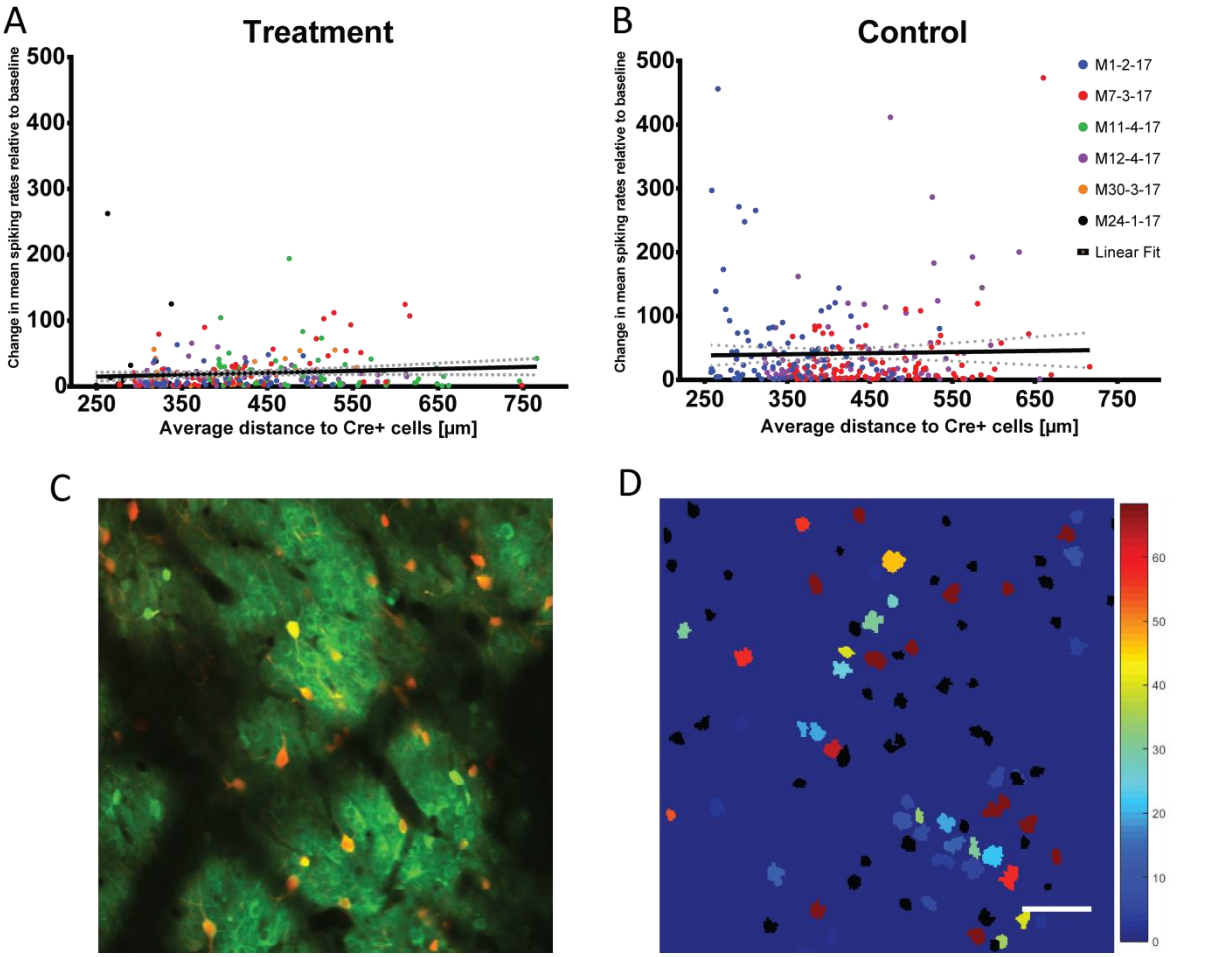

Figure 42. Relation between the average distance to manipulated Cre$^+$ cells and average change of spiking activity compared to initial spiking activity before Kir2.1 induced silencing of Cre$^+$ cells (n= ~260 cells analyzed for each experiment; Linear regression fit analysis). A) Treatment: No significant distance-dependent effect of silenced Cre$^+$ cells to the activity of the surrounding neuronal network (p=0.0967, R^2= 0.009892) B) Control: No correlation between distance to Cre$^+$ cells and change of spiking activity for the control brain hemisphere (p=0.6966; R^2= 0.0005746) Dashed line: 95 % confidence intervals). C) Composite image of an example region from experiment M24-1-17. D) The same region color coded with changes in average spiking relative to the initial activity over all recordings. The positions of targeted Cre$^+$ cells are displayed in black. (Scale bar: 100 µm; n=6 for each condition)

3.14.2 Proximity to manipulated PV interneurons

Silencing PV cells leads to increased activity of surrounding neuronal populations. It is unclear however, if this change in firing rates depends on the distance to the manipulated PV cells. Consequently, the average distance of each neuron to PV cells in the field of view was determined. The average activity changes of each of these cells over the entire experiment were compared to the initial activity levels before Doxycycline administration. These two parameters, average activity changes and average distance to PV cells, were then correlated (Chapter 2.5.8).

The results showed a significant relation between proximity of PV cells and the change in activity levels of each neuron (Figure 43). This effect was anticipated, as one would expect more synaptic

connections between nearby cells compared to distant ones. Hence, these cells would be under a higher influence of the manipulated PV cells, as they probably share more connections. The same correlation could not be observed for the control brain hemisphere, where PV cells were not manipulated.

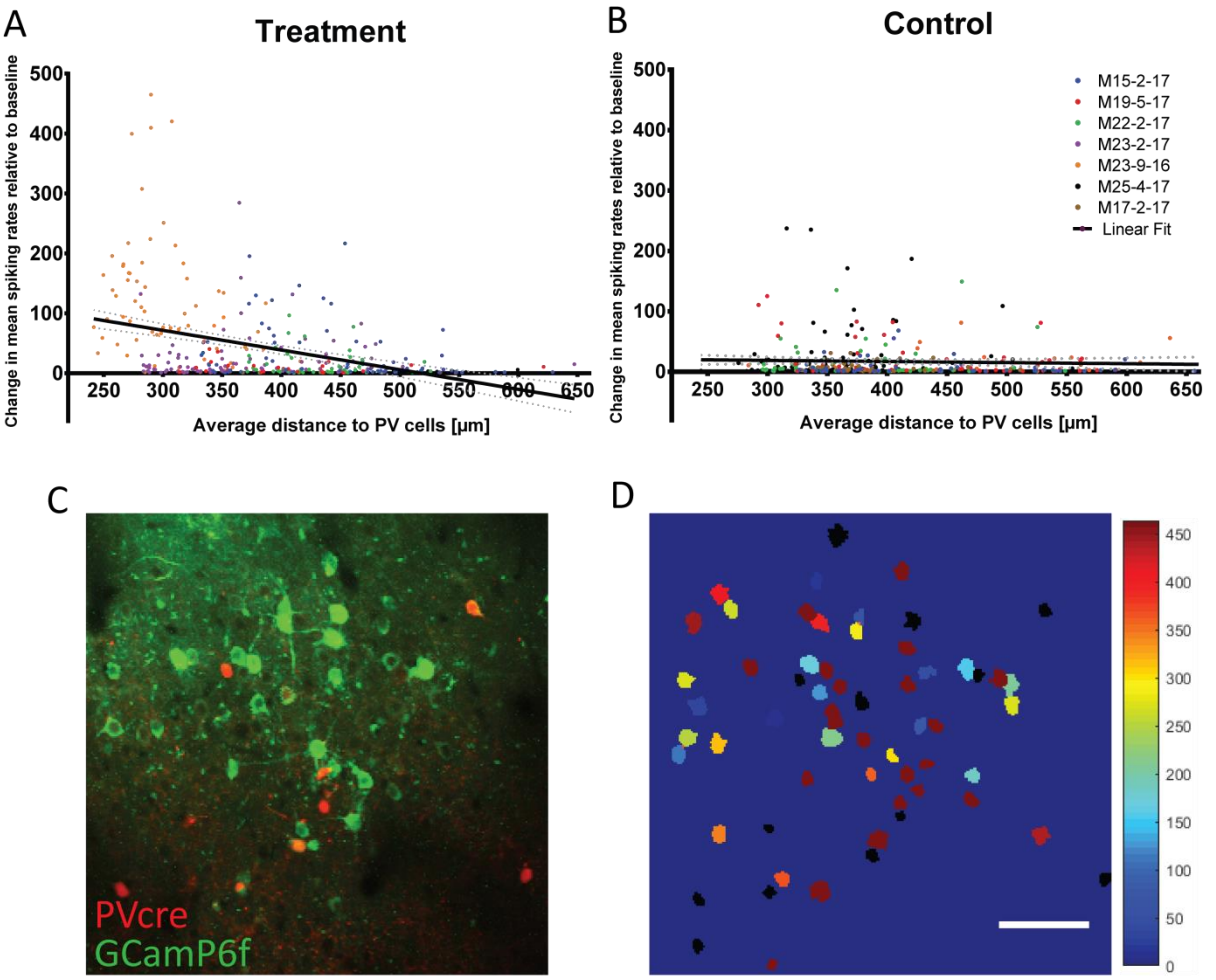

Figure 43. Relation between the average distance to all PV cells and average change of spiking activity compared to initial spiking activity before Kir2.1 induced silencing of PV cells. It is apparent that there is a strong effect of silenced PV cells to the activity of the surrounding neuronal network. The more proximal PV cells are, the higher the activity changes became. No such correlation between distance to PV cells and change of spiking activity can be observed for the control brain hemisphere where PV cell activity was not silenced. (n= ~320 cells analyzed for each experiment; Linear regression fit analysis: A) Treatment: p=>0.0001, R^2=0.1503; B) Control: p=0.4246; R^2=0.002058; Dashed line: 95 % confidence intervals). C) Composite image of an example region from experiment M23-9-16. D) The same region color coded with changes in average spiking relative to the initial activity over all recordings. The positions of PV cells are displayed in black. (Scale bar: 100 µm; n=7 for each condition)

These results also are in good agreement with the morphological characteristics of PV cells, that have been described before (Halasy et al., 1996). In this publication, the dendritic 'reach' of PV cells was described to be around 760 ± 130 µm on average. My results suggest an average influential reach on the surrounding neuronal network of maximal 525 µm. Conceivably PV cells do not appear to have a

big influence on cells if there are further away. This might be due to the fact, that PV cells presumably have more connections to nearby neurons and their silencing thus has stronger effects on their firing activity. As the inhibitory signals from nearby PV cells get weaker after Kir2.1 induction, the surrounding neurons increase their spiking activity. The effect gets weaker with an increasing distance to PV cells. Thus, my data suggest that non PV cells can have average distances from PV cells that vary two-fold and more and that this distance determines how much the firing of these non PV cells is affected by PV cells.

3.15 Assessing morphological changes after induced expression of Kir2.1

Burrone and co-workers previously showed that silencing neurons with Kir2.1 *after* synaptogenesis had occurred, did not lead to homeostatic morphological changes, i.e. spine loss or spine increase (Burrone et al., 2002). I am now in the position to reproduce and validate these published *in vitro* data in an *in vivo* setting. Because the silenced cells express Cre-dependet tdTomato, I could use the red fluorescence for morphological analyses before and after Kir2.1 induction.

For the Dilute Cre experiments the image quality of the stacks was suboptimal which made it challenging to determine stretches of dendrites with spines in a Pre-Doxycycline (Predox) and Post-Doxycycline (Postdox) time point. From four different animals, suitable stretches of dendrite were chosen before and ~75 h after Doxycycline administration. The counting was performed by a blinded observer (Figure 44).

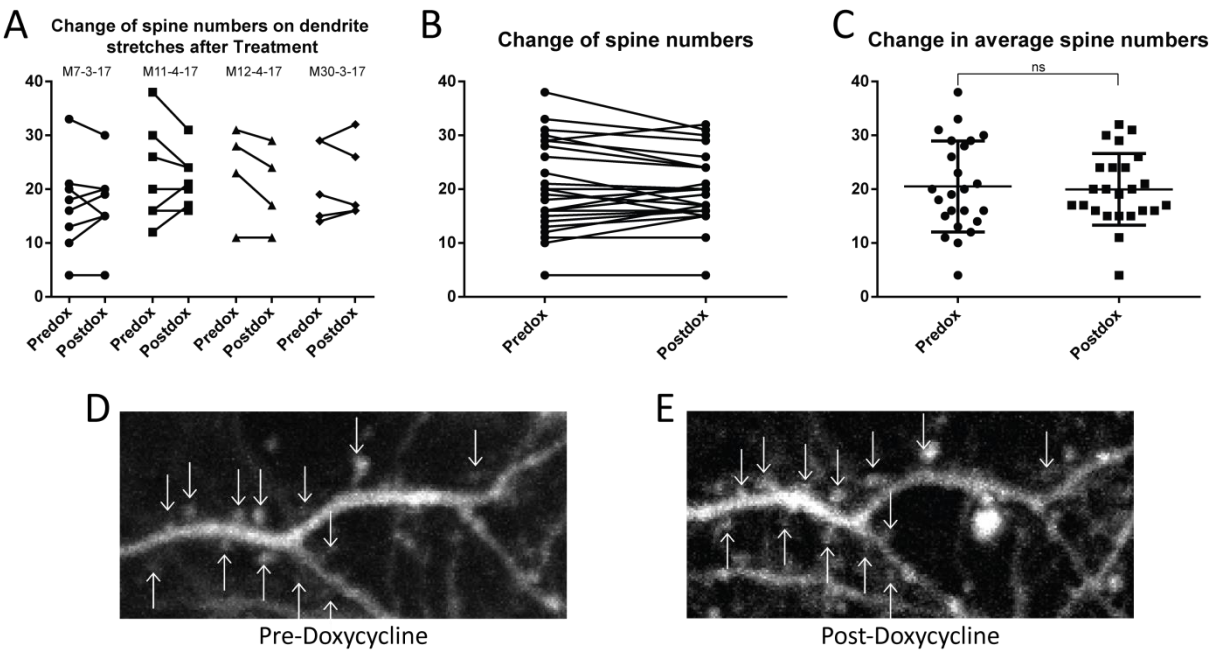

Figure 44. No significant changes in spine number were detected 75 h after induction of silencing Kir2.1 in the Dilute Cre animals. A) 4 to 8 dendrite stretches from four animals were compared regarding their spine number before induction (Predox), and 75 h after Kir2.1 induction (Postdox). No experiment did produce significant differences (M7-3-17, p=0.7813; M11-4-17, p=0.6250; M12-4-17, p=0.2500; M30-3-17, p>0.9999). B) Pooled display of data from A. C) No significant difference could be determined for changes in average spine number before and after Kir2.1 induction (p=0.4774; n=4 animals; Predox n=492 spines, Postdox n=479 spines). (Statistical test: nonparametric Wilcoxon matched-pairs signed ranked test). D) Example stretch of a dendrite from animal M11-4-17 acquired before and E) 75 h after Doxycycline induced Kir2.1 expression. Arrows depict spines.

The results showed no significant changes of spine numbers after extensive Kir2.1 mediated silencing of neurons. These results validate for the first time the results by Burrone and co-workers who observed that silencing of neurons *in vitro* after the synaptic connections were established ("adult-like"), did not have a significant effect on spine numbers (Burrone et al., 2002). These results suggest that, at least in the time window up to 80 h after induction, neurons do not change spine numbers *in vivo* even after experiencing prolonged periods on inactivity.

It was not possible to do morphological analyses with stacks acquired from PVcre *in vivo* experiments. The image resolution/signal was not suited to detect any morphological changes. Also, Parvalbumin interneurons are mainly aspiny, which would have made it even more complicated to compare morphological structures before and after treatment.

4 Discussion

4.1 Advantages of the established paradigm

For my thesis a TetOn based system was optimized to address previously reported leakiness issues. My method additionally offers the possibility to target specific cell types by incorporation of the Cre/lox system. I could combine this system with two-photon microscopy *in vivo* to monitor neuronal activity and morphology before, during, and after the induction of transgenes. All components of the TetOn system are rAAV based and thus can be delivered to neuronal cells or any other tissue via injection. To be able to monitor neuronal activity with calcium imaging required the development of an analysis pipeline. Minor and major changes of spontaneous activity induced by targeted expression of transgenes to the targeted cells and the surrounding, untargeted cells can now be assessed. In fact, with this pipeline it is possible to follow the changes of activity of single cells over days and possibly weeks by consecutive imaging sessions in the living animal.

I am convinced that the main accomplishment of my thesis was the successful combination of many different existing methods and tools into a robust, straightforward pipeline. Especially for the transgene expression my system incorporates some of the advantages of the individual methods and circumvents some of their disadvantages in this new experimental setting.

For instance, the use of Cre/lox transgenic animals has been a corner stone of biological research for the last two decades. Many transgenic mouse lines have been generated that express Cre recombinase in a cell-type specific manner and thus is the system of choice for conditional manipulation of genes in the desired subpopulation of cells. However, while the inducible Cre/lox system based on fusion of Cre to a mutated Estradiol receptor (CreERT2) and Tamoxifen improved the temporal resolution, transgene induction within hours is not possible. Moreover, transient transgene expression cannot be achieved because the Cre mediated recombination is essentially irreversible.

The method I developed uses the power of the Cre/lox system to target the TetOn system to specific cell types. This circumvents the need to use promoters in rAAVs to direct expression of the transgene. By making the transgenic expression dependent on the TetOn system rapid induction occurs within hours after the administration of Doxycycline. Therefore, scientists can choose the exact time of induction. Since the inducible transgene is not immediately expressed upon viral delivery one can wait until the other viral transgenes are fully expressed, which might vary from transgene to transgene. Thus, with my system one can deliver all the rAAVs at once and choose the time of induction as desired. The possibility to induce transgenic expression in specific cell types at

any time point combined with the optimized tightness of the TetOn system is the great advantage of this method compared to the previously available tools. This sophisticated combination thus allows acute (within hours), transient (theoretically adjustable by the Doxycycline concentration), and cellular resolved ("piggy-backing" the Cre/lox system) transgene expression in the living animal.

4.2 Results confirm previous studies of the scientific field

The results from my experiments conform to literature knowledge. In particular, I could show that silencing of PV inhibitory interneurons leads to an increase of neuronal activity in the proximity of these cells. This supports the importance of these interneurons for balanced activity (Hu et al., 2014). Conversely, no such network effects were observed when a small, random subpopulation of neurons was silenced by induced expression of Kir2.1 in the dilute Cre experiments. This is discussed in more detail below in chapter 4.7.

The initial idea that led to the start and the establishment of my method was based on the publication of Burrone and co-workers (Burrone et al., 2002). In their study they could show that homeostatic effects *in vitro* modulate synapse formation and stabilization before and after synaptic maturation of neurons. At low temporal resolution, the authors analyzed network homeostasis after transfection of Kir2.1 or a Kir2.1 mutant *in vitro*. With my experimental approach I could confirm their results by the induced expression of Kir2.1 *in vivo* with a more precise temporal resolution and the additional assessment of neuronal population activity. The authors analyzed the activity of transfected neurons and found that Kir2.1 compared to mutant Kir2.1 did change the neuronal activity of adult-like neurons (>DIV10) but did not lead to a change in spine numbers. On the contrary, if Kir2.1 mediated silencing of neuronal activity occurred in young neurons (<DIV10) they could observe decreased numbers of developed spines. In my experiments, I could follow the activity changes of the same neurons before and after the expression of Kir2.1, which was not possible with their experimental approach. Silencing *in vitro* was for about 96 h (because of the transfection, the timing is difficult to estimate) while silencing *in vivo* was for ~75 h. To my knowledge this is the first time, that these results could be confirmed *in vivo* with my experimental approach (Chapter 3.15).

4.3 Comparison to available tools

4.3.1 Transgene induction with the TetOn system

To my knowledge Tet-based systems are the only commonly used transgene induction methods used for research in mammals, besides the CreERT2 system which induces recombination. The combination of rtTA and tTR has been successfully used before (Freundlieb et al., 1999), but is not regularly used by the community for reasons that are unclear, but perhaps researchers did not want to introduce a third component for the Tet system. Notably, in my approach the TetOn proteins rtTA and tTR are combined within one single rAAV. In regard to tightness, efficacy, and temporal resolution, my system compares well with the results of Freundlieb and co-workers. Yet, most of the recent publications utilizing the TetOn system did not incorporate a tTR (Dogbevia et al., 2015) and were therefore possibly experiencing high levels of leakiness. The advantage of incorporating tTR for *in vivo* applications I demonstrated in this thesis (Chapter 3.1.3). To my knowledge the DriverTET construct I produced is the only available rAAV to deliver rtTA and tTR polycistronically to the target cells. As DriverTET is expected to generate approximately stoichiometric amounts of rtTA and tTR, leakiness should not be originating from uneven expression levels of the two proteins.

4.3.2 Conditional transgene expression system Cre/lox

For cell-type specificity, my method depends on the availability of Cre/lox transgenic animals with cell-type specific promoters. Transgenic animals are superior compared to delivery of the transgenes with a cell-type specific promoter via viruses or transfection. Cell-type specific promoter sequences are often very long and therefore problematic to fit into viral vectors. By homologous recombination or by the use of BACs (Bacterial Artificial Chromosomes) Cre recombinase can be controlled by endogenous promoters, which confer the desired specificity – temporally, spatially, or in respect to cell types. Due to their size, the delivery of BACs is usually limited to direct microinjections into the pronucleus of fertilized mouse oocytes and therefore cannot be applied in adult animals. With the combinatorial power of the Cre/lox system, one can express any floxed transgene under a ubiquitous promoter by crossing it to a line with Cre under a cell-type specific promoter. There have been other attempts to combine the Cre/lox with the Tet system, namely various tet-dependet Cre mice (Belteki et al., 2005; Hasan et al., 2013) or mice with reporter genes such as GCamP6f that are Cre and Tet dependent (Madisen et al., 2015; Sadakane et al., 2015). Nevertheless, I am not aware of any attempt to express non-reporter transgenes with the Cre/Tet combination.

As my system utilizes the Cre/lox system to target cell types, it enables additional experimental approaches. Basically any time that inducibility at a desired time point is needed, *and* in a specific cell type. Also, the Tet-dependent expression is transient. This makes this approach more flexible and powerful compared to the on-off only modality of the standard Cre/lox system.

4.3.3 The chemogenetic DREADD system

The chemogenetic DREADD system is utilized to modify neuronal activity by administration of a chemical compound after expression of a transgene, while for my chemogenetic system, first Doxycycline is administered and then transgene expression occurs. DREADDs modify the resting membrane potential, and I adopted the TetOn system to do the same through the induced expression of a hyperpolarizing (Kir2.1) or hypopolarizing (NaChBac) channel protein. For both systems, the spatial resolution is dependent on targeting of the proteins in a cell-type specific manner. The temporal resolution of DREADDs on the other hand is slightly superior to my system, as the DREADD compounds CNO/Clozapine were found to affect neuronal activity within ~30 min (Smith et al., 2016). My system depends on the time course of protein expression and is therefore dependent on the cellular machinery to produce and process the proteins which cannot be shortened. Albeit not significant *in vitro*, I see a trend in neuronal activity within one hour. Hasan and co-workers also observe expression of Luciferase within one hour *in vivo*, although this was not statistically quantified (Hasan et al., 2001). Thus, the DREADD system is faster than the TetOn system but the speed of inducing changes is not as relevant for the temporal resolution as is the "predictability" when things occur after action was taken (i.e. injection of the compounds). Presumably, the DREADD system has more of an on-off kinetic despite the recent finding that CNO first needs to be converted to the biologically active Clozapine (Gomez et al., 2017). Tet-dependent Kir2.1 expression on the other hand is gradually increasing over hours and then the channel remains in the neurons and silences them for at least three days without the need for future treatment. In addition, despite having a better temporal resolution, DREADDs are limited to hyperpolarizing or hypopolarizing membranes, whereas my system is far more flexible, as any transgene of interest can be expressed.

4.4 Validation of *in vivo* transgene induction was not possible with simultaneous assessment of neuronal activity with GCamP6f

One critical aspect of the inducible transient transgene expression is the time window during which overexpression lasts. This is important for being able to correlate any late phenotypic changes to the effect of transgene expression. The most straight forward approach to characterize the time window of transgene expression would be to detect the overexpressed protein product. As described in the results section 3.5.1 it was impossible to validate the successful induction either by mtagBFP fluorescence or antibody staining for the HA-Tag of Kir2.1. The efficacy of the bidirectional Tet promoter was shown by the fluorescence reporter mVenus which is comparable in structure to the other arm of the promoter that induced Kir2.1 (Chapter 3.7). Similarly, the induction of the fluorescence reporter mtagBFP in the Cre dependent constructs was also not possible *in vivo*, only *in vitro*. Having the mtagBFP targeted to the nucleus by a NLS sequence to accumulate the fluorescence signal in a smaller volume was not sufficient for *in vivo* detection. One reason for this might be the physical limitations of a blue spectrum fluorescent reporter for *in vivo* two-photon microscopy. Its emission wavelength of 454 nm is unfortunately prone to substantial absorption by the brain tissue (Phan and Bullen, 2010), which also increases with the thickness of the brain tissue (Al-Juboori et al., 2013).

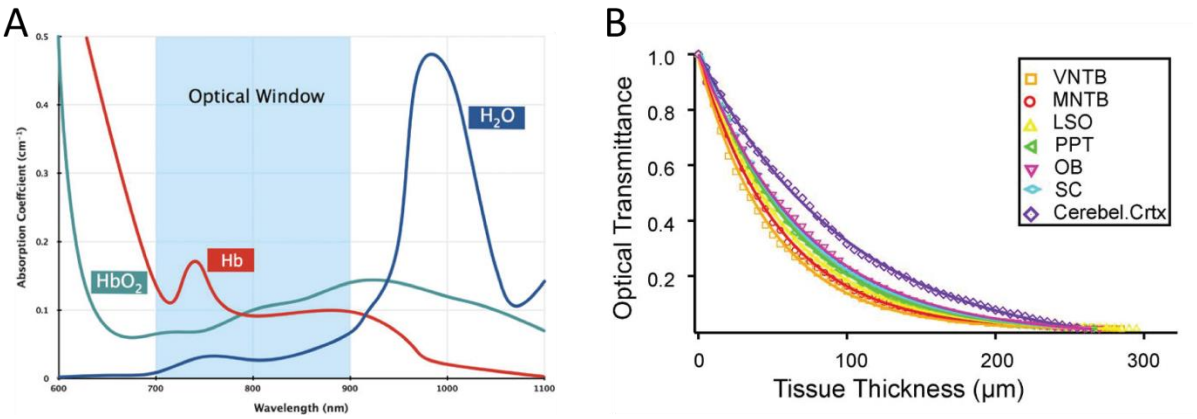

Figure 45. Tissue properties as a limitation for effective two-photon microscopy. A) Absorption spectrum of Hemoglobin (Hb) as the main fluorescence absorbent in brain tissue [From (Phan and Bullen, 2010)]. This limits the effective window for the collection of emitted photons beginning with wavelengths at around 500 nm. B) Optical transmittance of different types of brain tissue in relation to its thickness using light of 453 nm wavelength [From (Al-Juboori et al., 2013)]. The thicker the tissue, the more photons are absorbed by the tissue. Both these factors greatly influence and limit the effective use of blue fluorescence for *in vivo* experiments.

Also, the reporter mtagBFP is a far less bright fluorescent protein (32.8 x $10^{-3}M^{-1}cm^{-1}$) compared to mVenus (52.5 x $10^{-3}M^{-1}cm^{-1}$) (Cranfill et al., 2016). The combination of these three factors might be the reason for the inability to detect mtagBFP with two-photon microscopy in depths of ~100 µm.

The fluorescent reporter mtagBFP had been chosen because its emitted fluorescence would neither overlap much with GCamP6f nor with the tdTomato fluorescent reporter. The idea was to be able to do three color imaging and validate the expression levels of all three fluorescent proteins during the *in vivo* experiments. *In vitro* the induced mtagBFP fluorescence has also not been as intense as the bright emitted fluorescence of mVenus. mtagBFP fluoresence was sufficient to validate induction, but not strong enough to enable the experimenter to do morphological studies. For such experiments, I would therefore strongly suggest using mVenus as a fluorescent reporter if possible.

But also the *post-hoc* detection in brain slices after the *in vivo* experiments was not possible either for mtagBFP fluorescence or with antibody staining for HA-Tag of the Kir2.1 protein. However, *in vitro* Kir2.1 induction could be followed by immunofluorescence staining for the HA-Tag. The experiments indicate that Kir2.1 was present for at least 96 h after doxycycline exposure. More importantly, the 'Dilute Cre' experiments showed that Kir2.1 was not only present at least up to 80 h but also functional as neuronal activity in the targeted cells was silenced (Chapter 3.12).

The combination of both, the *in vitro* detection and the *in vivo* silencing for at least 80 h demonstrate long-lasting presence of Kir2.1 in neurons after single pulse induction with Doxycycline.

4.5 Determining the activity of Parvalbumin interneurons

Different approaches were tried to assess the activity levels of Parvalbumin neurons with GCamP6f. As the PV cells were not expressing the viral synapsin promoter driven GCamP6f sufficiently, floxed CAG driven GCamP6f rAAVs were co-injected with the mixture (1:10). With this approach the expression levels were strong enough to visually observe GCamP6f fluorescence in these cells. Interestingly, most bleaching that was notable during two-photon image acquisition was observed within these cells. Generally the CAG promoter is one of the strongest available ubiquitous promoters used in the research field. Hence, it is even more puzzling that bleaching could repeatedly be observed during the image acquisition phases. A possible explanation for this might be that the GCamP6f levels were not saturated and therefore a decrease in fluorescence due to bleaching was more readily detected. However, despite sufficiently high expression of GCamP6f in PV cells, only rarely could calcium transients be recorded by imaging.

Presumably, the activity levels of this high-frequency firing interneurons were too high to measure them with GCamP6f. The intracellular calcium levels of these cells are fluctuating at very high levels that cannot be resolved with a calcium sensor like GCamP6f (Badura et al., 2014; Helassa et al., 2016). At least not when trying to observe unevoked spontaneous activity of these interneurons.

Most publications in which PV cells were studied by imaging the experimenters used strong and distinct stimuli (Hofer et al., 2011), or instead used much more sensitive electrical recordings (McCormick et al., 1985).

The pattern of the recorded calcium traces appeared like “busy” noise most of the time without any distinct peaks or other features (Figure 33). Also higher image acquisition rates of 30 Hz did not improve transient detection. The most likely reason is the insufficient on-off kinetics of GCamP6f as a calcium indicator to measure such high frequency activities. To my knowledge, there is currently no possibility to measure spontaneous PV cell activity with genetically encoded calcium indicators. To measure PV cell activity with confidence, one would either have to try chemical calcium sensors or use electrical recordings.

Also, the light anesthesia during the recordings might impair measureable fluctuations of activity. Habituating the animals and acquiring data with awake animals might be helpful to gather more useful information.

4.6 High variability of the recordings

Establishing conditions for reproducible *in vivo* recordings have been a major obstacle for the whole study. Only with breathing rate controlled anesthesia, comparability of the recordings could be achieved successfully. Still, high differences between different animals were observed. Each animal reacted differently to the same amount of Isoflurane, which might be due to their body weights. In general, the Isoflurane levels had to be monitored and adjusted throughout the entire recordings. Otherwise, the neuronal activity would change rapidly so that the entire recording would have to be repeated after the breathing rates were adjusted to the desired value of ~120 Breaths/min again.

Another source for variability turned out to be the intrinsic properties of the imaged cortical areas. During rAAV injections, areas with few big blood vessels were chosen regardless of any specific brain regions, but roughly somewhere in the S1 somatosensory cortex. Injected areas with sufficient GCamP6f expression were then imaged. Of these, some areas later turned out to have very low neuronal activity or no observable activity at all. Other areas showed high levels of neuronal activity with a lot of variability also among neurons in the same field of view (see error bars in Figure 38). Thus, it was very difficult to identify a cortical area that would have homogeneous neuronal activity levels in all the animals. The quality of the injections also varied quite a lot which reduced the cortical areas for effective recording additionally. In general, it was much easier to find suitable GCamp6f expressing regions in control brain hemispheres. This might be due to the reason that commercial

GCamp6f rAAVs were injected in control hemispheres without the TetOn rAAVs. The injections were much easier due to less cloaking of the injection electrode and the expression levels have therefore been higher as more viral volume could successfully be injected. Also, even though the number of injected viral GCamP6f particles was the same for the treatment and control hemispheres, the presence of the TetOn viral particles probably reduced the "effectivity" of the GCamP6f particles on the treatment side. This could partially be corrected by adjusting the laser power, but the reduced GCamP6f fluorescence was still a limiting factor. This problem can be appreciated in Figure 37, where the control brain hemispheres (Control) have a much higher average activity level compared to the treatment brain hemispheres (Targeted). Choosing regions for imaging in the PV animals also made it necessary to find a good 'balance' between having PV cells in the field of view together with GCamP6f expressing cells in the surrounding areas. Imaging was always performed in cortical depths of ~100 µm. Thus, the imaging depth can probably be excluded as a source for additional variability.

The subsequent analysis pipeline should not add any additional variability. The only source might be the imperfect image registration that might lead to some deviations, as the ROIs are not adjusted for every acquired movie separately, but are chosen from a projection of all the recordings of one brain region. The later spike inference with MLspike was calibrated to the original publication data and any error created should also be a systematic one, which therefore cannot be a source for variability.

Taken together, in light of all these different sources of variability, including surgery, injection quality, biological differences between animals, anesthesia adjustment, and analysis pipeline, the achieved level of reproducibility is a great success in my opinion. The only way to further decrease the variability might be to habituate the animals to the recordings and use wake animals, and/or use specific stimuli to evoke neuronal activity that can be stimulus locked and readily correlated.

4.7 Influences of transgenic manipulations on neuronal network

Observing adjustments of the neuronal network activity as a consequence of acute genetic manipulations of a subset of neuronal populations could be achieved successfully. The effect was most obvious when PV cells were silenced by induced expression of Kir2.1 (Chapter 3.13). Even though the activity changes of the PV cells themselves could not be measured successfully, the surrounding neurons did increase their activity as expected, since the inhibitory input from PV cells decreased. To my knowledge this is the first time, that this effect has been shown on *in vivo* with genetic manipulations, rather than pharmacologic or optogenetic ones. Also, recording spontaneous activity and not evoked activity, the observed effect is a physiologic one and less likely to be an

artifact. Using this experimental approach I could show that the proximity and potentially the number of synaptic connections must be a crucial factor for balancing neuronal activity levels homeostatically (Chapter 3.14.2). The effect of the induced expression of Kir2.1 on the PV cells must have been quite large as they decreased their activity so much that even the surrounding neuronal activity was increased (Figure 40). This confirms previous findings (Jiang et al., 2016; Kim et al., 2016; Sessolo et al., 2015) that PV cells must play an important role in balancing neuronal activity levels locally and act as some sort of pace maker to regulate activity of principal neurons in their vicinity.

Silencing a random population of neurons by Cre mediated targetingdid not show a comparable effect on neuronal network activity levels (Figure 37). The reasons for this observation are unclear. Presumably, the overall strength of the synaptic connections between principal cells is less than the strength between PV and principal cells. This could be reflected by the localization of the synaptic connections (soma vs. dendrites), the number of synaptic connections between the cells, or the synaptic strength of individual connecting synapses. I did not detect any proximity effect, which one could have expected at least for very nearby and potentially more connected neurons (Chapter 3.14.1).

It thus appears, that these cells might be less affected by proximal activity changes, and possibly have a more stable activity pattern. In this study, silencing of a small percentage of neurons did not lead to changes in activity levels of the network. Though, it might be very interesting to determine the percentage of neurons that need to be silenced to have an effect on the neuronal network activities.

This finding supports the idea, that inhibitory interneurons are an essential component of the main regulatory homeostatic system (Isaacson and Scanziani, 2011). One should also keep in mind that potentially different cell types are manipulated by the ‘Dilute Cre’ approach, compared to the cell type specific silencing of PV interneurons. Therefore, silencing a more diverse group of neurons, possibly both excitatory and inhibitory neurons, has much less of a predictable effect on the surrounding cells.

4.7.1 Observation of spine dynamics in Dilute Cre experiments

Burrone and co-workers (Burrone et al., 2002) showed *in vitro* that cell-autonomous silencing of neurons with Kir2.1 after synapse formation had occurred, did not lead to significant changes in spine numbers. More than one decade later, to our knowledge I am the first to corroborate these results *in vivo*. In fact, my experiments were conducted with a much higher spatial (969 µm x 969 µm field of view at cellular resolution vs. none) and temporal (>8 time points vs. 1 time point) resolution.

While it is possible that morphological spine changes occur only after more than 80 h of silencing, reported induced spine changes occur within a time frame of minutes to hours in the hippocampus (Oh et al., 2013; Wiegert and Oertner, 2013). Even though there were no obvious signs of toxicity after 80 h of silencing, spine changes that occur later might be a reflection of neuronal degeneration because of silencing rather than homeostatic mechanisms.

There are studies showing that loss of sensory input leads to a decrease in spine numbers of GAD65 inhibitory interneurons in the visual cortex already within 6 hours (Keck et al., 2011). Because of this rapid response, the authors of this study suggest that spine plasticity of interneurons might precede the plasticity of excitatory pyramidal neurons. For excitatory pyramidal neurons spine turnover is considered to be slower and taking place in a time frame of days to weeks rather than hours (Wefelmeyer et al., 2016). There might be big differences in the very heterogenic group of interneurons, though (Holtmaat et al., 2006). It seems that excitatory and inhibitory neurons have very different and often opposing compensatory mechanisms of rebalancing activity after big sensory input changes (Marik et al., 2010). To my knowledge there is no study available that focused on global silencing of excitatory neurons (for example with Tetrodotoxin, TTX) and the subsequent cortical spine morphology *in vivo*, which would be a suitable comparison to the conducted experiments of this study. Only studies are available that studied morphological changes in sliced brain cultures either with global silencing of neuronal activity (Mitra et al., 2011) or inhibition of glutamatergic synaptic transmission (Lu et al., 2013). Still, both studies could not find major morphological changes of spine numbers despite dramatic changes of neuronal activity. Conversely, previous studies could show that it is in fact possible to induce outgrowth of spines by LTP-like stimuli (Engert and Bonhoeffer, 1999; Kwon and Sabatini, 2011). It might be the case that dynamic homeostatic adaptation of neuronal activity in adult mouse excitatory neurons does not necessarily require acute morphological changes, but only long-term morphological adaptations (Lu et al., 2013).

Another critical point is, the image quality of the acquired stacks. Tiny, delicate, filopodia-like or immature spines that are more amenable to morphological dynamics could not be well resolved microscopically. The predominant spines that were observed were big, mature ones, which are supposed to be very stable despite changes in cellular dynamics (Meyer et al., 2014) (Figure 46). It is commonly accepted that big, mature, and stable spines in general are swelling or decreasing as a consequence of activity changes rather than completely disappearing (Berry and Nedivi, 2017).

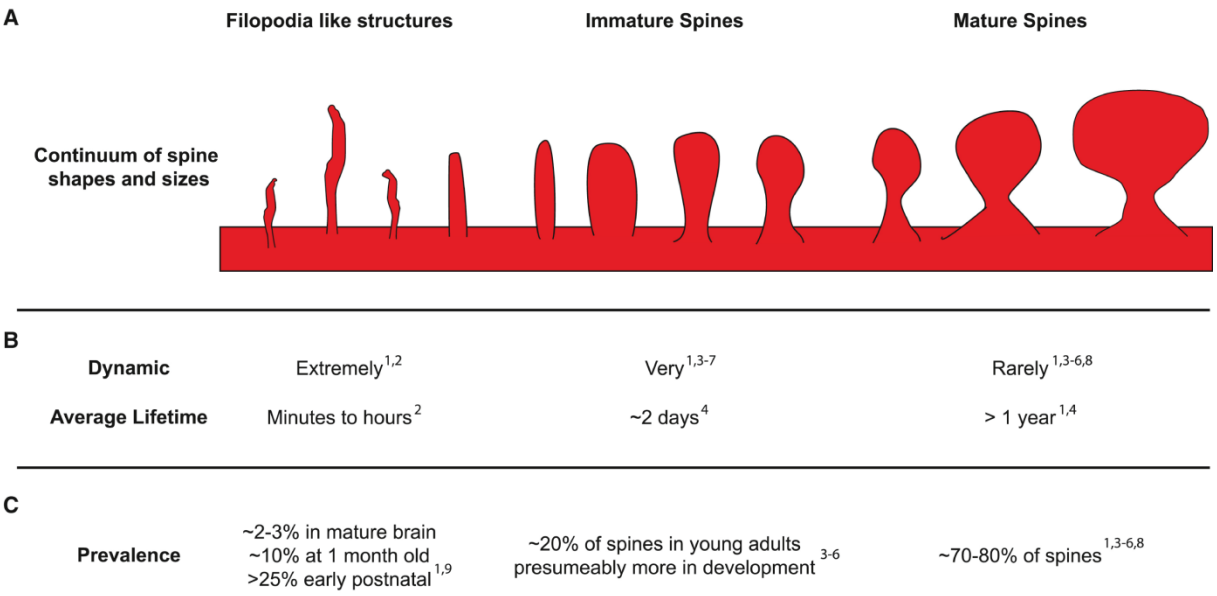

Figure 46. Overview of spine morphologies from filopodia-like structures to mature spines. A) Continuum of spine shapes and sizes. Spines are usually grouped into three different categories, filopodia-like structures, immature spines, and mature spines. B) Correlation of dynamics and average lifetime of spines in regard to the category they belong to. C) Estimates of the prevalence of each spine structure in different states of brain development. [Modified from (Berry and Nedivi, 2017)]

Taken together, with my research I could observe that silencing pyramidal neurons did not lead to a significant change in mature spine numbers, suggesting that the principles of homeostatic mechanisms Burrone and co-workers established in dissociated cell culture also hold true in an *in vivo* paradigm.

4.8 Limitations of the TetOn system for *in vivo* experiments

In general, the results of the viral TetOn system *in vitro* could be well extrapolated to the *in vivo* experiments. Robustness and inducibility of transgene expression was high in both cases. In the first *in vivo* experiments, the induction efficiency did vary more often, according to the mVenus fluorescence used as readout (Chapter 3.7). Most probably the reasons for the variability were the many different experimental steps necessary for the *in vivo* experimentation. In principle the entire surgery and its successful outcome depended on many factors. For example, the minor damage introduced to the brain surface was different for every animal. Also, sometimes brains of the animals would swell during surgery which can cause additional damage to the brain tissue, which might further impair the successful outcome of the experiments. The efficacy of the rAAV injections was probably the most varying factor of the *in vivo* experiments. Depending on the rAAV preparations and their viscosity the injections have been very challenging, as sometimes the injection electrodes

would be blocked by the particles in the suspension. In my experience, the complications and variability also increased with increasing number of rAAV types in the injection mixture. The simpler, initial experiments to assess the functionality, leakiness, and Doxycycline administration routes with only two rAAVs (DriverTET and RTETbi-mVenus-Kir2.1) were seemingly more robust (Chapter 3.7). With only two rAAVs, the mKO fluorescence signal of the DriverTET could be detected. For the later *in vivo* experiments with four different rAAVs (DriverTET, pAM-RTETbi-NLSmtagBFP-DIO-Kir2.1, Cre, GCamP6f) the only detectable fluorescence signal was originating from the GCamP6f as all the other fluorescent signals were too weak (Chapter 3.12). Because the (floxed) GCamP6f and the Cre virus were much more concentrated than necessary, I could mix the viruses in a 1:1:0.1:0.1 (DriverTET:ResponderTET:GCamP6f:Cre or floxed GCamP6f) relation. Since I always injected the same volume of ~1.5 µL the concentration of DriverTET and ResponderTET in the 4-fold mixture was only ~10 % less compared to injecting DriverTET and ResponderTET only.

Of course, there is a finite rAAV uptake capacity for transduction. The presence of GCamP6f and the other virus limits the extent of transduction with DriverTET and ResponderTET, which in turn lead to decreased mKO fluorescence. Not surprisingly, the overall transduction efficacy also varied so that injected cortical areas showed high variabilities of average fluorescence levels. Fortunately, these variabilities could easily be corrected for with adjustments of the laser power and did not impair the experimental approach. Still, experimenters should take this “dilution effect” into account and use as few different rAAVs as possible to keep this source of variability limited.

High leakiness of the ResponderTET construct RTETbi-mVenus-Kir2.1 could be observed if it was injected alone or without tTR transrepressor. We were excited to see that leakiness had essentially dropped to or below the detection limit if the tTR transrepressor had been incorporated into the DriverTET construct. In my experience, leakiness was not observed *in vivo* if the injection mixture contained DriverTET with the tTR transrepressor protein, at least for the fluorescence detection. A more sensitive assessment of the leakiness levels *in vivo* remains to be done. For example this could be achieved with highly sensitive assays, such as RNA detections via single cell sequencing (Ofengeim et al., 2017).

For *in vitro* experiments, the beneficiary effect of the tTR transrepressor was less striking. For instance, the levels of basal leakiness were not significantly different from the experiments without tTR. Only the Doxycycline dose-response curve was different – a steady increase without tTR versus a binary mode and step-like function with tTR (Chapter 3.1.2). To determine if leakiness levels are a true concern one could test this by using a toxic transgene such as Diphtheria toxin that would kill the cells if any basal expression is originating from the construct.

4.8.1 Viral delivery limitations and transgenic tissue

A more general limitation of this rAAV based approach is the size limitation of rAAV capsids. The effective size for a transgene can be maximally ~3800 bp, if one excludes the WPRE (used to stabilize viral transgene expression) sequence and only uses a unidirectional promoter without an inducible fluorescent reporter. Otherwise the effective size for a transgene is limited to ~ 3300 bp for a tet promoter inducible construct. Having an inducible reporter in a bidirectional ResponderTET construct will limit the maximum size of transgenes to about 2200 bp. This biophysical limitation is probably the biggest drawback of rAAV constructs in general. These limitations could be avoided if the system was transferred to viral vectors such as Adenoviruses (~36 kb) or Lentiviruses (~7 kb) (Davidson and Breakefield, 2003). This might introduce other disadvantages, but would solve the size limitation issue easily and enable the use of this system with larger transgenes of interest.

Another problem of the used rAAV serotypes 1/2 is their tropism for certain neuronal cell types (Aschauer et al., 2013) which might limit the use of this system or at least introduce a bias towards certain cell types. This cell-type specificity exists for all viral gene transfer systems and therefore it will not be possible to avoid that completely. Thus, one has to choose the viral vector system carefully for the specific requirements of the experimental approach.

Also, one has to keep in mind the amount of transgenic tissue and the arising complexity of it. For example, for the PVcre *in vivo* experiments double-transgenic animals were injected with a cocktail of four different rAAVs. Leading to sextuple transgenic tissue that was inducible by Doxycycline administration to the animal. The successful handling of this complexity is an accomplishment by itself and has been achieved only by few laboratories in the world, if at all.

4.9 Further optimizations

The main source of concern of using the TetOn system has mostly been the leakiness issue that did limit a lot of experimental approaches. While I improved the leakiness substantially, further optimizations should address this issue. One could think about two different approaches to tackle this problem. First, by optimizing the tTR to bind more tightly to the Tet promoter and prevent any transcription in the absence of Doxycycline. Second, by optimizing the synthetic Tet promoter itself, possibly by replacement of the CMVmin promoter with a weaker minimal promoter to minimize background expression (Loew et al., 2010).

Furthermore, the transfer of the system to Lentiviral vectors will allow the use of bigger transgenes that do not fit in rAAV vectors. Of course, one could also consider utilizing other cell-type specific

promoters for the DriverTET construct instead of the pan-neuronal synapsin promoter, i.e. the GFAP promoter for astrocytes. This way one could also target other cell types than neuronal populations.

Moreover, it was difficult to validate the successful induction of the transgene by any reporter protein other than mVenus. With the green fluorescence channel being heavily used because of other indicators such as GCamP6f, mVenus is therefore not suitable for many applications. Unfortunately, since the red fluorescence channel was occupied by the signal of tdTomato, only blue and far-red fluorescence remained as alternatives. Both appear to be suboptimal as reporter genes for *in vivo* 2P microscopy, because of their brightness and signal-to-noise ratios. Despite a lot of effort, mtagBFP or even the *post-hoc* HA-Tag staining was not a satisfactory proxy for monitoring transgene expression. Certainly, a reporter that can be monitored *in vivo* would be very useful. Moreover, this reporter could also be tagged to certain cellular compartments, which could be used for more detailed analysis of the manipulated cells.

4.10 Possible applications of the established method

In general, inducible transgene expression is important for a wide variety of possible applications. My system in particular is interesting for applications where the effect of acute transgene expression should be observed in a limited time window within a specific cell-type or population. In general, research of cell-type specific contributions to organ function should greatly benefit from this method. Additionally, all applications where the previous leakiness issues prevented scientists from using the TetOn system. Still, in my opinion leakiness is intrinsic to any inducible transgene expression method and will never be eliminated entirely. Of course, in my system a minor level of leakiness is to be expected, although being lower.

In respect to possible future applications of my method, the generation of *in vivo* induced pluripotent stem cells comes to mind (Carey et al., 2010; Haenebalcke et al., 2013). Reprogramming by the induction of certain transgenes to a stem cell-like status, and following their cellular transition until integration as newly generated neurons into the circuitry could be an exciting project. Also, one could think about inducing apoptosis in astroglia or other neuronal populations and monitor the effects on neuronal network activities with high spatio-temporal resolution.

Moreover, this system could be used for gene therapeutic treatment of chronic diseases where transgene expression is necessary periodically. For example, applications in retinopathies where uncontrolled growth of blood vessels impairs vision. In these cases the periodic expression of sFlt1 (Soluble fms-like tyrosine kinase-1) could counteract the pathological release of VEGF (Vascular

Endothelial Growth Factor) by sequestration. VEGF release is thought to be the main cause of neovascularization in the retina. Treatments with anti-VEGF drugs showed promising results in the past (Evans and Virgili, 2014). This sort of neovascularization is often observed in diabetic, or hypertension patients, and in age-related macular degeneration. Being able to tightly control VEGF levels transiently with a conditional gene therapy should improve such applications, potentially even by attempting cell-type specific release of sFlt1 in humans.

In the end, just about any experimental approach that requires the expression of transgenes at a desired time in a specific cell-type can utilize this system as long as the desired transgenes fit in the viral vectors.

5 References

Ai, H.W., Shaner, N.C., Cheng, Z., Tsien, R.Y., and Campbell, R.E. (2007). Exploration of new chromophore structures leads to the identification of improved blue fluorescent proteins. Biochemistry *46*, 5904-5910.

Al-Juboori, S.I., Dondzillo, A., Stubblefield, E.A., Felsen, G., Lei, T.C., and Klug, A. (2013). Light scattering properties vary across different regions of the adult mouse brain. PloS one *8*, e67626.

Alexander, G.M., Rogan, S.C., Abbas, A.I., Armbruster, B.N., Pei, Y., Allen, J.A., Nonneman, R.J., Hartmann, J., Moy, S.S., Nicolelis, M.A.*, et al.* (2009). Remote control of neuronal activity in transgenic mice expressing evolved G protein-coupled receptors. Neuron *63*, 27-39.

Armbruster, B.N., Li, X., Pausch, M.H., Herlitze, S., and Roth, B.L. (2007). Evolving the lock to fit the key to create a family of G protein-coupled receptors potently activated by an inert ligand. Proceedings of the National Academy of Sciences of the United States of America *104*, 5163-5168.

Arrenberg, A.B., Stainier, D.Y., Baier, H., and Huisken, J. (2010). Optogenetic control of cardiac function. Science *330*, 971-974.

Aschauer, D.F., Kreuz, S., and Rumpel, S. (2013). Analysis of transduction efficiency, tropism and axonal transport of AAV serotypes 1, 2, 5, 6, 8 and 9 in the mouse brain. PloS one *8*, e76310.

Badura, A., Sun, X.R., Giovannucci, A., Lynch, L.A., and Wang, S.S. (2014). Fast calcium sensor proteins for monitoring neural activity. Neurophotonics *1*, 025008.

Banker, G., and Goslin, K. (1998). Culturing nerve cells, 2nd edn (Cambridge, Mass.: MIT Press).

Baron, U., Schnappinger, D., Helbl, V., Gossen, M., Hillen, W., and Bujard, H. (1999). Generation of conditional mutants in higher eukaryotes by switching between the expression of two genes. Proceedings of the National Academy of Sciences of the United States of America *96*, 1013-1018.

Becnel, J., Johnson, O., Majeed, Z.R., Tran, V., Yu, B., Roth, B.L., Cooper, R.L., Kerut, E.K., and Nichols, C.D. (2013). DREADDs in Drosophila: a pharmacogenetic approach for controlling behavior, neuronal signaling, and physiology in the fly. Cell Rep *4*, 1049-1059.

Belteki, G., Haigh, J., Kabacs, N., Haigh, K., Sison, K., Costantini, F., Whitsett, J., Quaggin, S.E., and Nagy, A. (2005). Conditional and inducible transgene expression in mice through the combinatorial use of Cre-mediated recombination and tetracycline induction. Nucleic acids research *33*, e51.

Berry, K.P., and Nedivi, E. (2017). Spine Dynamics: Are They All the Same? Neuron *96*, 43-55.

Bezaire, M.J., and Soltesz, I. (2013). Quantitative assessment of CA1 local circuits: knowledge base for interneuron-pyramidal cell connectivity. Hippocampus *23*, 751-785.

Blankenship, A.G., Ford, K.J., Johnson, J., Seal, R.P., Edwards, R.H., Copenhagen, D.R., and Feller, M.B. (2009). Synaptic and extrasynaptic factors governing glutamatergic retinal waves. Neuron *62*, 230-241.

Boyden, E.S., Zhang, F., Bamberg, E., Nagel, G., and Deisseroth, K. (2005). Millisecond-timescale, genetically targeted optical control of neural activity. Nat Neurosci *8*, 1263-1268.

Buetfering, C., Allen, K., and Monyer, H. (2014). Parvalbumin interneurons provide grid cell-driven recurrent inhibition in the medial entorhinal cortex. Nat Neurosci *17*, 710-718.

Burrone, J., O'Byrne, M., and Murthy, V.N. (2002). Multiple forms of synaptic plasticity triggered by selective suppression of activity in individual neurons. Nature *420*, 414-418.

Carey, B.W., Markoulaki, S., Beard, C., Hanna, J., and Jaenisch, R. (2010). Single-gene transgenic mouse strains for reprogramming adult somatic cells. Nature methods *7*, 56-59.

Chagnac-Amitai, Y., and Connors, B.W. (1989). Horizontal spread of synchronized activity in neocortex and its control by GABA-mediated inhibition. Journal of neurophysiology *61*, 747-758.

Chen, T.W., Wardill, T.J., Sun, Y., Pulver, S.R., Renninger, S.L., Baohan, A., Schreiter, E.R., Kerr, R.A., Orger, M.B., Jayaraman, V.*, et al.* (2013a). Ultrasensitive fluorescent proteins for imaging neuronal activity. Nature *499*, 295-300.

Chen, Y., Cao, L., Luo, C., Ditzel, D.A., Peter, J., and Sprengel, R. (2013b). RANGE: Gene Transfer of Reversibly Controlled Polycistronic Genes. Mol Ther Nucleic Acids *2*, e85.

Cranfill, P.J., Sell, B.R., Baird, M.A., Allen, J.R., Lavagnino, Z., de Gruiter, H.M., Kremers, G.J., Davidson, M.W., Ustione, A., and Piston, D.W. (2016). Quantitative assessment of fluorescent proteins. Nature methods *13*, 557-562.

Dave, A.S., and Margoliash, D. (2000). Song replay during sleep and computational rules for sensorimotor vocal learning. Science *290*, 812-816.

Davidson, B.L., and Breakefield, X.O. (2003). Viral vectors for gene delivery to the nervous system. Nat Rev Neurosci *4*, 353-364.

DeFelipe, J., Lopez-Cruz, P.L., Benavides-Piccione, R., Bielza, C., Larranaga, P., Anderson, S., Burkhalter, A., Cauli, B., Fairen, A., Feldmeyer, D.*, et al.* (2013). New insights into the classification and nomenclature of cortical GABAergic interneurons. Nat Rev Neurosci *14*, 202-216.

Deneux, T., Kaszas, A., Szalay, G., Katona, G., Lakner, T., Grinvald, A., Rozsa, B., and Vanzetta, I. (2016). Accurate spike estimation from noisy calcium signals for ultrafast three-dimensional imaging of large neuronal populations in vivo. Nature communications *7*, 12190.

Denk, W., Strickler, J.H., and Webb, W.W. (1990). Two-photon laser scanning fluorescence microscopy. Science *248*, 73-76.

Deuschle, U., Meyer, W.K., and Thiesen, H.J. (1995). Tetracycline-reversible silencing of eukaryotic promoters. Mol Cell Biol *15*, 1907-1914.

Dogbevia, G.K., Marticorena-Alvarez, R., Bausen, M., Sprengel, R., and Hasan, M.T. (2015). Inducible and combinatorial gene manipulation in mouse brain. Frontiers in cellular neuroscience *9*, 142.

Dubbs, A., Guevara, J., and Yuste, R. (2016). moco: Fast Motion Correction for Calcium Imaging. Front Neuroinform *10*, 6.

Dumermuth, G., Walz, W., Scollo-Lavizzari, G., and Kleiner, B. (1972). Spectral analysis of EEG activity in different sleep stages in normal adults. Eur Neurol *7*, 265-296.

Egorov, A.V., and Draguhn, A. (2013). Development of coherent neuronal activity patterns in mammalian cortical networks: common principles and local hetereogeneity. Mech Dev *130*, 412-423.

Ehlers, M.D. (2003). Activity level controls postsynaptic composition and signaling via the ubiquitin-proteasome system. Nat Neurosci *6*, 231-242.

Eldridge, M.A., Lerchner, W., Saunders, R.C., Kaneko, H., Krausz, K.W., Gonzalez, F.J., Ji, B., Higuchi, M., Minamimoto, T., and Richmond, B.J. (2016). Chemogenetic disconnection of monkey orbitofrontal and rhinal cortex reversibly disrupts reward value. Nat Neurosci *19*, 37-39.

Engert, F., and Bonhoeffer, T. (1999). Dendritic spine changes associated with hippocampal long-term synaptic plasticity. Nature *399*, 66-70.

Evans, J., and Virgili, G. (2014). Anti-VEGF drugs: evidence for effectiveness. Community Eye Health *27*, 48.

Fauth, M., and Tetzlaff, C. (2016). Opposing Effects of Neuronal Activity on Structural Plasticity. Front Neuroanat *10*, 75.

Freund, T.F., and Buzsaki, G. (1996). Interneurons of the hippocampus. Hippocampus *6*, 347-470.

Freundlieb, S., Schirra-Muller, C., and Bujard, H. (1999). A tetracycline controlled activation/repression system with increased potential for gene transfer into mammalian cells. The journal of gene medicine *1*, 4-12.

Gomez, J.L., Bonaventura, J., Lesniak, W., Mathews, W.B., Sysa-Shah, P., Rodriguez, L.A., Ellis, R.J., Richie, C.T., Harvey, B.K., Dannals, R.F*., et al.* (2017). Chemogenetics revealed: DREADD occupancy and activation via converted clozapine. Science *357*, 503-507.

Gossen, M., and Bujard, H. (1992). Tight control of gene expression in mammalian cells by tetracycline-responsive promoters. Proceedings of the National Academy of Sciences of the United States of America *89*, 5547-5551.

Gossen, M., Freundlieb, S., Bender, G., Muller, G., Hillen, W., and Bujard, H. (1995). Transcriptional activation by tetracyclines in mammalian cells. Science *268*, 1766-1769.

Grienberger, C., and Konnerth, A. (2012). Imaging calcium in neurons. Neuron *73*, 862-885.

Haenebalcke, L., Goossens, S., Dierickx, P., Bartunkova, S., D'Hont, J., Haigh, K., Hochepied, T., Wirth, D., Nagy, A., and Haigh, J.J. (2013). The ROSA26-iPSC mouse: a conditional, inducible, and exchangeable resource for studying cellular (De)differentiation. Cell Rep *3*, 335-341.

Halasy, K., Buhl, E.H., Lorinczi, Z., Tamas, G., and Somogyi, P. (1996). Synaptic target selectivity and input of GABAergic basket and bistratified interneurons in the CA1 area of the rat hippocampus. Hippocampus *6*, 306-329.

Harris, K.D., Quiroga, R.Q., Freeman, J., and Smith, S.L. (2016). Improving data quality in neuronal population recordings. Nat Neurosci *19*, 1165-1174.

Hasan, M.T., Hernandez-Gonzalez, S., Dogbevia, G., Trevino, M., Bertocchi, I., Gruart, A., and Delgado-Garcia, J.M. (2013). Role of motor cortex NMDA receptors in learning-dependent synaptic plasticity of behaving mice. Nature communications *4*, 2258.

Hasan, M.T., Schonig, K., Berger, S., Graewe, W., and Bujard, H. (2001). Long-term, noninvasive imaging of regulated gene expression in living mice. Genesis *29*, 116-122.

Hebb, D.O. (1949). The organization of behavior. A neuropsychological theory., Vol 2002 (Mahwah, NJ: Erlbaum Books).

Helassa, N., Podor, B., Fine, A., and Torok, K. (2016). Design and mechanistic insight into ultrafast calcium indicators for monitoring intracellular calcium dynamics. Sci Rep *6*, 38276.

Hensch, T.K., Fagiolini, M., Mataga, N., Stryker, M.P., Baekkeskov, S., and Kash, S.F. (1998). Local GABA circuit control of experience-dependent plasticity in developing visual cortex. Science *282*, 1504-1508.

Higley, M.J., and Sabatini, B.L. (2012). Calcium signaling in dendritic spines. Cold Spring Harb Perspect Biol *4*, a005686.

Hippenmeyer, S., Vrieseling, E., Sigrist, M., Portmann, T., Laengle, C., Ladle, D.R., and Arber, S. (2005). A developmental switch in the response of DRG neurons to ETS transcription factor signaling. PLoS Biol *3*, e159.

Hofer, S.B., Ko, H., Pichler, B., Vogelstein, J., Ros, H., Zeng, H., Lein, E., Lesica, N.A., and Mrsic-Flogel, T.D. (2011). Differential connectivity and response dynamics of excitatory and inhibitory neurons in visual cortex. Nat Neurosci *14*, 1045-1052.

Holtmaat, A., Bonhoeffer, T., Chow, D.K., Chuckowree, J., De Paola, V., Hofer, S.B., Hubener, M., Keck, T., Knott, G., Lee, W.C*., et al.* (2009). Long-term, high-resolution imaging in the mouse neocortex through a chronic cranial window. Nat Protoc *4*, 1128-1144.

Holtmaat, A., Wilbrecht, L., Knott, G.W., Welker, E., and Svoboda, K. (2006). Experience-dependent and cell-type-specific spine growth in the neocortex. Nature *441*, 979-983.

Hu, H., Gan, J., and Jonas, P. (2014). Interneurons. Fast-spiking, parvalbumin(+) GABAergic interneurons: from cellular design to microcircuit function. Science *345*, 1255263.

Ikegaya, Y., Aaron, G., Cossart, R., Aronov, D., Lampl, I., Ferster, D., and Yuste, R. (2004). Synfire chains and cortical songs: temporal modules of cortical activity. Science *304*, 559-564.

Ikegaya Y, A.G., Cossart R, Aronov D, Lampl I, Ferster D, Yuste R. (2004). Synfire chains and cortical songs: temporal modules of cortical activity. In Science.

Isaacson, J.S., and Scanziani, M. (2011). How inhibition shapes cortical activity. Neuron *72*, 231-243.

Jann, M.W., Lam, Y.W., and Chang, W.H. (1994). Rapid formation of clozapine in guinea-pigs and man following clozapine-N-oxide administration. Arch Int Pharmacodyn Ther *328*, 243-250.

Jiang, X., Lachance, M., and Rossignol, E. (2016). Involvement of cortical fast-spiking parvalbumin-positive basket cells in epilepsy. Prog Brain Res *226*, 81-126.

Kalderon, D., Roberts, B.L., Richardson, W.D., and Smith, A.E. (1984). A short amino acid sequence able to specify nuclear location. Cell *39*, 499-509.

Keck, T., Scheuss, V., Jacobsen, R.I., Wierenga, C.J., Eysel, U.T., Bonhoeffer, T., and Hubener, M. (2011). Loss of sensory input causes rapid structural changes of inhibitory neurons in adult mouse visual cortex. Neuron *71*, 869-882.

Khazipov, R., Leinekugel, X., Khalilov, I., Gaiarsa, J.L., and Ben-Ari, Y. (1997). Synchronization of GABAergic interneuronal network in CA3 subfield of neonatal rat hippocampal slices. The Journal of physiology *498 (Pt 3)*, 763-772.

Kilman, V., van Rossum, M.C., and Turrigiano, G.G. (2002). Activity deprivation reduces miniature IPSC amplitude by decreasing the number of postsynaptic GABA(A) receptors clustered at neocortical synapses. The Journal of neuroscience : the official journal of the Society for Neuroscience *22*, 1328-1337.

Kim, D., Jeong, H., Lee, J., Ghim, J.W., Her, E.S., Lee, S.H., and Jung, M.W. (2016). Distinct Roles of Parvalbumin- and Somatostatin-Expressing Interneurons in Working Memory. Neuron *92*, 902-915.

Koester, H.J., and Sakmann, B. (2000). Calcium dynamics associated with action potentials in single nerve terminals of pyramidal cells in layer 2/3 of the young rat neocortex. The Journal of physiology *529 Pt 3*, 625-646.

Kovacevic, N., Henderson, J.T., Chan, E., Lifshitz, N., Bishop, J., Evans, A.C., Henkelman, R.M., and Chen, X.J. (2005). A three-dimensional MRI atlas of the mouse brain with estimates of the average and variability. Cereb Cortex *15*, 639-645.

Krashes, M.J., Koda, S., Ye, C., Rogan, S.C., Adams, A.C., Cusher, D.S., Maratos-Flier, E., Roth, B.L., and Lowell, B.B. (2011). Rapid, reversible activation of AgRP neurons drives feeding behavior in mice. The Journal of clinical investigation *121*, 1424-1428.

Kwon, H.B., and Sabatini, B.L. (2011). Glutamate induces de novo growth of functional spines in developing cortex. Nature *474*, 100-104.

Lewandoski, M. (2001). Conditional control of gene expression in the mouse. Nature reviews Genetics *2*, 743-755.

Liu, X., Ramirez, S., Pang, P.T., Puryear, C.B., Govindarajan, A., Deisseroth, K., and Tonegawa, S. (2012). Optogenetic stimulation of a hippocampal engram activates fear memory recall. Nature *484*, 381-385.

Lobbestael, E., Reumers, V., Ibrahimi, A., Paesen, K., Thiry, I., Gijsbers, R., Van den Haute, C., Debyser, Z., Baekelandt, V., and Taymans, J.M. (2010). Immunohistochemical detection of transgene expression in the brain using small epitope tags. BMC Biotechnol *10*, 16.

Loew, R., Heinz, N., Hampf, M., Bujard, H., and Gossen, M. (2010). Improved Tet-responsive promoters with minimized background expression. BMC Biotechnol *10*, 81.

Lu, W., Bushong, E.A., Shih, T.P., Ellisman, M.H., and Nicoll, R.A. (2013). The cell-autonomous role of excitatory synaptic transmission in the regulation of neuronal structure and function. Neuron *78*, 433-439.

Madisen, L., Garner, A.R., Shimaoka, D., Chuong, A.S., Klapoetke, N.C., Li, L., van der Bourg, A., Niino, Y., Egolf, L., Monetti, C.*, et al.* (2015). Transgenic mice for intersectional targeting of neural sensors and effectors with high specificity and performance. Neuron *85*, 942-958.

Madisen, L., Zwingman, T.A., Sunkin, S.M., Oh, S.W., Zariwala, H.A., Gu, H., Ng, L.L., Palmiter, R.D., Hawrylycz, M.J., Jones, A.R.*, et al.* (2010). A robust and high-throughput Cre reporting and characterization system for the whole mouse brain. Nat Neurosci *13*, 133-140.

Malinow, R., and Malenka, R.C. (2002). AMPA receptor trafficking and synaptic plasticity. Annu Rev Neurosci *25*, 103-126.

Marik, S.A., Yamahachi, H., McManus, J.N., Szabo, G., and Gilbert, C.D. (2010). Axonal dynamics of excitatory and inhibitory neurons in somatosensory cortex. PLoS Biol *8*, e1000395.

McCormick, D.A., Connors, B.W., Lighthall, J.W., and Prince, D.A. (1985). Comparative electrophysiology of pyramidal and sparsely spiny stellate neurons of the neocortex. Journal of neurophysiology *54*, 782-806.

Meyer, D., Bonhoeffer, T., and Scheuss, V. (2014). Balance and stability of synaptic structures during synaptic plasticity. Neuron *82*, 430-443.

Mitra, A., Mitra, S.S., and Tsien, R.W. (2011). Heterogeneous reallocation of presynaptic efficacy in recurrent excitatory circuits adapting to inactivity. Nat Neurosci *15*, 250-257.

Mohns, E.J., and Blumberg, M.S. (2008). Synchronous bursts of neuronal activity in the developing hippocampus: modulation by active sleep and association with emerging gamma and theta rhythms. The Journal of neuroscience : the official journal of the Society for Neuroscience *28*, 10134-10144.

Muir, D.R., and Kampa, B.M. (2014). FocusStack and StimServer: a new open source MATLAB toolchain for visual stimulation and analysis of two-photon calcium neuronal imaging data. Front Neuroinform *8*, 85.

Murthy, V.N., Schikorski, T., Stevens, C.F., and Zhu, Y. (2001). Inactivity produces increases in neurotransmitter release and synapse size. Neuron *32*, 673-682.

Nelson, S.B. (1991). Temporal interactions in the cat visual system. III. Pharmacological studies of cortical suppression suggest a presynaptic mechanism. The Journal of neuroscience : the official journal of the Society for Neuroscience *11*, 369-380.

O'Brien, R.J., Kamboj, S., Ehlers, M.D., Rosen, K.R., Fischbach, G.D., and Huganir, R.L. (1998). Activity-dependent modulation of synaptic AMPA receptor accumulation. Neuron *21*, 1067-1078.

Ofengeim, D., Giagtzoglou, N., Huh, D., Zou, C., and Yuan, J. (2017). Single-Cell RNA Sequencing: Unraveling the Brain One Cell at a Time. Trends Mol Med *23*, 563-576.

Oh, W.C., Hill, T.C., and Zito, K. (2013). Synapse-specific and size-dependent mechanisms of spine structural plasticity accompanying synaptic weakening. Proceedings of the National Academy of Sciences of the United States of America *110*, E305-312.

Personius, K.E., Chang, Q., Mentis, G.Z., O'Donovan, M.J., and Balice-Gordon, R.J. (2007). Reduced gap junctional coupling leads to uncorrelated motor neuron firing and precocious neuromuscular synapse elimination. Proceedings of the National Academy of Sciences of the United States of America *104*, 11808-11813.

Phan, T.G., and Bullen, A. (2010). Practical intravital two-photon microscopy for immunological research: faster, brighter, deeper. Immunol Cell Biol *88*, 438-444.

Prange, O., and Murphy, T.H. (1999). Correlation of miniature synaptic activity and evoked release probability in cultures of cortical neurons. The Journal of neuroscience : the official journal of the Society for Neuroscience *19*, 6427-6438.

Ramakers, G.J., Corner, M.A., and Habets, A.M. (1990). Development in the absence of spontaneous bioelectric activity results in increased stereotyped burst firing in cultures of dissociated cerebral cortex. Exp Brain Res *79*, 157-166.

Resendez, S.L., Jennings, J.H., Ung, R.L., Namboodiri, V.M., Zhou, Z.C., Otis, J.M., Nomura, H., McHenry, J.A., Kosyk, O., and Stuber, G.D. (2016). Visualization of cortical, subcortical and deep brain neural circuit dynamics during naturalistic mammalian behavior with head-mounted microscopes and chronically implanted lenses. Nat Protoc *11*, 566-597.

Roome, C.J., and Kuhn, B. (2014). Chronic cranial window with access port for repeated cellular manipulations, drug application, and electrophysiology. Frontiers in cellular neuroscience *8*, 379.

Rossi, F.M., Guicherit, O.M., Spicher, A., Kringstein, A.M., Fatyol, K., Blakely, B.T., and Blau, H.M. (1998). Tetracycline-regulatable factors with distinct dimerization domains allow reversible growth inhibition by p16. Nature genetics *20*, 389-393.

Roth, B.L. (2016). DREADDs for Neuroscientists. Neuron *89*, 683-694.

Rudy, B., and McBain, C.J. (2001). Kv3 channels: voltage-gated K+ channels designed for high-frequency repetitive firing. Trends in neurosciences *24*, 517-526.

Sadakane, O., Masamizu, Y., Watakabe, A., Terada, S., Ohtsuka, M., Takaji, M., Mizukami, H., Ozawa, K., Kawasaki, H., Matsuzaki, M.*, et al.* (2015). Long-Term Two-Photon Calcium Imaging of Neuronal Populations with Subcellular Resolution in Adult Non-human Primates. Cell Rep *13*, 1989-1999.

Saeed, I.A., and Ashraf, S.S. (2009). Denaturation studies reveal significant differences between GFP and blue fluorescent protein. Int J Biol Macromol *45*, 236-241.

Salomonnson, E., Mihalko, L.A., Verkhusha, V.V., Luker, K.E., and Luker, G.D. (2012). Cell-based and in vivo spectral analysis of fluorescent proteins for multiphoton microscopy. J Biomed Opt *17*, 96001.

Schindelin, J., Arganda-Carreras, I., Frise, E., Kaynig, V., Longair, M., Pietzsch, T., Preibisch, S., Rueden, C., Saalfeld, S., Schmid, B.*, et al.* (2012). Fiji: an open-source platform for biological-image analysis. Nature methods *9*, 676-682.

Sessolo, M., Marcon, I., Bovetti, S., Losi, G., Cammarota, M., Ratto, G.M., Fellin, T., and Carmignoto, G. (2015). Parvalbumin-Positive Inhibitory Interneurons Oppose Propagation But Favor Generation of Focal Epileptiform Activity. The Journal of neuroscience : the official journal of the Society for Neuroscience *35*, 9544-9557.

Smith, K.S., Bucci, D.J., Luikart, B.W., and Mahler, S.V. (2016). DREADDS: Use and application in behavioral neuroscience. Behav Neurosci *130*, 137-155.

Sohal, V.S., Zhang, F., Yizhar, O., and Deisseroth, K. (2009). Parvalbumin neurons and gamma rhythms enhance cortical circuit performance. Nature *459*, 698-702.

Sommer, J.M., Smith, P.H., Parthasarathy, S., Isaacs, J., Vijay, S., Kieran, J., Powell, S.K., McClelland, A., and Wright, J.F. (2003). Quantification of adeno-associated virus particles and empty capsids by optical density measurement. Molecular therapy : the journal of the American Society of Gene Therapy *7*, 122-128.

Sternson, S.M., and Roth, B.L. (2014). Chemogenetic tools to interrogate brain functions. Annu Rev Neurosci *37*, 387-407.

Subach, O.M., Gundorov, I.S., Yoshimura, M., Subach, F.V., Zhang, J., Gruenwald, D., Souslova, E.A., Chudakov, D.M., and Verkhusha, V.V. (2008). Conversion of red fluorescent protein into a bright blue probe. Chemistry & biology *15*, 1116-1124.

Sun, Y., Chen, X., and Xiao, D. (2007). Tetracycline-inducible expression systems: new strategies and practices in the transgenic mouse modeling. Acta Biochim Biophys Sin (Shanghai) *39*, 235-246.

Svoboda, K., and Yasuda, R. (2006). Principles of two-photon excitation microscopy and its applications to neuroscience. Neuron *50*, 823-839.

Thiagarajan, T.C., Piedras-Renteria, E.S., and Tsien, R.W. (2002). alpha- and betaCaMKII. Inverse regulation by neuronal activity and opposing effects on synaptic strength. Neuron *36*, 1103-1114.

Tischer, D., and Weiner, O.D. (2014). Illuminating cell signalling with optogenetic tools. Nat Rev Mol Cell Biol *15*, 551-558.

Tsai, H.C., Zhang, F., Adamantidis, A., Stuber, G.D., Bonci, A., de Lecea, L., and Deisseroth, K. (2009). Phasic firing in dopaminergic neurons is sufficient for behavioral conditioning. Science *324*, 1080-1084.

Turrigiano, G.G., Leslie, K.R., Desai, N.S., Rutherford, L.C., and Nelson, S.B. (1998). Activity-dependent scaling of quantal amplitude in neocortical neurons. Nature *391*, 892-896.

Turrigiano, G.G., and Nelson, S.B. (2004). Homeostatic plasticity in the developing nervous system. Nat Rev Neurosci *5*, 97-107.

Wang, L., Wang, Z., Zhang, F., Zhu, R., Bi, J., Wu, J., Zhang, H., Wu, H., Kong, W., Yu, B.*, et al.* (2016). Enhancing Transgene Expression from Recombinant AAV8 Vectors in Different Tissues Using Woodchuck Hepatitis Virus Post-Transcriptional Regulatory Element. Int J Med Sci *13*, 286-291.

Wang, R., and Brattain, M.G. (2007). The maximal size of protein to diffuse through the nuclear pore is larger than 60kDa. FEBS letters *581*, 3164-3170.

Wefelmeyer, W., Puhl, C.J., and Burrone, J. (2016). Homeostatic Plasticity of Subcellular Neuronal Structures: From Inputs to Outputs. Trends in neurosciences *39*, 656-667.

Westbrook, G. (2013). Seizures and epilepsy. In Principles of Neural Science (New York: McGraw-Hill), pp. 1116-1139.

Wiegert, J.S., and Oertner, T.G. (2013). Long-term depression triggers the selective elimination of weakly integrated synapses. Proceedings of the National Academy of Sciences of the United States of America *110*, E4510-4519.

Wu, Z., Yang, H., and Colosi, P. (2010). Effect of genome size on AAV vector packaging. Molecular therapy : the journal of the American Society of Gene Therapy *18*, 80-86.

Zehendner, C.M., Luhmann, H.J., and Yang, J.W. (2013). A simple and novel method to monitor breathing and heart rate in awake and urethane-anesthetized newborn rodents. PloS one *8*, e62628.

Zhu, P., Aller, M.I., Baron, U., Cambridge, S., Bausen, M., Herb, J., Sawinski, J., Cetin, A., Osten, P., Nelson, M.L.*, et al.* (2007). Silencing and un-silencing of tetracycline-controlled genes in neurons. PloS one *2*, e533.

Zipfel, W.R., Williams, R.M., and Webb, W.W. (2003). Nonlinear magic: multiphoton microscopy in the biosciences. Nature biotechnology *21*, 1369-1377.

Ziv, Y., Burns, L.D., Cocker, E.D., Hamel, E.O., Ghosh, K.K., Kitch, L.J., El Gamal, A., and Schnitzer, M.J. (2013). Long-term dynamics of CA1 hippocampal place codes. Nat Neurosci *16*, 264-266.

6 Appendix

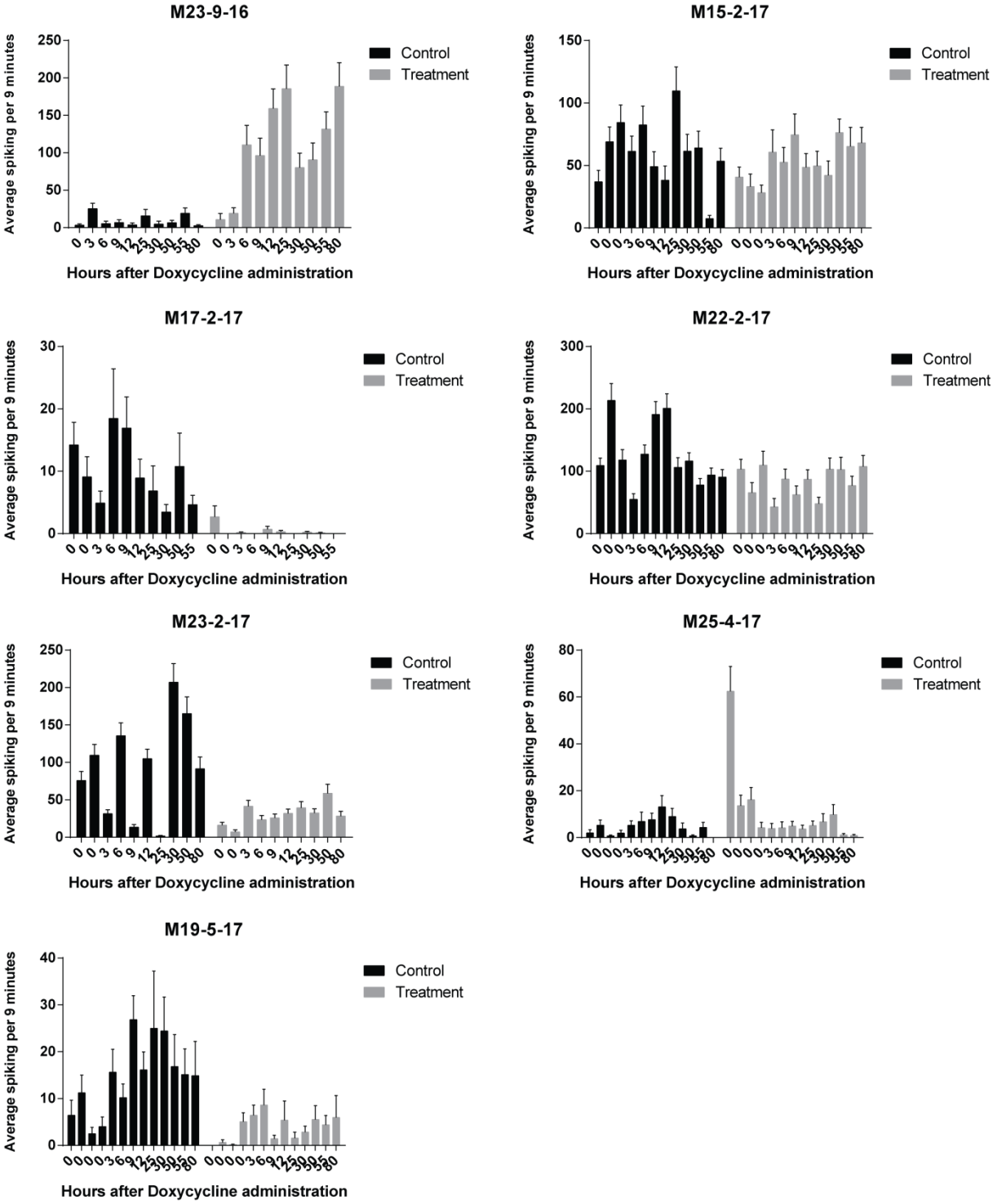

Figure 47. Inferred average spiking of single *in vivo* experiments from PVcre animals over consecutive time points. (Error bars: SEM)

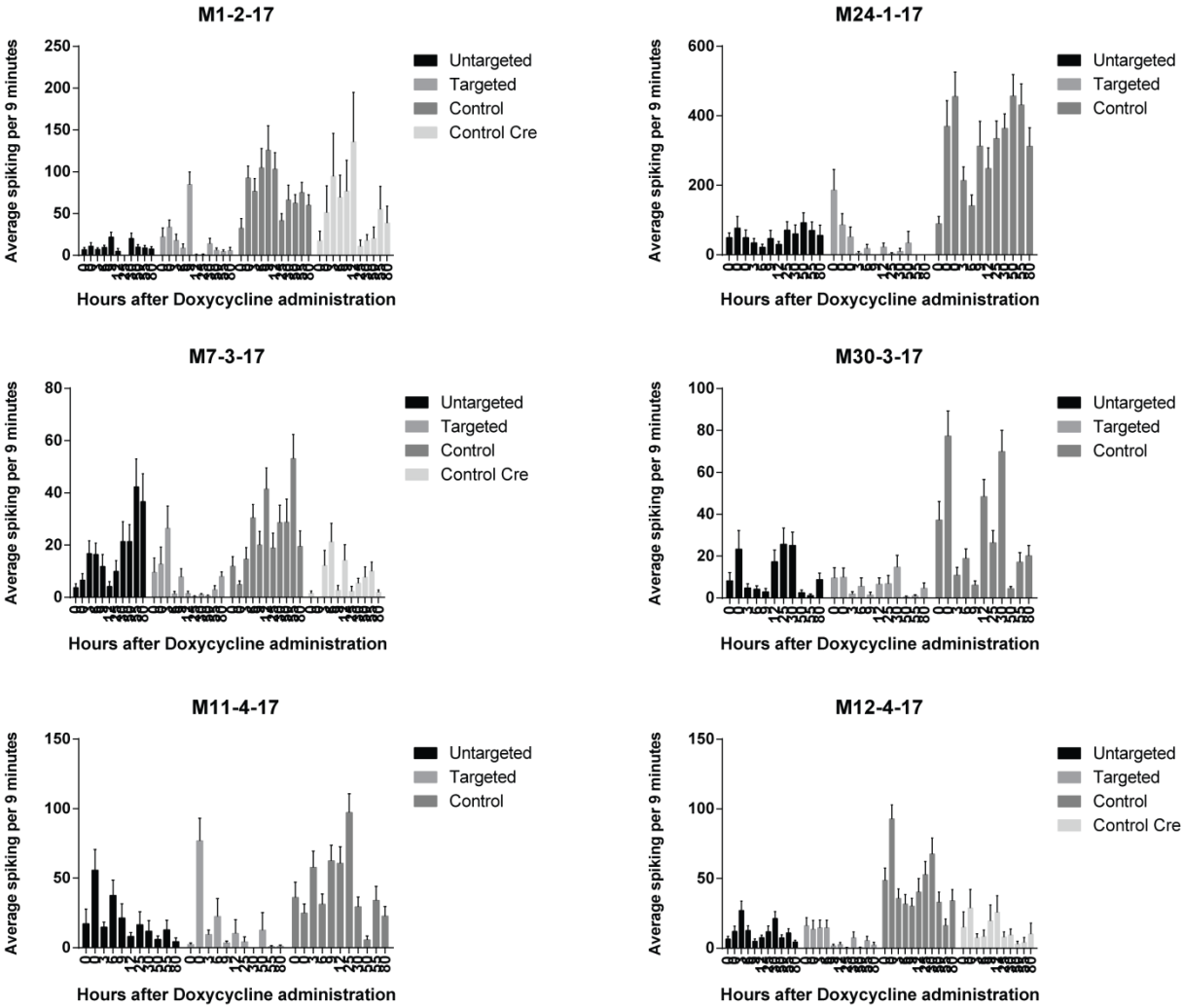

Figure 48. Inferred average spiking of single *in vivo* experiments from Dilute Cre animals over consecutive time points. (Error bars: SEM)

7 Declaration

Hereby I declare that in this thesis I presented my original research results. I have written this thesis by myself and marked the sources of any materials previously published or written by another person.

The work has been done under the guidance of Prof. Dr. Thomas Kuner at the Department of Functional Neuroanatomy, University of Heidelberg, Germany and was supervised by Dr. Sidney Cambridge.

This thesis is being submitted for the degree of Doctor of Natural Sciences at the University of Heidelberg.

Heidelberg,

Firat Terzi